

1-1-2010

Modeling of Bimolecular Nitroxide Mediated Radical Polymerization of Styrene in Batch Reactor and Steady State Analysis of CSTR Reactor

Basma Matti
Ryerson University

Follow this and additional works at: <http://digitalcommons.ryerson.ca/dissertations>

 Part of the [Polymer Science Commons](#)

Recommended Citation

Matti, Basma, "Modeling of Bimolecular Nitroxide Mediated Radical Polymerization of Styrene in Batch Reactor and Steady State Analysis of CSTR Reactor" (2010). *Theses and dissertations*. Paper 1293.

This Thesis is brought to you for free and open access by Digital Commons @ Ryerson. It has been accepted for inclusion in Theses and dissertations by an authorized administrator of Digital Commons @ Ryerson. For more information, please contact bcameron@ryerson.ca.

**MODELING OF BIMOLECULAR NITROXIDE MEDIATED
RADICAL POLYMERIZATION OF STYRENE IN BATCH
REACTOR AND STEADY STATE ANALYSIS OF CSTR
REACTOR**

by

Basma Matti

B.Sc. in Chemical Engineering - University of Technology - Iraq 2001

M.Sc. in Chemical Engineering - University of Technology - Iraq 2005

A thesis presented to

Ryerson University

in partial fulfillment of the requirement

for the degree of

Master of Applied Science

in the program of

Chemical Engineering

Toronto, Ontario, Canada, 2010

© Basma Matti 2010

Author's Declaration

I hereby declare that I am the sole author of this thesis. I authorize Ryerson University to lend this thesis to other institutions or individuals for the purpose of scholarly research.

I further authorize Ryerson University to reproduce this thesis by photocopying or by other means, in total or in part, at the request of other institutions or individuals for the purpose of scholarly research.

Borrower's Page

Ryerson University requires the names and signatures of all persons using or photocopying this thesis. Please sign below and provide address and date.

Modeling of Bimolecular Nitroxide Mediated Radical Polymerization of Styrene in Batch Reactor and Steady State Analysis of CSTR Reactor

Basma Matti, M.A.Sc., Chemical Engineering, Ryerson University, Toronto, 2010

Abstract

Controlled radical polymerization (CRP) is a rapidly developing area in polymer science. Its versatility and ability to produce novel polymer structures are the main reasons which attract both academic and industrial interests. In particular, Nitroxide Mediated Radical Polymerization (NMRP) is currently one of the three popular approaches in CRP. Polymeric materials synthesized by NMRP can be utilized for coatings, adhesives, lubricants, gels, thermoplastic, and also for biomedical applications.

Open literature shows an academic controversy over the kinetic mechanisms of NMRP and also over the kinetic reaction rate parameters. In this study, a kinetic mechanism describing the bimolecular NMRP was thoroughly discussed, reviewed and improved. In fact, two side reactions have been added to the most updated NMRP reaction scheme. Therefore, a kinetic model for a NMRP polymer reactor operating in batch and CSTR modes was developed based on a detailed reaction mechanism for thermal polymerization of styrene and also for bimolecular NMRP of styrene using benzoyl peroxide (BPO) as initiator and 2,2,6,6-tetramethyl-1-piperidinyloxy (TEMPO) as a radical controller. The kinetic model, consisting of a set of ordinary differential equations, was numerically integrated and validated with a set of experimental data obtained at temperature 120°C and [TEMPO]/[BPO] molar ratio 1.1. This model validation was done by means of a parameter estimation scheme to determine the “best” kinetic parameters. The model predictions were compared with data at 120 and 130°C for [TEMPO]/[BPO] molar ratios of 0.9, 1.1, 1.2, and 1.3. A good to very good agreement was obtained between the prediction and data.

The non-linear behavior of the CSTR polymerization reactor was also analyzed using Matlab continuation program Matcont package. Typical hysteresis behavior, input and output multiplicities, as well as disjoint bifurcations were determined for this reactor. The bifurcation

parameters selected are the coolant flow rate, feed stream temperature, residence time, initiator feed stream concentration and controller feed stream concentration. Bifurcation analyses reveal the stable and unstable operating regions of the reaction. Thus, the results obtained can be employed as a guide to develop a process control strategy for a better and safer operation of the NMRP polymerization reactors. Finally, a steady state optimization for the CSTR reactor was carried out in order to identify the optimal operating conditions of the NMRP process.

Acknowledgements

First and foremost I offer my sincerest gratitude to my supervisor, Dr. Ramdhane Dhib, who has supported me throughout my thesis with his patience and knowledge. I attribute the level of my Master's degree to his encouragement and effort and without him this thesis would not have been completed or written. One simply could not wish for a better or friendlier supervisor. I would like to thank NSERC of Canada for their financial support to complete this study. I am very thankful to the faculty members in Chemical Engineering department, and also to the oral examining committee members: Dr. Chil-Hung Cheng, Dr. Ginette Turcotte, and Dr. Daniel Foucher.

I would like to thank Mr. Noel Jacob for his great help and useful advice in programming. I also would like to thank Mr. Tondar Tajrobehkar, Mrs. Caltha Rimmer, and Mrs. Isabella Fernandes for their endless help during the completion of this study. I am grateful to my friends Miss Erlita Mastan, Mr. Ruston Bedasie and Mr. Farshid Sanjabi for their help.

I am thankful and grateful to the whole family especially my parents-in-law for their understanding and their help in taking care of my son during my study. I am grateful to my parents for taking care of me in the first place, for educating me, for their prayers and endless support. I am also thankful to my sisters as well as my sister-in-law for their support. I also would like to thank aunt Neena for her prayers. Words fail to express my appreciation to my husband and my son. Yaser, thank you for letting me live my dream. I was blessed to receive your patience, understanding, encouragement and endless love through the entire process. Raphael, in these two years, I was not always beside you when you wanted to share your happiness, sadness or fears with me. But I always tried to send my love to you through the prayers. Thank you for being patient. You are a great son for me. I'm proud of you, my sun!

Finally, I offer my regards and blessing to all of those who supported me in any respect during the completion of my study. I also want to apologize for not being able to mention them personally one by one. Thank you for your support.

Dedication

To my husband for his unconditional love, endless support, encouragement, understanding and patience in my life as well as during my study.

A special dedication to my lovely son, for his love and patience.

Table of Contents

Author's Declaration.....	iii
Borrower's Page.....	iv
Acknowledgements.....	vii
Dedication	viii
List of Tables	xii
List of Figures	xiii
Chapter 1: Introduction.....	1
Chapter 2: Background and Literature Review.....	3
2.1 What is Controlled Radical Polymerization (CRP)?.....	3
2.2 Classification of Controlled Radical Polymerization Systems	4
2.2.1 Atom Transfer Radical Polymerization (ATRP)	5
2.2.2 Reversible Addition Fragmentation Transfer (RAFT)	5
2.2.3 Nitroxide Mediated Radical Polymerization (NMRP)	6
Chapter 3: Kinetic Models in Batch Reactor	16
3.1 Mechanism and Model of Thermal Polymerization of Styrene	16
3.2 Bimolecular Nitroxide Mediated Radical Polymerization (NMRP) of Styrene	26
3.2.1 Previous Mechanisms and Models of NMRP of Styrene	26

3.2.2	Proposed Kinetic Mechanism for NMRP of Styrene.....	28
3.3	Kinetic Model of Bimolecular NMRP of Styrene in a Batch Reactor	33
3.4	Dimensionless Form of the Bimolecular NMRP of Styrene Kinetic Model in Batch Reactor	37
3.5	Validation of the Bimolecular NMRP of Styrene Model with Data	41
3.5.1	Parameter Estimation	42
3.5.2	Comparison of Model Predictions with Data.....	46
Chapter 4: Bimolecular NMRP of Styrene in CSTR Reactor.....		51
4.1	Literature Review of the Steady State Analysis of the Continuous Stirred Tank Reactor (CSTR) Polymerization Reactors.....	51
4.2	Bimolecular NMRP of Styrene in a CSTR Reactor	53
4.2.1	Continuous Stirred Tank Reactor (CSTR) Design.....	53
4.2.2	Kinetic Model	55
4.3	Dimensionless Form of the Bimolecular NMRP of Styrene Kinetic Model in CSTR	58
4.4	Steady State Bifurcation Analysis.....	63
4.4.1	Numerical Algorithm.....	63
4.5	Result Analysis.....	65
4.5.1	The Effect of Coolant Flow Rate as a Main Bifurcation Parameter	68
4.5.2	The Effect of Feed Stream Temperature as a Main Bifurcation Parameter.....	74
4.5.3	The Effect of Residence Time as a Main Bifurcation Parameter	80

4.5.4 The Effect of Initiator Feed Stream Concentration as a Main Bifurcation Parameter ...	86
4.5.5 The Effect of Controller Feed Stream Concentration as a Main Bifurcation Parameter	92
Chapter 5: Optimal Operating Conditions of CSTR.....	98
5.1 Conversion Maximization.....	100
5.2 Conversion and PDI Optimization	104
5.3 Conversion, PDI and Mw Optimization.....	107
Chapter 6: Conclusions and Recommendations	110
6.1 Concluding Remarks	110
6.2 Recommendations	111
Nomenclature	113
References	119
Appendix A : Molar Balances for Kinetic Model Development	126
Appendix B : Calculating the Heat Transfer Coefficient.....	128
Appendix C : Steady State Bifurcation Plots	131

List of Tables

<u>Table 3.1</u> : Mechanism of thermal polymerization of styrene	18
<u>Table 3.2</u> : Kinetic rate constants for thermal polymerization of styrene	23
<u>Table 3.3</u> : Kinetic mechanism of NMRP of styrene	26
<u>Table 3.4</u> : Kinetic mechanism of bimolecular NMRP of styrene: modified version	31
<u>Table 3.5</u> : Dimensionless variables for batch reactor model	37
<u>Table 3.6</u> : Simplifying expressions in the dimensionless batch reactor model	38
<u>Table 3.7</u> : Kinetic rate constants for bimolecular NMRP of styrene	44
<u>Table 4.1</u> : Reactor dimensions	54
<u>Table 4.2</u> : Dimensionless variables for CSTR	58
<u>Table 4.3</u> : Simplifying expressions in the dimensionless CSTR model	59
<u>Table 4.4</u> : Reactor operating conditions and physical properties	66
<u>Table 4.5</u> : Selection of bifurcation parameters	67
<u>Table 5.1</u> : Optimal operating conditions of NMRP of styrene to maximize conversion	103
<u>Table 5.2</u> : Optimal operating conditions of NMRP of styrene conversion and PDI	106
<u>Table 5.3</u> : Optimal operating conditions of NMRP of styrene conversion, PDI and \overline{M}_w	109

List of Figures

<u>Figure 2.1</u> : A general CRP equilibrium between dormant and active species.....	4
<u>Figure 2.2</u> : Schematic CRP reaction scheme	7
<u>Figure 2.3</u> : Examples of molecular structures attained through CRP.....	8
<u>Figure 2.4</u> : Structures of some nitroxide radicals employed in NMRP	9
<u>Figure 2.5</u> : Bimolecular initiation approach in NMRP.....	10
<u>Figure 2.6</u> : Structures of some alkoxyamines employed in NMRP	11
<u>Figure 2.7</u> : Unimolecular initiation approach in NMRP	11
<u>Figure 3.1</u> : Mechanism of thermal polymerization of styrene.....	17
<u>Figure 3.2</u> : Model predictions of thermal polymerization of styrene at 120°C	24
<u>Figure 3.3</u> : Model predictions of thermal polymerization of styrene at 130°C	25
<u>Figure 3.4</u> : Comparison of model predictions with experimental data.....	28
<u>Figure 3.5</u> : Mechanism for reaction between BPO and TEMPO	29
<u>Figure 3.6</u> : Model predictions (optimal estimates) for ratio [TEMPO]/[BPO]=1.1 and T=120°C	46
<u>Figure 3.7</u> : Model predictions for ratio [TEMPO]/[BPO]=1.2 and T=120°C	47
<u>Figure 3.8</u> : Model predictions for ratio [TEMPO]/[BPO]=0.9 and T=120°C	48
<u>Figure 3.9</u> : Model predictions for ratio [TEMPO]/[BPO]=1.1 and T=130°C	49
<u>Figure 3.10</u> : Model predictions for ratio [TEMPO]/[BPO]=1.3 and T=130°C	49

<u>Figure 4.1</u> : Schematic diagram of a jacketed CSTR	53
<u>Figure 4.2</u> : Bifurcation diagrams with coolant flow rate as the main bifurcation parameter and feed stream temperature as the secondary bifurcation parameter	69
<u>Figure 4.3</u> : Bifurcation diagrams with coolant flow rate as the main bifurcation parameter and residence time as the secondary bifurcation parameter	71
<u>Figure 4.4</u> : Bifurcation diagrams with coolant flow rate as the main bifurcation parameter and ratio $R=[\text{TEMPO}]/[\text{BPO}]$ as the secondary bifurcation parameter	73
<u>Figure 4.5</u> : Bifurcation diagrams with feed stream temperature as the main bifurcation parameter and coolant flow rate as the secondary bifurcation parameter	75
<u>Figure 4.6</u> : Bifurcation diagrams with feed stream temperature as the main bifurcation parameter and residence time as the secondary bifurcation parameter	77
<u>Figure 4.7</u> : Bifurcation diagrams with feed stream temperature as the main bifurcation parameter and ratio $R=[\text{TEMPO}]/[\text{BPO}]$ as the secondary bifurcation parameter	79
<u>Figure 4.8</u> : Bifurcation diagrams with residence time as the main bifurcation parameter and feed stream temperature as the secondary bifurcation parameter	81
<u>Figure 4.9</u> : Bifurcation diagrams with residence time as the main bifurcation parameter and coolant flow rate as the secondary bifurcation parameter	83
<u>Figure 4.10</u> : Bifurcation diagrams with residence time as the main bifurcation parameter and $[\text{TEMPO}]/[\text{BPO}]$ ratio as the secondary bifurcation parameter	85
<u>Figure 4.11</u> : Bifurcation diagrams with initiator feed stream concentration as the main bifurcation parameter and feed stream temperature as the secondary bifurcation parameter	87

<u>Figure 4.12</u> : Bifurcation diagrams with initiator feed stream concentration as the main bifurcation parameter and coolant flow rate as the secondary bifurcation parameter...	89
<u>Figure 4.13</u> : Bifurcation diagrams with initiator feed stream concentration as the main bifurcation parameter and residence time as the secondary bifurcation parameter.....	91
<u>Figure 4.14</u> : Bifurcation diagrams with TEMPO feed stream concentration as the main bifurcation parameter and feed stream temperature as the secondary bifurcation parameter	93
<u>Figure 4.15</u> : Bifurcation diagrams with TEMPO feed stream concentration as the main bifurcation parameter and coolant flow rate as the secondary bifurcation parameter...	95
<u>Figure 4.16</u> : Bifurcation diagrams with TEMPO feed stream concentration as the main bifurcation parameter and residence time as the secondary bifurcation parameter.....	97
<u>Figure C.1</u> : Bifurcation diagrams with feed stream temperature as the main bifurcation parameter and coolant flow rate as the secondary bifurcation parameter	132
<u>Figure C.2</u> : Bifurcation diagrams with feed stream temperature as the main bifurcation parameter and residence time as the secondary bifurcation parameter	133

Chapter 1: Introduction

In the last two decades, significant advances have been made in the field of controlled/ living free radical polymerization (CRP). Free radical polymerization is widely employed in industry and academia. There exist three techniques of CRP: atom transfer radical polymerization (ATRP), reversible addition fragmentation chain transfer (RAFT), and Nitroxide Mediated Radical Polymerization (NMRP). These techniques provide polymers with narrow molecular weight distributions and low polydispersities. CRP techniques can be used to polymerize complete monomer families, such as styrene, (meth)acrylates, acrylamides, acrylonitriles, dienes, and vinylpyridines (Fukuda et al., 2000).

Nitroxide Mediated Radical Polymerization (NMRP) is the least sensitive to impurities in comparison with the other two mentioned techniques. There are two NMRP techniques: unimolecular NMRP and bimolecular NMRP. The first one uses unimolecular initiators such as alkoxyamines which decompose into primary radicals that initiate the polymerization and nitroxide radicals that act as a controller. The second uses a conventional initiator that generates primary radicals and stable free nitroxide radicals as controllers. Polymeric materials synthesized by NMRP can be used for coatings, adhesives, surfactants, dispersants, lubricants, gels, additives and thermoplastic elastomers, as well as for biomedical applications (Greszta and Matyjaszewski, 1996).

The focus of this study was to investigate the kinetic mechanism and develop a kinetic model for bimolecular NMRP of styrene using benzoyl peroxide (BPO) as a conventional initiator and nitroxide stable free radical 2,2,6,6-tetramethyl-1-piperidinyloxy (TEMPO) as the controller. The main objectives of this study included the following points:

- Develop a kinetic mechanism for the bimolecular NMRP of styrene and update the corresponding kinetic rate constants.
- Develop a mathematical model which is experimentally verifiable.

- Investigate the non-linear bifurcation analysis of styrene bimolecular NMRP in a continuous stirred tank reactor (CSTR).
- Determine optimal operating conditions of NMRP of styrene in CSTR reactor.

Chapter 2 provides a background and reviews past studies done on controlled radical polymerization (CRP). Literature on NMRP is extensive. In Chapter 3, a mathematical model is developed based on a detailed reaction mechanism for thermal polymerization of styrene as well as bimolecular NMRP of styrene. In this work, two side reactions were proposed for the NMRP mechanism. Parameter estimation and simulation runs were done for two kinetic models.

A review of previous bifurcation studies is covered in Chapter 4. Detailed analysis of the steady state bifurcation behavior of the CSTR kinetic models of the bimolecular NMRP of styrene was performed using Matlab continuation program Matcont package. Typical hysteresis behaviors, input and output multiplicities, as well as disjoint bifurcations were determined for this reactor. The bifurcation parameters selected were the coolant flow rate, feed stream temperature, residence time, initiator feed stream concentration and controller feed stream concentration.

In Chapter 5, an optimization technique was carried out in order to determine the optimal operating conditions of the CSTR polymer reactor. Few objective functions were selected to maximize the monomer conversion and the weight average molecular weight, and to also minimize the polydispersity index, coolant flow rate and residence time. All the optimal results satisfied the constraints. Chapter 6 summarizes the main concluding remarks along with recommendations for future work.

Chapter 2: Background and Literature Review

This chapter gives a review of past studies on controlled radical polymerization (CRP) with extensive details on nitroxide mediated radical polymerization (NMRP).

2.1 What is Controlled Radical Polymerization (CRP)?

Controlled Radical Polymerization (CRP) has proved to be a procedure to prepare organic polymers with low polydispersities and polymeric architecture under mild conditions from 120 to 140°C, with moderate requirements for purification of monomers and solvents (Boutevin and Bertin, 1999; Fukuda et al., 2000).

In the past few decades, few techniques have been developed to synthesize well defined polymers via controlled radical polymerization. A common feature of the variant CRP's is the existence of equilibrium between active free radicals and dormant species. The exchange between active radicals and dormant species allows slow but simultaneous growth of all chains while keeping the concentration of radicals low enough to minimize termination (Otsu and Yoshida, 1982; Fukuda et al., 2000).

The core reaction in CRP systems is shown in Figure 2.1. The dormant species R_n-X undergoes homolytic bond breakage, either by heating or by a more complex process of activation caused by an added reagent. The reaction produces one active and one stable free radicals. The activation and deactivation rate constants are represented by k_a and k_d , respectively. In the presence of monomer M , the active radical R_n^{\bullet} propagates. The corresponding propagating radical can either be deactivated by the stable radical X^{\bullet} or it can terminate with other growing radicals (Fukuda et al., 2000).

There are three prerequisites that should be satisfied in order to achieve controlled conditions,

- Fast and quantitative initiation compared to propagation;
- Small contribution of chain breaking reactions like termination and transfer reactions;
- Fast exchange between active and dormant species.

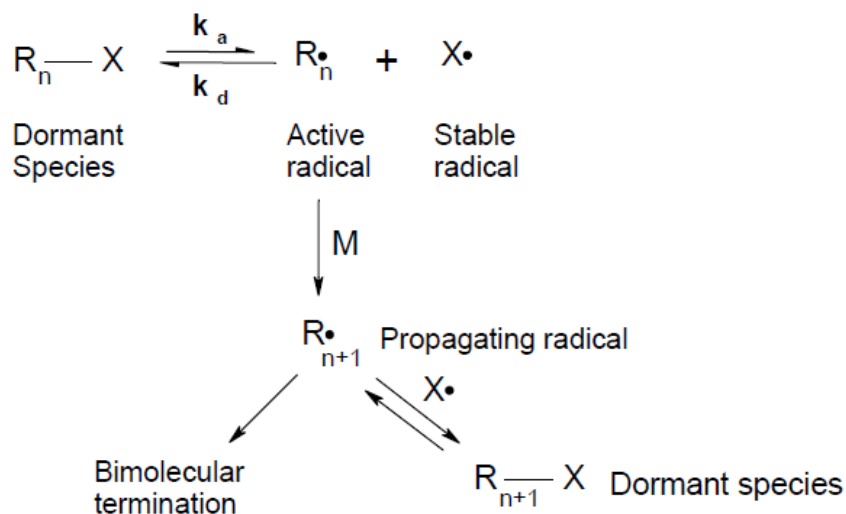


Figure 2.1: A general CRP equilibrium between dormant and active species (Fukuda et al., 2000)

A major difference between conventional radical and controlled radical polymerizations (CRP) is the lifetime of the propagating radicals during the course of the reaction. In conventional free radical polymerizations, radicals generated by decomposition of the initiator undergo propagation and bimolecular termination reactions within a short time. In contrast, the lifetime of a growing radical can be extended to several hours in a CRP, enabling the preparation of polymers with predefined molar masses, low polydispersity, controlled compositions, and functionality (Pyun and Matyjaszewski, 2001). Unlike conventional radical processes, CRP requires the use of persistent radical (deactivator) species, or highly active transfer agents to react with propagating radicals. These persistent radicals/transfer agents react with radicals to form the dormant species. Conversely, propagating radicals are generated from the dormant species by an activation reaction.

2.2 Classification of Controlled Radical Polymerization Systems

There are few approaches which have been proposed to put light on controlled radical polymerization, and presume some sort of dynamic equilibrium between the growing free radicals and various types of dormant species. The equilibrium exchange process is at the core of the CRP methods and can be approached in different ways depending on the structure of the

dormant and deactivating species, the presence of a catalyst and the particular kinetic mechanism of the exchange.

In fact, currently three methods appear to be the most efficient and could lead to commercial applications:

- Atom Transfer Radical Polymerization (ATRP)
- Reversible Addition Fragmentation Transfer (RAFT)
- Nitroxide Mediated Radical Polymerization (NMRP)

2.2.1 Atom Transfer Radical Polymerization (ATRP)

The technical literature on ATRP has been growing very rapidly ever since the first successful study on atom transfer radical addition (ATRA) proposed by Wang and Matyjaszewski (1995).

The radical generation in ATRP involves an organic halide undergoing a reversible redox process catalyzed by a transition metal compound such as $\text{Cu}^{(\text{I})}$, $\text{Ru}^{(\text{II})}$, $\text{Mo}^{(0)}$, $\text{Fe}^{(\text{II})}$ and a halogen atom playing a similar role as TEMPO in NMRP (further clarification about NMRP can be found in section 2.2.3).

Most of the ATRP initiators use either chlorides or bromides, and some investigators have used iodine as the halogen atom in the initiator (Wang and Matyjaszewski, 1995).

2.2.2 Reversible Addition Fragmentation Transfer (RAFT)

As reported by Chiefari et al. (1998), Reversible Addition Fragmentation Transfer (RAFT) polymerization controls chain growth through reversible chain transfer. It involves the reaction of polymeric radical species (R_m^\bullet, R_n^\bullet) that transfers reversibly the capping group (or chain transfer agent X) back and forth:



Where K_{exch} is the equilibrium rate constant. The structures of R_m-X and R_n-X are essentially assumed identical, except that the number of monomer repeat units present may be different. The RAFT polymerization involves a conventional radical initiator like peroxide or azobisisobutyronitrile, and a chain transfer agent X which contains a dithioester, dithiocarbamate, trithiocarbonate or xanthate moiety. The key to the success of RAFT polymerizations lies in the high reactivity of the thiocarbonyl group towards propagating radicals (Chiefari et al., 1998; Moad et al., 2005).

2.2.3 Nitroxide Mediated Radical Polymerization (NMRP)

Nitroxide mediated radical polymerization is a polymerization technique that provides high molecular weight polymers with low polydispersities and molecular weights increasing linearly with conversion. The basic molecular control principle consists of introducing in the reacting system a species like a nitroxide stable radical, that is able to reversibly trap the propagating chains by capping the active radical species. The trapping reaction is given by Eq. 2.2 as follows (Butte et al., 1999):



Where R_n^\bullet represents the propagating (or active) radical, X^\bullet represents the nitroxide stable radical and $R_n - X$ represents the trapped (or dormant) species; k_a is the activation rate constant (forward reaction) and k_d is the deactivation rate constant. The reaction equilibrium is shifted strongly to the left side. The concentration of the active species is lower in the NMRP in comparison with conventional free radical polymerization. At low temperatures (between 40 to 60°C), the dormant species is stable and therefore the nitroxide group behaves as an inhibitor (Moad et al., 1981). However, at elevated temperatures between 100 and 140°C, the dormant chain can undergo homolytic cleavage (dissociation) leading to a polymer radical and nitroxide group (Georges et al., 1993). The polymer radical can grow, terminate or couple with the nitroxide group again to form a dormant species.

The dissociation mechanism of $R_n - X$ is still not well understood. Shown in Figure 2.2 is the scheme proposed by Fischer (2001) who considered a reactant system with both monomer M and initiating adduct $R_n - X$ at time $t = 0$. According to this reaction concept, the dissociation of $R_n - X$ can start the polymerization. This scheme was re-used by Mesa et al. (2005). It was assumed that the same quantity of R_n^\bullet and X^\bullet was produced per unit time. At first, concentrations of $[R_n^\bullet]$ and $[X^\bullet]$ increase linearly with time. Once $[R_n^\bullet]$ and $[X^\bullet]$ reach a certain level, bimolecular termination among the active radicals R_n^\bullet and the reaction between R_n^\bullet and X^\bullet became significant, as shown in Figure 2.2.

As the termination of R_n^\bullet results in a decrease of $[R_n^\bullet]$ relative to $[X^\bullet]$, so $[X^\bullet]$ steadily increases, and therefore the reaction between R_n^\bullet and X^\bullet becomes more and more important, thus reversing the formation of $R_n - X$. This eventually leads to a balance between the rate of deactivation, $k_d[R_n^\bullet][X^\bullet]$, and that of activation, $k_a[R_n - X]$ (quasi equilibrium condition will hold). Furthermore, while the quasi equilibrium condition holds, $[R_n^\bullet]$ must be a decreasing function of time and termination continues to occur. The concentration of $[R_n^\bullet]$ passes through a maximum and will start to decrease.

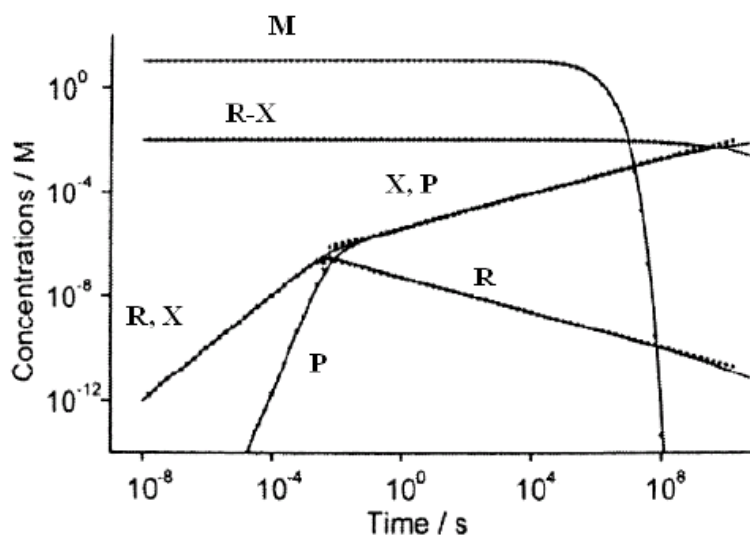


Figure 2.2: Schematic CRP reaction scheme (Fischer, 2001)

This trend has been termed the persistent radical effect (PRE), which is widely accepted nomenclature in describing the kinetics of ATRP and NMRP. This kinetic scheme of $R_n - X$ dissociation will help to understand the dormant living exchange reactions in Table 3.4.

2.2.3.1 Types of Nitroxide Mediated Radical Polymerization (NMRP)

The main reason behind the success of the NMRP can be related to the ability of stable nitroxide free radicals (such as TEMPO) to react with the carbon-centered free radical of the growing polymer chain end in a thermally reversible process. This reaction tends to lower the concentration of free radicals in the polymerization system (Pyun and Matyjaszewski, 2001). Furthermore, the nitroxide free radicals hold back to initiate new chain growth which sustains the controlled polymerization. The polymer structures obtainable via CRP are presented in Figure 2.3.

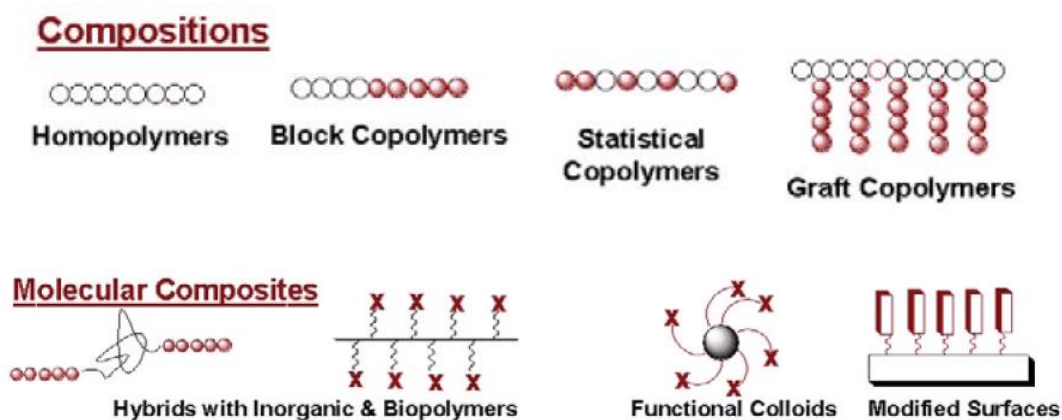


Figure 2.3: Examples of molecular structures attained through CRP (Pyun and Matyjaszewski, 2001)

Basically, Nitroxide Mediated Radical Polymerization (NMRP) depends on the type of initiator used to initiate the polymerization as described next.

A. Bimolecular initiator

First, according to studies on CRP (Georges et al., 1994; Boutevin and Bertin, 1999; Fukuda et al., 2000; Hawker et al., 2001), the nitroxide stable radical can have different active structures, some of which are shown in Figure 2.4.

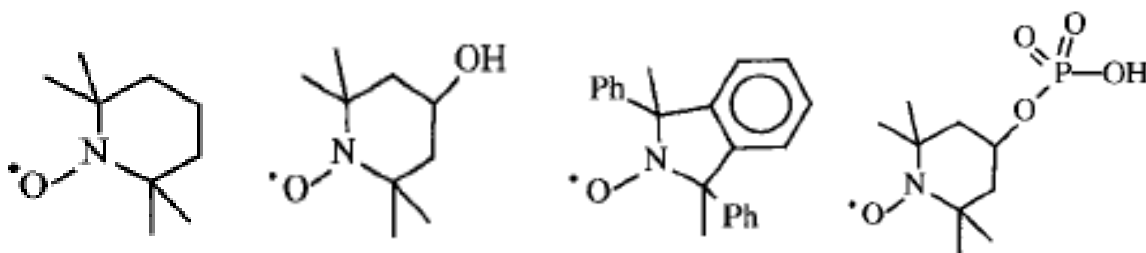


Figure 2.4: Structures of some nitroxide radicals employed in NMRP (Georges et al., 1994; Hawker et al., 2001)

Bimolecular NMRP, which is demonstrated to a wide audience, is conducted with any of these nitroxide stable radicals along with a conventional initiator such as benzoyl peroxide (BPO) or azobisisobutyronitrile (AIBN). This approach was first introduced by Georges et al. (1993) at XEROX (Mississauga, Canada) describing the preparation of low polydispersity polystyrene. The key feature of their work was the production of high molecular weight and low polydispersity materials. It was proved that nitroxides can behave as polymerization inhibitors at low temperatures (less than 100°C) and they can behave as polymerization mediators at elevated temperatures (higher than 100°C).

In this thesis, benzoyl peroxide (BPO) was selected as the initiator and 2,2,6,6-tetramethyl-1-piperidinyloxy (TEMPO) as the radical controller, which is the first radical in the left hand side in Figure 2.4. Under the polymerization conditions, the initiator (BPO) decomposes into primary radicals of high reactivity which initiate the polymerization of monomer. The TEMPO radical then makes a labile bond (C–O) with the radical chain, leading to the formation of alkoxyamines in situ. The C–O bond is weak enough to reversibly dissociate at temperature greater than 100°C, thus establishing the activation-deactivation equilibrium between dormant and active chains as shown in Figure 2.5.

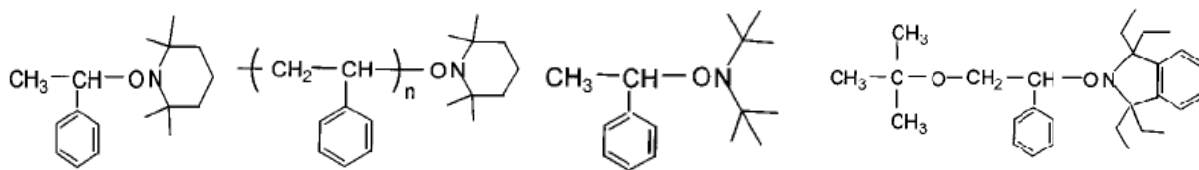


Figure 2.6: Structures of some alkoxyamines employed in NMRP (Fukuda et al., 2000)

The C-O bond of the small molecule alkoxyamine derivative is therefore expected to be thermolytically unstable and decompose on heating to give an initiating radical, (i.e., the R-methylbenzyl radical) as well as the mediating nitroxide radical. Following initiation, the polymerization would proceed as previously described for the bimolecular case to give the polystyrene derivative according to the reaction scheme in Figure 2.7.

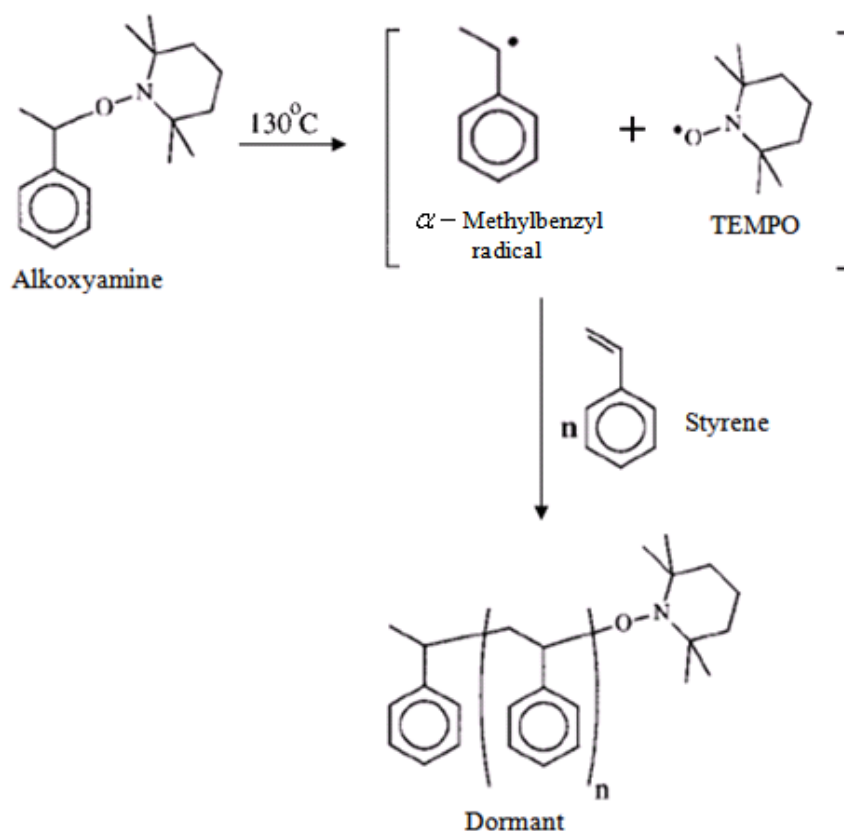


Figure 2.7: Unimolecular initiation approach in NMRP (Hawker et al., 2001)

2.2.3.2 Past Studies on Nitroxide Mediated Radical Polymerization (NMRP)

The literature on the NMRP process is extensive and growing. Several research groups have proposed new synthesis routes and have used new nitroxides and/or alkoxyamines. Moad et al. (1981, 1982) did pioneer work on NMRP. They established their work using nitroxides such as 2, 2, 6, 6-tetramethylpiperidinyloxy (TEMPO) react at near diffusion controlled rates with carbon-centered free radicals at low temperatures (40-60°C). The resulting alkoxyamine derivatives were essentially stable at these temperatures and did not participate in the reaction any further, thus acting as radical traps. Also, Solomon et al. (1986) applied a similar concept at higher temperature (80-100°C) to synthesize low molecular weight oligomers, primarily with acrylates and nitroxides such as TEMPO. The polymerization led to the production of poorly defined materials with uncontrolled molecular weights and high polydispersities.

In a procedure similar to Georges et al. (1993), Veregin et al. (1993) focused on the first step of the bimolecular NMRP which is the “promoted dissociation reaction”. They reported a rapid reaction between TEMPO and BPO compared to BPO thermal decomposition.

Later, Greszta and Matyjaszewski (1996) proposed a kinetic model validated with data for the TEMPO-mediated polymerization of styrene at 120°C. They showed the necessity to include thermal polymerization of styrene, transfer, and irreversible decomposition of intermediate alkoxyamines in addition to the reversible cleavage of the TEMPO-polymeric radical adduct.

In parallel, Fukuda et al. (1996) studied the unimolecular bulk polymerization of styrene at 125°C. Their results were consistent with the proposed kinetic scheme where it was assumed the existence of a stationary state with respect to both polymeric and nitroxyl radical concentrations. They also showed that in order for the “living” radical polymerization mediated by a stable nitroxyl radical (SNR) to proceed successfully, a constant supply of initiating radicals (by e.g. thermal polymerization) was essential as well as the frequent reversible combination of polymeric and nitroxyl radicals. The total number of initiating radicals to be supplied in this way may be small compared with the number of polymer-SNR adducts so that they have no important influence on the molecular weight and its distribution of the product.

Connolly and Scaiano (1997) discussed that stable radical TEMPO reacted with styrene and polystyrene under conditions typically used for polymerization. Consequently, the nitroxide is not inert at elevated temperature.

Boutevin and Bertin (1999) studied the thermal polymerization of styrene in the presence of TEMPO at 120°C. At the end of the bulk polymerizations, the concentration of macromolecular chains was high. The main conclusion was that not all macromolecular chains are controlled by nitroxide radicals. The presence of TEMPO in a thermal polymerization of styrene was shown to have an influence on the rate of the radicals formation generated by Diels-Alder reaction: a transfer reaction of TEMPO to the dimer of styrene was confirmed through kinetic studies. The rate of radicals formation was proportional to the TEMPO concentration.

Butte et al. (1999) developed a mathematical model suitable for handling both processes (ATRP and NMRP). The performance of their model was compared with experimental data.

Also, the mechanisms and kinetics of several variants of living radical polymerization were discussed in the work of Fukuda et al. (2000) on the basis of experimental data and theoretical results. The focus was on two main issues, the polymerization rate and the activation rate constant. The authors reported that, because of bimolecular termination, which is inevitable in LRP as well as in conventional radical polymerization, the time-conversion curves of LRP exhibit some characteristic features depending on the experimental conditions, such as the presence or absence of conventional initiation. Despite the presence of termination (and initiation, in some cases), polymers obtained by LRP can have a low polydispersity, provided that the number of terminated chains is small compared to the number of potentially active chains. A large rate constant of activation is another fundamental requisite for low polydispersities.

A thorough chemistry description of bimolecular and unimolecular NMRP has been reported by Hawker et al. (2001). They discussed the development of a variety of TEMPO-based unimolecular initiators to examine the effects of structural variation on the efficiency and usefulness of these derivatives as unimolecular initiators. They also discussed the synthesis of complex macromolecular architectures like star, hyperbranched and dendritic polymers as well as block and graft copolymers. Also, Zhang and Ray (2002) reported a kinetic mechanism for

living radical polymerization and a comprehensive model, which was validated using experimental data for both NMRP and ATRP.

Bonilla et al. (2002) presented a kinetic model based on a detailed general reaction mechanism for the nitroxide mediated radical polymerization (NMRP) of styrene. The model was validated using experimental data. Non-linear estimation procedure was used to estimate the unknown kinetic rate constants.

Later, an experimental work done by Schulte et al. (2004) discussed the effect of the variation of the alkoxyamine concentration on the conversion and polydispersity of the NMRP of styrene. Four different types of alkoxyamines were used. In addition, simulations for the nonlinear dynamics were discussed. In their study they concluded that at high alkoxyamine concentrations, the conversions vary to a small extent for all the types of alkoxyamines they studied; as long as the conversion remains high, the polydispersity index remains small.

On one hand, Saldivar-Guerra et al. (2006) discussed the kinetic mechanism of the induction period and the initial polymerization stages in the nitroxide mediated autopolymerization of styrene at 120-125°C. On the other hand, Pfaendner (2006) discussed the benefits of using nitroxyl derivatives in polymerization and grafting processes.

An experimental study on bimolecular NMRP of styrene at 120 and 130°C using TEMPO and BPO with molar ratios of 0.9 to 1.5 was carried out by Roa-Luna et al. (2007). However, comparison of their experimental data with predictions of a kinetic model previously reported in literature (Bonilla et al., 2002) shows a model discrepancy which reflects either a poor understanding of the reaction mechanism or a low accuracy of the kinetic rate constants.

Belincanta-Ximenes et al. (2007) proposed a study on simulation of polymerization rate, molecular weight development and evaluation of the concentration of species participating in the NMRP reaction mechanism of styrene over a range of operating conditions.

Nabifar et al. (2008) presented a comprehensive experimental investigation of nitroxide mediated radical polymerization (NMRP) of styrene using TEMPO as the controller. Polymerization with BPO was carried out at 120 and 130°C, with TEMPO/BPO molar ratios ranging from 0.9 to 1.5. The results of their study indicate that increasing temperature favors the rate of polymerization

and slightly decreases the molecular weights. It was also observed that increasing the ratio of TEMPO/BPO lowered both the rate of polymerization and molecular weights.

Based on the literature survey done, the kinetic mechanism of NMRP is not well understood. Therefore, there exists a large variation in the published NMRP mechanisms, which inherently resulted in large variations in the reaction rate constants. Thus, the mathematical models previously developed in these studies cannot predict all the experimental data. Therefore, the scope of this study addresses these issues. It reviews the most common mechanisms and proposes a modification. In fact, the thesis proposes a new kinetic model based on the reaction mechanism proposed. Parameter estimation has been conducted for model validation and also a steady-state analysis has been done to determine the operating range of a CSTR reactor. Finally, an optimization strategy was also conducted to determine the optimal operating conditions of the reactor.

Chapter 3: Kinetic Models in Batch Reactor

First, the kinetic mechanism and the related model of thermal polymerization of styrene are discussed. Then, the second part of the chapter discusses the various kinetic mechanisms and models of bimolecular Nitroxide Mediated Radical Polymerization (NMRP) of styrene in a batch reactor.

3.1 Mechanism and Model of Thermal Polymerization of Styrene

It is well known that styrene exhibits thermal polymerization at temperatures over 100°C (Mayo, 1968; Hui and Hamielec, 1972; Almeida et al., 2008). Similarly, Nitroxide Mediated Radical Polymerization (NMRP) of styrene is typically conducted at temperatures higher than 100°C (Nabifar et al., 2009). Thermal polymerization may help maintain a reasonable reaction rate as it generates continuously radicals to compensate for loss of radicals due to termination reactions. Also, radicals produced through styrene self initiation can be captured by added nitroxides to give unimolecular initiators.

Several researchers have studied the phenomenon of thermal polymerization of styrene. Flory (1937) was the first who suggested that this polymerization might be initiated by the combination of two molecules of styrene to produce a diradical. However, further statistical analysis indicated that these diradicals react very fast in order to start a polymerization.

Preliminary studies on thermal polymerization of styrene were extensively conducted and the occurrence of styrene thermal polymerization was proved according to the Mayo mechanism as in Figure 3.1 (Mayo, 1968). The first stage of the mechanism is a reaction between two styrene molecules M to form a Diels-Alder adduct D . This reaction is a dimerization, followed by reaction of D with a styrene molecule M to form two benzylic radicals D^\bullet and M^\bullet , that can add to a monomer to initiate the polymerization.

When discussing the polymerization kinetics of styrene, it is obvious to mention the kinetic model of the thermal polymerization proposed by Hui and Hamielec (1972). In their article, the authors did an experimental study of thermal polymerization of styrene at temperatures from 100

to 200°C. They also established kinetic constants of the reaction, considering that all the reaction rate constants are independent of the size of the polymer chain, but may vary with conversion.

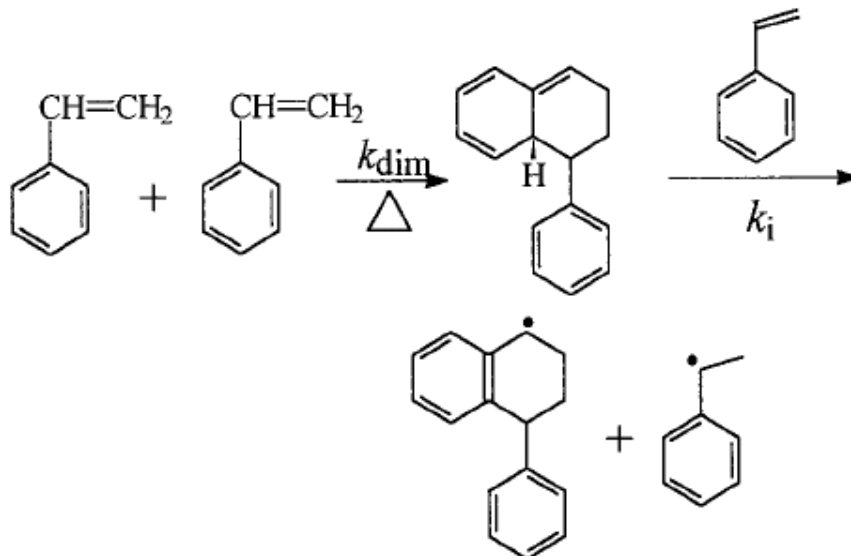


Figure 3.1: Mechanism of thermal polymerization of styrene (Mayo, 1968)

Since styrene thermal polymerization plays an important role in NMRP of styrene, it is worthwhile to have a good idea about the behavior of the polymerization without initiator (BPO) and nitroxide mediating agent (TEMPO). Nabifar et al. (2009) conducted an experimental study on styrene polymerization at 120 and 130°C with no BPO and no TEMPO. Their data have been used in validating the model of thermal polymerization of styrene in this study.

Table 3.1 shows the mechanism of thermal polymerization of styrene with three main steps: initiation, propagation and termination. In accordance with the mechanism proposed by Mayo (1968), the initiation reaction leads to the first polymeric unit R_1^\bullet which will initiate the polymerization. In the propagation step, the monomer M , adds to the primary radical R_n^\bullet and results in a live polymeric radicals with chain length $r+1$. Finally, the termination step is obtained by a combination reaction of two live polymer radicals. It can also be achieved through two transfer reactions.

Table 3.1: Mechanism of thermal polymerization of styrene

Step	Description
Thermal Initiation	
$M + M \xrightarrow{k_{dim}} D$	Mayo dimerization
$M + D \xrightarrow{k_{ia}} D^\bullet + M^\bullet$	Thermal initiation
$M^\bullet + M \xrightarrow{k_{p1}} R_1^\bullet$	Thermal initiation
$D^\bullet + M \xrightarrow{k_{p1}} R_1^\bullet$	Thermal initiation
Propagation	
$R_r^\bullet + M \xrightarrow{k_p} R_{r+1}^\bullet$	$r \geq 1$
Termination and chain transfer agent	
$R_r^\bullet + R_s^\bullet \xrightarrow{k_t} P_{r+s}$	Termination by combination
$R_r^\bullet + M \xrightarrow{k_{fM}} P_r + M^\bullet$	Transfer to monomer
$R_r^\bullet + D \xrightarrow{k_{fD}} P_r + D^\bullet$	Transfer to dimer

Referring to Table 3.1, the symbols M, D, R_r^\bullet and P_r represent the monomer (styrene), the dimer, the temporary polymer radical and the dead polymer radical, respectively. All other symbols defined in Table 3.1 are reported in the nomenclature.

A kinetic model is obtained by means of molar balance. Therefore, performing a molar balance of the reaction species M, D, M^\bullet and D^\bullet leads to the set of differential equations given below, respectively:

$$\frac{d[M]}{dt} = -2k_{\text{dim}}[M]^2 - k_{ia}[M][D] - k_{p1}[M]([D^\bullet] + [M^\bullet]) - k_p[M][\lambda_0] - k_{fM}[M][\lambda_0] \quad (3.1)$$

$$\frac{d[D]}{dt} = +k_{\text{dim}}[M]^2 - k_{ia}[D][M] - k_{fD}[\lambda_0][D] \quad (3.2)$$

$$\frac{d[M^\bullet]}{dt} = +k_{ia}[M][D] - k_{p1}[M][M^\bullet] + k_{fM}[M][\lambda_0] \quad (3.3)$$

$$\frac{d[D^\bullet]}{dt} = +k_{ia}[M][D] - k_{p1}[M][D^\bullet] + k_{fD}[D][\lambda_0] \quad (3.4)$$

The symbols k 's represent the kinetic rate constants, and any symbol in [] represent the species concentration.

where λ_0 is the total concentration of all live polymer radicals and it is theoretically given by:

$$\lambda_0 = \sum_{r=1}^{\infty} R_r^\bullet \quad (3.5)$$

Since the polymer chains do not have the same molecular weight. A statistical distribution is usually developed based on the concepts of moments. The moments are defined as below for the live and dead polymer chains, respectively (Dhib et al., 2000):

$$\lambda_i = \sum_{r=0}^{\infty} r^i R_r^\bullet \quad (3.6)$$

$$\mu_i = \sum_{r=0}^{\infty} r^i P_r \quad (3.7)$$

Where $i=0$, $i=1$, and $i=2$ denote the zeroth, first, and second moment, respectively.

Hence, doing a molar balance of the live polymer radicals gives the differential equations model below:

$$\frac{d(\lambda_0)}{dt} = +k_{p1}[M]([M^\bullet] + [D^\bullet]) - k_t[\lambda_0]^2 - k_{fM}[\lambda_0][M] - k_{fD}[D][\lambda_0] \quad (3.8)$$

$$\frac{d(\lambda_1)}{dt} = +k_{p1}[M]([M^\bullet] + [D^\bullet]) + k_p[M][\lambda_0] - k_t[\lambda_0][\lambda_1] - k_{fM}[\lambda_1][M] - k_{fD}[D][\lambda_1] \quad (3.9)$$

$$\begin{aligned} \frac{d(\lambda_2)}{dt} = & +k_{p1}[M]([M^\bullet] + [D^\bullet]) + k_p[M](\lambda_0 + 2[\lambda_1]) - k_t[\lambda_0][\lambda_2] - k_{fM}[\lambda_2][M] \\ & - k_{fD}[D][\lambda_2] \end{aligned} \quad (3.10)$$

$$\frac{d(\mu_0)}{dt} = +\frac{1}{2}k_t[\lambda_0]^2 + k_{fM}[\lambda_0][M] + k_{fD}[\lambda_0][D] \quad (3.11)$$

$$\frac{d(\mu_1)}{dt} = +k_t[\lambda_0][\lambda_1] + k_{fM}[\lambda_1][M] + k_{fD}[\lambda_1][D] \quad (3.12)$$

$$\frac{d(\mu_2)}{dt} = +k_t([\lambda_0][\lambda_2] + [\lambda_1]^2) + k_{fM}[\lambda_2][M] + k_{fD}[\lambda_2][D] \quad (3.13)$$

Based on the moments of the polymer populations, the number and weight average molecular weights are given, respectively, by:

$$\overline{Mn} = MW_M \left(\frac{\mu_1 + \lambda_1}{\mu_0 + \lambda_0} \right) \quad (3.14)$$

$$\overline{Mw} = MW_M \left(\frac{\mu_2 + \lambda_2}{\mu_1 + \lambda_1} \right) \quad (3.15)$$

where MW_M is the monomer molecular weight.

Since the live radicals are short lived, let assume a steady state hypothesis for polymer live radicals, therefore Eq. (3.8) becomes:

$$k_{p1}[M]([M^\bullet] + [D^\bullet]) - k_t[\lambda_0]^2 - k_{fM}[\lambda_0][M] - k_{fD}[D][\lambda_0] = 0 \quad (3.16)$$

Solving for λ_0 gives:

$$\lambda_0 = \frac{1}{2} \sqrt{\frac{(k_{fM}[M] + k_{fD}[D])^2}{k_t^2} + \frac{4k_{p1}[M]([M^\bullet] + [D^\bullet])}{k_t}} - \frac{k_{fM}[M] + k_{fD}[D]}{k_t}} \quad (3.17)$$

The rate of polymerization is defined by:

$$R_p = k_p[M][\lambda_0] \quad (3.18)$$

Equation (3.17) helps to easily express the rate of polymerization R_p . However, we can still keep equations (3.9) and (3.10) in transient form or put them in steady-state form. It will not make any difference. Integration of the model above requires values of the kinetic parameters and also an initial value of each species.

All the kinetic rate constants are written according to Arrhenius equation (Avery, 1974); the symbols A and E are the kinetic parameters in the Arrhenius equation.

$$k = A \exp(-E/RT) \quad (3.19)$$

Parameter Estimation and Simulation for Thermal polymerization of Styrene

In this part, literature provides information to verify the kinetic rates to be used in the model of this study. Also, an important point has been noticed that which k_p may not have the same numerical value in the thermal initiation step and propagation step. Therefore, it is represented by k_{p1} in the thermal initiation step as in Table 3.1. The parameters ($k_{dim}, k_{ia}, k_{p1}, k_{fM}, k_{fD}$) were adjusted in order to validate the model using experimental data from literature (Nabifar et al.,

2009) for thermal polymerization of styrene at 120°C. The parameter estimation was done according to the objective function below:

$$\min_z J(z) = \sum_{i=1}^N [w_1(C_{mi}(t, z)/C_{di} - 1)^2 + w_2(\overline{Mw}_{mi}(t, z)/\overline{Mw}_{di} - 1)^2 + w_3(\overline{Mn}_{mi}(t, z)/\overline{Mn}_{di} - 1)^2] \quad (3.20)$$

subject to:

$$\text{The model Eqs. (3.1) to (3.4), Eqs. (3.8) to (3.13), and Eq. (3.17).} \quad (3.21)$$

$$\text{where } z = [A_{\text{dim}}, E_{\text{dim}}, A_{ia}, E_{ia}, A_{p1}, E_{p1}, A_{fM}, E_{fM}, A_{fD}, E_{fD}]^T \quad (3.22)$$

Here C_{mi} represents the theoretical monomer conversion, C_{di} is the experimental data of the monomer conversion, \overline{Mw}_{mi} represents the theoretical weight average molecular weight, \overline{Mw}_{di} is the experimental data of weight average molecular weight. \overline{Mn}_{mi} represents the theoretical number average molecular weight, \overline{Mn}_{di} is the experimental data of number average molecular weight. Finally, w_1 , w_2 , and w_3 denote weight factors used to bring the conversion, the weight average molecular weight, and number average molecular weight to the same scale. In this case, $w_1 = w_2 = w_3 = 1$ since conversion, weight average molecular weight, and number average molecular weight are scaled to be equally important.

The Matlab optimization tool box was employed to solve the constrained optimization problem (3.20) and (3.21). On solving this problem, we got the optimal values of kinetic parameters z^* as defined in Eq. (3.22). These optimal values are given in the fourth column of Table 3.2.

Figure 3.2 show the model predictions with experimental data for thermal polymerization of styrene at 120°C. It is clear that the monomer conversion prediction demonstrate a very good agreement with data, whereas the number and weight average molecular weight model predictions show fairly good match with experimental data. The parameters determined in the previous run at 120°C were used in the model to test the model predictions with the experimental data at 130°C (Nabifar et al., 2009). In fact, plots in Figure 3.3 demonstrate a very good prediction of the conversion and moderate prediction of the number and weight average molecular weights of the polymer.

Table 3.2: Kinetic rate constants for thermal polymerization of styrene

Variable	Kinetic rate expressions	Reference	Kinetic rate expressions	Reference
k_{dim} $L .mol^{-1} min^{-1}$	$1.134 \times 10^4 \exp\left(-\frac{16185.1}{RT}\right)$	Belincanta -Ximenes et al.,2007	$944.85 \exp\left(-\frac{2.0231 \times 10^4}{RT}\right)$	This study $L .mol^{-1} min^{-1}$
k_{ia} $L .mol^{-1} min^{-1}$	$3.815 \times 10^{14} \exp\left(-\frac{36598.55}{RT}\right)$	Belincanta - Ximenes et al.,2007	$6.359 \times 10^8 \exp\left(-\frac{2.9279 \times 10^4}{RT}\right)$	This study $L .mol^{-1} min^{-1}$
k_{p1} $L^2 .mol^{-2} min^{-1}$	$1.314 \times 10^7 \exp\left(-\frac{27440}{RT}\right)$	Dhib et al., 2000	$1.3140 \times 10^5 \exp\left(-\frac{1.0976 \times 10^3}{RT}\right)$	This study $L^2 .mol^{-2} min^{-1}$
k_p $L .mol^{-1} min^{-1}$	$2.560 \times 10^9 \exp\left(-\frac{7769.17}{RT}\right)$	Zhang and Ray, 2002	$1.302 \times 10^9 \exp\left(-\frac{7.75923 \times 10^3}{RT}\right)$	Dhib et al., 2000 $L .mol^{-1} min^{-1}$
k_t $L .mol^{-1} min^{-1}$	$1.201 \times 10^{12} \exp\left(-\frac{3081.84}{RT}\right)$	Zhang and Ray, 2002	$4.92 \times 10^{11} \exp\left(-\frac{3471.29}{RT}\right)$	Dhib et al., 2000 $L .mol^{-1} min^{-1}$
k_{fM} $L .mol^{-1} min^{-1}$	$5.626 \times 10^8 \exp\left(-\frac{13372}{RT}\right)$	Zhang and Ray, 2002	$8.5792 \times 10^8 \exp\left(-\frac{1.3585 \times 10^4}{RT}\right)$	This study $L .mol^{-1} min^{-1}$
k_{fD} $L .mol^{-1} min^{-1}$	50	Greszta and Matyjasze wski,1996	$9.376 \times 10^3 \exp\left(-\frac{3343}{RT}\right)$	This study $L .mol^{-1} min^{-1}$

Note: T (K) and R (cal mol⁻¹ K⁻¹)

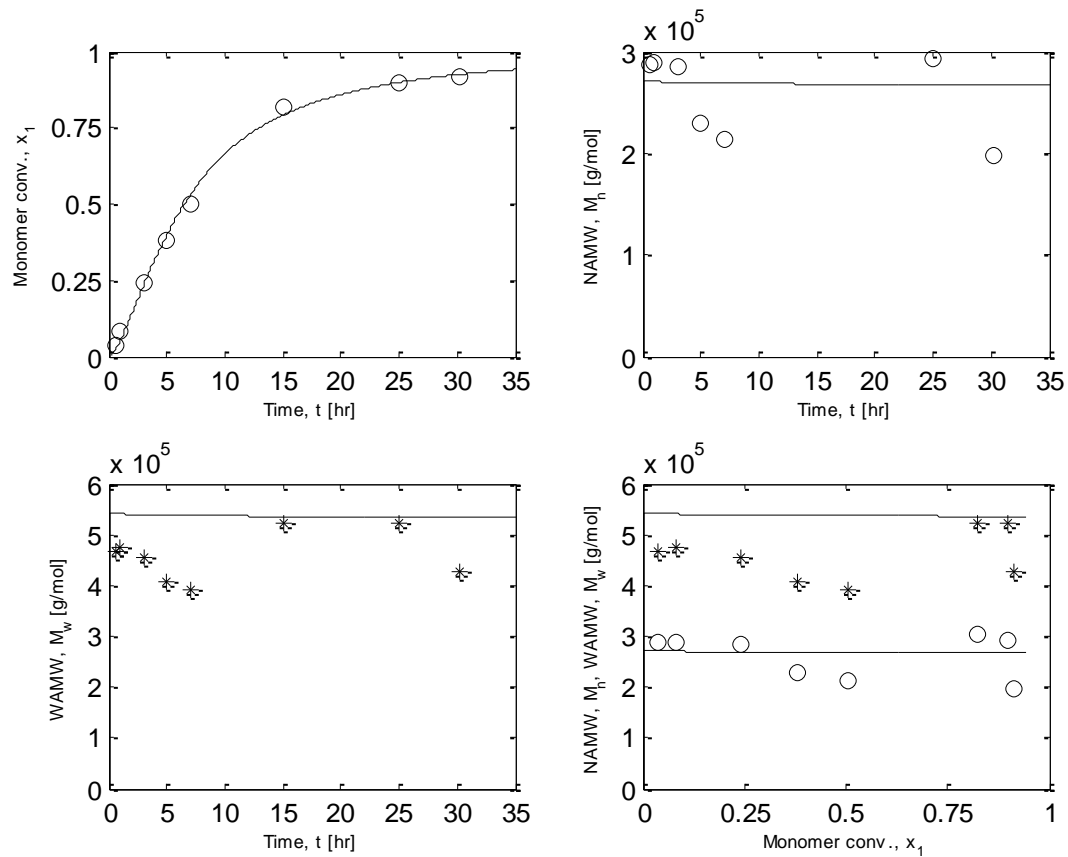


Figure 3.2: Model predictions of thermal polymerization of styrene at 120°C
 (—) model, (*,o) experimental data (Source of data: Nabifar et al., 2009)

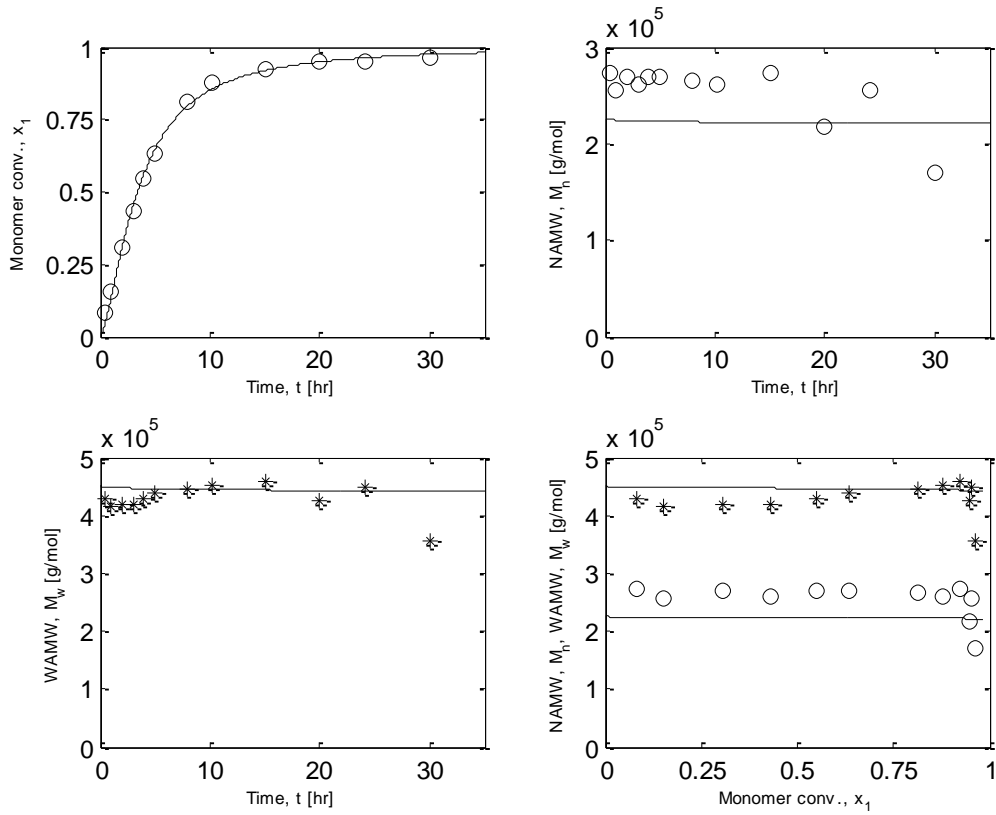


Figure 3.3: Model predictions of thermal polymerization of styrene at 130°C
 (—) model, (*,o) experimental data (Source of data: Nabifar et al., 2009)

In the next section, the kinetic mechanism demonstrates the involvement of the initiator (BPO) and the nitroxide stable radical (TEMPO) in the NMRP of styrene.

3.2 Bimolecular Nitroxide Mediated Radical Polymerization (NMRP) of Styrene

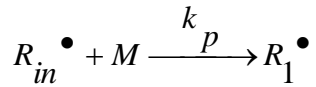
3.2.1 Previous Mechanisms and Models of NMRP of Styrene

Styrene polymerizations was studied for a number of years in the presence of the nitroxide stable free radical TEMPO, used as a controller, and of a conventional initiator BPO (Veregin et al., 1993; Veregin et al., 1996; Fukuda et al., 2000; Hawker et al., 2001; Bonilla et al., 2002; Mesa et al., 2005; Belincanta-Ximenes et al., 2007; Roa-Luna et al., 2007; Nabifar et al., 2008).

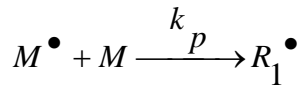
Yet, the mechanism of bimolecular NMRP of styrene is not fully understood. There has been controversy over the number of reactions describing the NMRP processes with the literature also reporting different reaction rate constants. This issue is the main reason for this study. In particular, Bonilla et al. (2002) proposed a kinetic mechanism for NMRP of styrene which is shown in Table 3.3. Roa-Luna et al. (2007) used the model to fit their data as in Figure 3.4. Since, the model does not predict all the data, Roa-Luna et al. (2007) concluded that the disagreement between data and model predictions may be due to the following reasons: either the reaction system was not well understood, or some of the kinetic rate constants reported in the literature were not accurate, or both.

Table 3.3: Kinetic mechanism of NMRP of styrene (Bonilla et al., 2002)

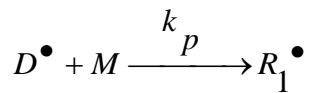
Step	Description
$I \xrightarrow{k_d} 2R_{in}^{\bullet}$	Chemical initiation
$M + M \xrightarrow{k_{dim}} D$	Mayo dimerization
$M + D \xrightarrow{k_{ia}} D^{\bullet} + M^{\bullet}$	Thermal initiation



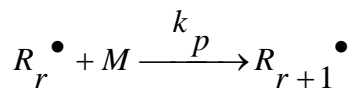
First propagation (primary radicals)



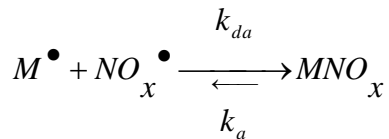
First propagation (monomeric radicals)



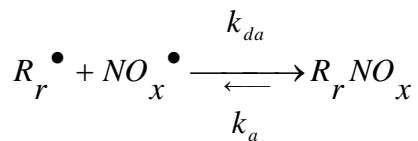
First propagation (dimeric radicals)



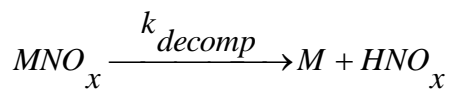
Propagation



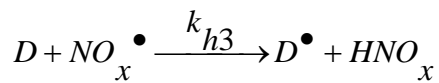
Dormant living exchange (monomeric alkoxyamine)



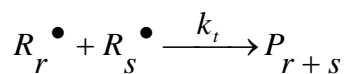
Dormant living exchange (polymeric alkoxyamine)



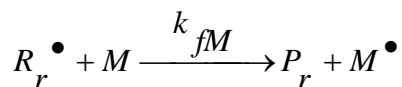
Alkoxyamine decomposition



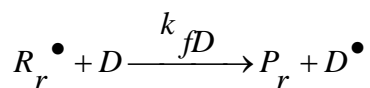
Rate enhancement reaction



Termination by combination



Transfer to monomer



Transfer to dimer

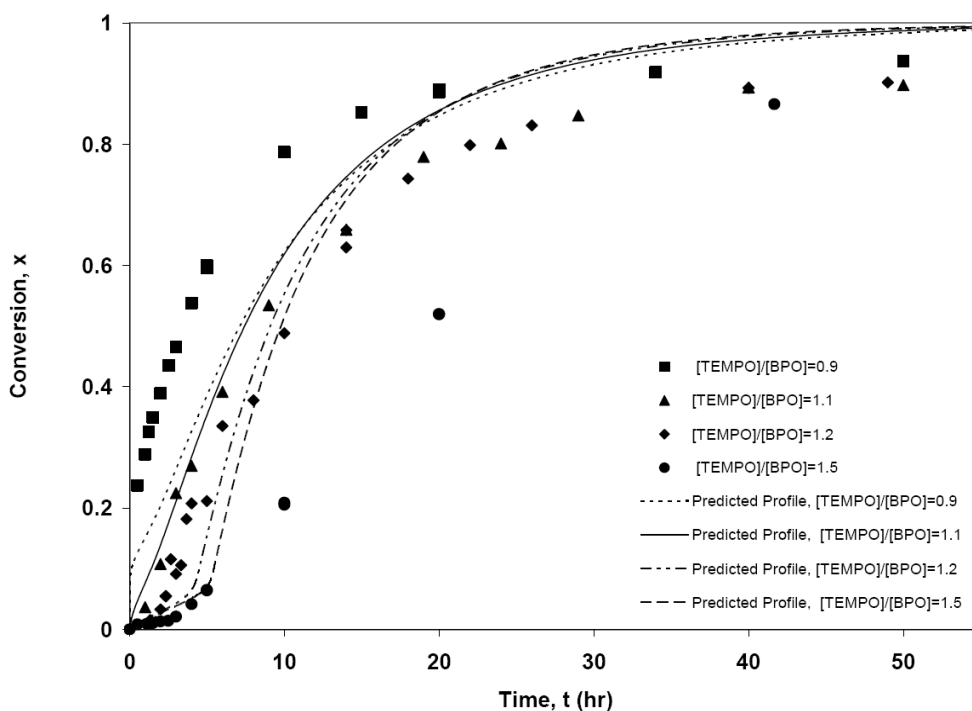


Figure 3.4: Comparison of model predictions with experimental data (Roa-Luna et al., 2007)

3.2.2 Proposed Kinetic Mechanism for NMRP of Styrene

3.2.2.1 New Side Reactions

In this study, we propose to modify the general mechanism reported by Bonilla et al. (2002) by adding two side reactions that were not considered in the mechanism presented in the literature. First, one side reaction is the “promoted dissociation” of BPO, which takes place between TEMPO and BPO as suggested by Moad et al. (1981). This reaction was further clarified by Veregin et al. (1993) and recently considered by Roa-Luna et al. (2007).



According to Veregin et al. (1993), this reaction is faster than BPO decomposition. Besides, formation of the benzyloxy radical can occur either by a thermal or promoted dissociation of

BPO. They showed that at a temperature below 80°C, the promoted dissociation is the dominant reaction whereas at higher temperatures the thermal dissociation mechanism plays a more important role. The promoted dissociation begins with an one-electron transfer from TEMPO to BPO to give an oxoammonium cation, a carboxylate anion and a benzoyloxy radical as shown in Figure 3.5.

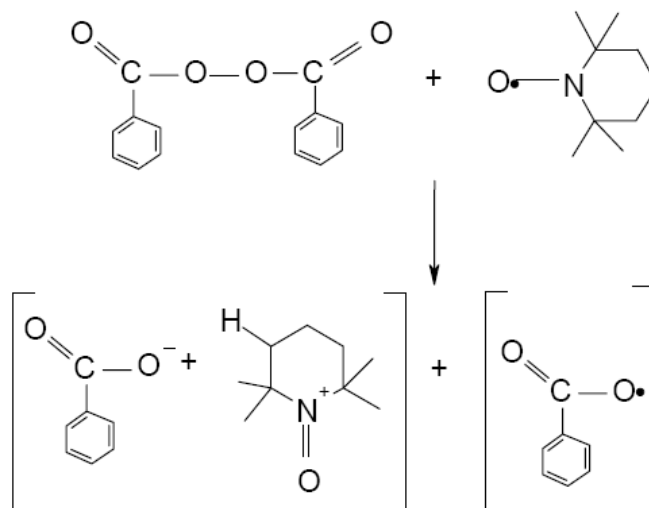


Figure 3.5: Mechanism for reaction between BPO and TEMPO (Moad et al., 1981)

It is important to keep in mind that the experimental data we collected from literature (Roa-Luna et al., 2007) were obtained at temperatures of 120 and 130°C. But during the preparation and handling of ampoules, the authors claimed that the reaction stock solutions were maintained at room temperature causing the occurrence of the side reaction (Roa-Luna et al., 2007).

Moreover, another side reaction named “Dormant living exchange” (Dimeric alkoxyamine) is given by Eq. (3.24). It was reported by Saldivar-Guerra et al. (2006). In this study, we added to the mechanism that was previously proposed by Bonilla et al. (2002).



D^\bullet is a dormant radical, and it can get easily trapped by NO_x^\bullet . Similar situation may occur for the NO_x^\bullet radical when trapping M^\bullet , a “Dormant living exchange” (monomeric alkoxyamine) and R_r^\bullet “Dormant living exchange” (polymeric alkoxyamine). In other words, reaction (3.24) is as important as the two reactions below which are already in the mechanism:



Even though several interesting studies have been done on nitroxide mediated radical polymerization (NMRP); the polymerization mechanism is not fully understood.

3.2.2.2 Full Bimolecular NMRP of Styrene

This section presents a detailed kinetic reaction mechanism for the bimolecular NMRP of styrene. The reaction mechanism summarized in Table 3.4 includes the following reactions:

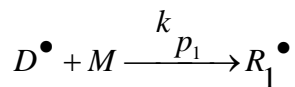
- Chemical initiation: when thermal decomposition of BPO into benzoyloxy primary radicals with high reactivity which initiates the polymerization of styrene by attacking the carbon–carbon double bond;
- Promoted dissociation reaction: first propagation (initiator radicals), monomer dimerization (Mayo dimerization), thermal initiation;
- Propagation;
- Living: reversible monomeric, dimeric and polymeric alkoxyamine formation (production of dormant species), alkoxyamine decomposition, rate enhancement;
- Termination: by combination and by transfer agent.

The addition of a nitroxide ‘controller’ molecule causes the pseudo-living character in the NMRP polymerization. The stable nitroxyl radical NO_x^\bullet can reversibly react with monomeric, dimeric and polymeric radicals to produce dormant monomeric, dimeric, and polymeric alkoxyamine species. These reactions are listed as dormant-living exchange (monomeric, dimeric and polymeric, respectively) in Table 3.4. Since the equilibrium is very much in favor of dormant chains as reported by He et al. (2000), the concentration of the polymer growing radicals is very low, and thus biradical termination is systematically suppressed. This leads to stepwise growth of molecular weight and slow polymerization rate. Detailed description of the activation/deactivation reactions is discussed in section 2.2.3.

The possible decomposition of the dormant monomeric alkoxyamine into styrene and the corresponding hydroxylamine is included in the reaction mechanism. Also, a possible reaction of the dimer with a stable nitroxyl radical produces a dimeric radical and a hydroxylamine. It is considered as an enhancement reaction. Only termination by combination and two transfer reactions are considered.

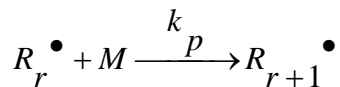
Table 3.4: Kinetic mechanism of bimolecular NMRP of styrene: modified version (this study)

Step	Description
Initiation	
$I \xrightarrow{k_d} 2R_{in}^\bullet$	Chemical initiation
$NO_x^\bullet + I \xrightarrow{K_{PR}} X + R_{in}^\bullet$	Promoted dissociation reaction
$R_{in}^\bullet + M \xrightarrow{k_1} R_1^\bullet$	First propagation (initiator radicals)
$M + M \xrightarrow{k_{dim}} D$	Mayo dimerization
$M + D \xrightarrow{k_{ia}} D^\bullet + M^\bullet$	Thermal initiation
$M^\bullet + M \xrightarrow{k_{p1}} R_1^\bullet$	Thermal initiation



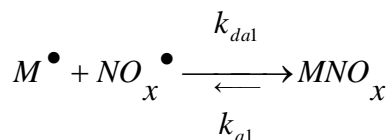
Thermal initiation

Propagation

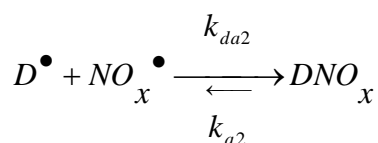


$r \geq 1$

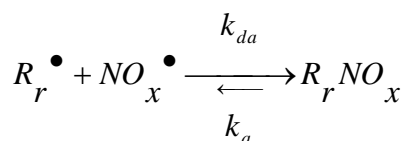
Living



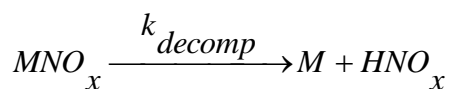
Dormant living exchange (monomeric alkoxyamine)



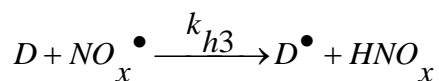
Dormant living exchange (dimeric alkoxyamine)



Dormant living exchange (polymeric alkoxyamine)

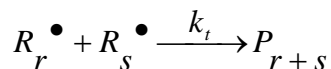


Alkoxyamine decomposition

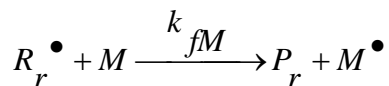


Rate enhancement reaction

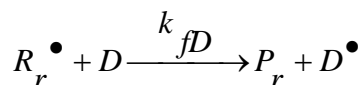
Termination and chain transfer agent



Termination by combination



Transfer to monomer



Transfer to dimer

Referring to Table 3.4, the symbols I, M, D, R_r^\bullet and P_r represent the initiator (BPO), the monomer (styrene), the dimer, the temporary polymer radical and the dead polymer radical, respectively. All other symbols defined in Table 3.4 are reported in the nomenclature.

3.3 Kinetic Model of Bimolecular NMRP of Styrene in a Batch Reactor

Based on the reaction mechanism presented above, the molar balance of each reaction species in a batch reactor is given below. The simplifying model assumptions are:

- Thermal polymerization of styrene does not depend on BPO and TEMPO;
- The diffusion-controlled effects (DC) as well as the gel effect are not expected to influence the NMRP system in a significant fashion, and are therefore neglected;
- All rate constants are assumed to be independent of chain length.

$$\frac{d[I]}{dt} = -k_d[I] - k_{PR}[I][NO_x^\bullet] \quad (3.27)$$

$$\begin{aligned} \frac{d[M]}{dt} = & -2fk_d[I] - k_{PR}[I][NO_x^\bullet] - 2k_{dim}[M]^2 - k_{ia}[M][D] - k_{p1}[M]([D^\bullet] + [M^\bullet]) \\ & - k_p[M][\lambda_0] + k_{decomp}[MNO_x] - k_{fM}[M][\lambda_0] \end{aligned} \quad (3.28)$$

$$\begin{aligned} \frac{d[NO_x^\bullet]}{dt} = & -k_{PR}[NO_x^\bullet][I] - k_{da1}[NO_x^\bullet][M^\bullet] + k_{a1}[MNO_x] - k_{da2}[D^\bullet][NO_x^\bullet] + k_{a2}[DNO_x] \\ & - k_{da}[\lambda_0][NO_x^\bullet] + k_a[\delta_0] - k_{h3}[D][NO_x^\bullet] \end{aligned} \quad (3.29)$$

$$\frac{d[M^\bullet]}{dt} = +k_{ia}[M][D] - k_{p1}[M][M^\bullet] - k_{da1}[NO_x^\bullet][M^\bullet] + k_{a1}[MNO_x] + k_{fM}[M][\lambda_0] \quad (3.30)$$

$$\begin{aligned} \frac{d[D^\bullet]}{dt} = & +k_{ia}[M][D] - k_{p1}[M][D^\bullet] - k_{da2}[D^\bullet][NO_x^\bullet] + k_{a2}[DNO_x] + k_{h3}[NO_x^\bullet][D] \\ & + k_{fD}[D][\lambda_0] \end{aligned} \quad (3.31)$$

$$\frac{d[HNO_x]}{dt} = +k_{decomp}[MNO_x] + k_{h3}[NO_x^\bullet][D] \quad (3.32)$$

$$\frac{d[MNO_x]}{dt} = +k_{dal}[NO_x^\bullet][M^\bullet] - k_{a1}[MNO_x] - k_{decomp}[MNO_x] \quad (3.33)$$

$$\frac{d[D]}{dt} = +k_{dim}[M]^2 - k_{ia}[D][M] - k_{h3}[D][NO_x^\bullet] - k_{fD}[\lambda_0][D] \quad (3.34)$$

$$\frac{d[DNO_x]}{dt} = +k_{da2}[NO_x^\bullet][D^\bullet] - k_{a2}[DNO_x] \quad (3.35)$$

The symbols k 's represent the kinetic rate constants, the symbol f represent the initiator efficiency with value equal to (0.5), and any symbol in [] represent the species concentration.

Given the fact that the initiator primary radical R_{in}^\bullet production is almost instantaneous, a steady state hypothesis was assumed; thus giving:

$$\frac{d[R_{in}^\bullet]}{dt} = +2fk_d[I] - k_1[M][R_{in}^\bullet] + k_{PR}[I][NO_x^\bullet] = 0 \quad (3.36)$$

which gives:

$$R_{in}^\bullet = \frac{2fk_d[I] + k_{PR}[I][NO_x^\bullet]}{k_1[M]} \quad (3.37)$$

The use of Eq. (3.37) is explained in Appendix A. There are three polymer populations in this system: live polymer radicals, dead polymer molecules, and dormant species. In similar manner to Eqs. (3.6) and (3.7), the moments of the dormant species is given by:

$$\delta_i = \sum_{r=0}^{\infty} r^i R_r NO_x \quad (3.38)$$

Once the molar balance equations for polymer molecules of all three polymer chain types are derived, the concept of the method of moments is applied. This leads to the polymer kinetic model:

Live polymer

$$\begin{aligned} \frac{d(\lambda_0)}{dt} = & 2fk_d[I] + k_{PR}[I][NO_x^\bullet] + k_{p1}[M]([M^\bullet] + [D^\bullet]) - k_{da}[NO_x^\bullet][\lambda_0] + k_a[\delta_0] \\ & - k_t[\lambda_0]^2 - k_{fM}[\lambda_0][M] - k_{fD}[D][\lambda_0] \end{aligned} \quad (3.39)$$

$$\begin{aligned} \frac{d(\lambda_1)}{dt} = & 2fk_d[I] + k_{PR}[I][NO_x^\bullet] + k_{p1}[M]([M^\bullet] + [D^\bullet]) + k_p[M][\lambda_0] - k_{da}[NO_x^\bullet][\lambda_1] + k_a[\delta_1] \\ & - k_t[\lambda_0][\lambda_1] - k_{fM}[\lambda_1][M] - k_{fD}[D][\lambda_1] \end{aligned} \quad (3.40)$$

$$\begin{aligned} \frac{d(\lambda_2)}{dt} = & 2fk_d[I] + k_{PR}[I][NO_x^\bullet] + k_{p1}[M]([M^\bullet] + [D^\bullet]) + k_p[M](\lambda_0 + 2[\lambda_1]) - k_{da}[NO_x^\bullet][\lambda_2] \\ & + k_a[\delta_2] - k_t[\lambda_0][\lambda_2] - k_{fM}[\lambda_2][M] - k_{fD}[D][\lambda_2] \end{aligned} \quad (3.41)$$

Dormant polymer

$$\frac{d(\delta_0)}{dt} = +k_{da}[NO_x^\bullet][\lambda_0] - k_a[\delta_0] \quad (3.42)$$

$$\frac{d(\delta_1)}{dt} = +k_{da}[NO_x^\bullet][\lambda_1] - k_a[\delta_1] \quad (3.43)$$

$$\frac{d(\delta_2)}{dt} = +k_{da}[NO_x^\bullet][\lambda_2] - k_a[\delta_2] \quad (3.44)$$

Dead polymer

$$\frac{d(\mu_0)}{dt} = +\frac{1}{2}k_t[\lambda_0]^2 + k_{fM}[\lambda_0][M] + k_{fD}[\lambda_0][D] \quad (3.45)$$

$$\frac{d(\mu_1)}{dt} = +k_t[\lambda_0][\lambda_1] + k_{fM}[\lambda_1][M] + k_{fD}[\lambda_1][D] \quad (3.46)$$

$$\frac{d(\mu_2)}{dt} = +k_t([\lambda_0][\lambda_2] + [\lambda_1]^2) + k_{fM}[\lambda_2][M] + k_{fD}[\lambda_2][D] \quad (3.47)$$

Based on the moments of the polymer populations, the number and weight average molecular weights are defined below:

$$\overline{Mn} = MW_M \left(\frac{\mu_1 + \lambda_1 + \delta_1}{\mu_0 + \lambda_0 + \delta_0} \right) \quad (3.48)$$

$$\overline{Mw} = MW_M \left(\frac{\mu_2 + \lambda_2 + \delta_2}{\mu_1 + \lambda_1 + \delta_1} \right) \quad (3.49)$$

where MW_n is the monomer molecular weight.

It is not possible to get an analytical solution of the kinetic model since Eqs. (3.27) to (3.35) and Eqs. (3.39) to (3.47) are coupled and highly nonlinear. Therefore, a numerical solution was attempted. But regarding the different scales of the species involved, a stable numerical solution may not be easy to obtain.

3.4 Dimensionless Form of the Bimolecular NMRP of Styrene Kinetic Model in Batch Reactor

In order to avoid numerical difficulties due to the stiffness of the differential system of equations, the kinetic model was transformed into a dimensionless form. This is common practice in chemical and polymer reaction engineering. Table 3.5 contains the dimensionless expressions and the scaling factors. Table 3.6 gives the model constants.

Table 3.5: Dimensionless variables for batch reactor model

$x_1 = \frac{I}{I_f}$	$x_2 = \frac{M}{M_f}$	$x_3 = \frac{NO_x^\bullet}{NO_{xf}^\bullet}$
$x_4 = \frac{M^\bullet}{M_0^\bullet}$	$x_5 = \frac{D^\bullet}{D_0^\bullet}$	$x_6 = \frac{HNO_x}{HNO_{x0}}$
$x_7 = \frac{MNO_x}{MNO_{x0}}$	$x_8 = \frac{D}{D_0}$	$x_9 = \frac{DNO_x}{DNO_{x0}}$
$x_{10} = \frac{\lambda_0 blmd_0}{M_f}$	$x_{11} = \frac{\lambda_1 blmd_1}{M_f}$	$x_{12} = \frac{\lambda_2 blmd_2}{M_f}$
$x_{13} = \frac{\delta_0 bsgm_0}{M_f}$	$x_{14} = \frac{\delta_1 bsgm_1}{M_f}$	$x_{15} = \frac{\delta_2 bsgm_2}{M_f}$
$x_{16} = \frac{\mu_0 bmu_0}{M_f}$	$x_{17} = \frac{\mu_1 bmu_1}{M_f}$	$x_{18} = \frac{\mu_2 bmu_2}{M_f}$
Scaling factors		
$blmd_0$	$blmd_1$	$blmd_2$
$bsgm_0$	$bsgm_1$	$bsgm_2$
bmu_0	bmu_1	bmu_2

Table 3.6: Simplifying expressions in the dimensionless batch reactor model

$a_0 = k_d \theta$	$a_1 = k_{PR} NO_{xf} \theta$	$a_2 = \frac{2fk_d I_f \theta}{M_f}$
$a_3 = \frac{k_{PR} I_f NO_{xf} \theta}{M_f}$	$a_4 = 2k_{dim} M_f \theta$	$a_5 = k_{ia} D_0 \theta$
$a_6 = k_{p1} M_0 \theta$	$a_7 = k_{p1} D_0 \theta$	$a_8 = k_p M_f \theta$
$a_9 = \frac{k_{decomp} MNO_{x0} \theta}{M_f}$	$a_{10} = k_{fM} M_f \theta$	$a_{11} = k_{PR} I_f \theta$
$a_{12} = k_{da1} M_0 \theta$	$a_{13} = \frac{k_{a1} MNO_{x0} \theta}{NO_{xf}}$	$a_{14} = k_{da2} D_0 \theta$
$a_{15} = \frac{k_{a2} DNO_{x0} \theta}{NO_{xf}}$	$a_{16} = k_{da} M_f \theta$	$a_{17} = \frac{k_a M_f \theta}{NO_{xf}}$
$a_{18} = k_{h3} D_0 \theta$	$a_{19} = \frac{k_{ia} M_f D_0 \theta}{M_0}$	$a_{20} = k_{p1} M_f \theta$
$a_{21} = k_{da1} NO_{xf} \theta$	$a_{22} = \frac{k_{a1} MNO_{x0} \theta}{M_0}$	$a_{23} = \frac{k_{fM} M_f^2 \theta}{M_0}$
$a_{24} = \frac{k_{ia} M_f D_0 \theta}{D_0}$	$a_{25} = k_{da2} NO_{xf} \theta$	$a_{26} = \frac{k_{a2} DNO_{x0} \theta}{D_0}$
$a_{27} = \frac{k_{h3} D_0 NO_{xf} \theta}{D_0}$	$a_{28} = \frac{k_{fD} M_f D_0 \theta}{D_0}$	$a_{29} = \frac{k_{decomp} MNO_{x0} \theta}{HNO_{x0}}$
$a_{30} = \frac{k_{h3} D_0 NO_{xf} \theta}{HNO_{x0}}$	$a_{31} = \frac{k_{da1} M_0 NO_{xf} \theta}{MNO_{x0}}$	$a_{32} = k_{a1} \theta$

$a_{33} = k_{decomp}\theta$	$a_{34} = \frac{k_{dim}M_f^2\theta}{D_0}$	$a_{35} = k_{ia}M_f\theta$
$a_{36} = k_{h3}NO_{xf}^*\theta$	$a_{37} = k_{fD}M_f\theta$	$a_{38} = k_{da}NO_{xf}^*\theta$
$a_{39} = k_a\theta$	$a_{40} = k_tM_f\theta$	$a_{41} = k_{fD}D_0\theta$
$a_{42} = \frac{k_tM_f\theta}{2}$	$a_{43} = \frac{k_{da2}D_0^*NO_{xf}^*\theta}{DNO_{x0}}$	$a_{44} = k_{a2}\theta$

The kinetic differential equations (3.27) to (3.35) are replaced with the dimensionless differential equations (3.50) to (3.58) and equations (3.39) to (3.47) with (3.59) to (3.67), respectively.

- Kinetic reactor model

$$\frac{dx_1}{dt} = -a_0x_1 - a_1x_1x_3 \quad (3.50)$$

$$\frac{dx_2}{dt} = -a_2x_1 - a_3x_1x_3 - a_4x_2^2 - a_5x_2x_8 - a_7x_2x_5 - a_6x_2x_4 - a_8x_2\frac{x_{10}}{blmd_0} + a_9x_7 - a_{10}x_2\frac{x_{10}}{blmd_0} \quad (3.51)$$

$$\frac{dx_3}{dt} = -a_{11}x_1x_3 - a_{12}x_3x_4 + a_{13}x_7 - a_{14}x_3x_5 + a_{15}x_9 - a_{16}x_3\frac{x_{10}}{blmd_0} + a_{17}\frac{x_{13}}{bsgm_0} - a_{18}x_3x_8 \quad (3.52)$$

$$\frac{dx_4}{dt} = a_{19}x_2x_8 - a_{20}x_2x_4 - a_{21}x_3x_4 + a_{22}x_7 + a_{23}x_2\frac{x_{10}}{blmd_0} \quad (3.53)$$

$$\frac{dx_5}{dt} = a_{24}x_2x_8 - a_{20}x_2x_5 - a_{25}x_3x_5 + a_{26}x_9 + a_{27}x_3x_8 + a_{28}x_8\frac{x_{10}}{blmd_0} \quad (3.54)$$

$$\frac{dx_6}{dt} = a_{29}x_7 + a_{30}x_3x_8 \quad (3.55)$$

$$\frac{dx_7}{dt} = a_{31}x_3x_4 - a_{32}x_7 - a_{33}x_7 \quad (3.56)$$

$$\frac{dx_8}{dt} = a_{34}x_2^2 - a_{35}x_2x_8 - a_{36}x_3x_8 - a_{37}x_8 \frac{x_{10}}{blmd_0} \quad (3.57)$$

$$\frac{dx_9}{dt} = a_{43}x_3x_5 - a_{44}x_9 \quad (3.58)$$

- Kinetic polymer model

$$\begin{aligned} \frac{dx_{10}}{dt} = blmd_0 \left[a_2x_1 + a_3x_1x_3 + a_6x_2x_4 + a_7x_2x_5 - a_{38}x_3 \frac{x_{10}}{blmd_0} + a_{39} \frac{x_{13}}{bsgm_0} - a_{40} \left(\frac{x_{10}}{blmd_0} \right)^2 \right. \\ \left. - a_{10}x_2 \frac{x_{10}}{blmd_0} - a_{41}x_8 \frac{x_{10}}{blmd_0} \right] \end{aligned} \quad (3.59)$$

$$\begin{aligned} \frac{dx_{11}}{dt} = blmd_1 \left[a_2x_1 + a_3x_1x_3 + a_6x_2x_4 + a_7x_2x_5 + a_8x_2 \frac{x_{10}}{blmd_0} - a_{38}x_3 \frac{x_{11}}{blmd_1} + a_{39} \frac{x_{14}}{bsgm_1} \right. \\ \left. - a_{40} \frac{x_{10}}{blmd_0} \frac{x_{11}}{blmd_1} - a_{10}x_2 \frac{x_{11}}{blmd_1} - a_{41}x_8 \frac{x_{11}}{blmd_1} \right] \end{aligned} \quad (3.60)$$

$$\begin{aligned} \frac{dx_{12}}{dt} = blmd_2 \left[a_2x_1 + a_3x_1x_3 + a_6x_2x_4 + a_7x_2x_5 + a_8x_2 \frac{x_{10}}{blmd_0} + 2a_8x_2 \frac{x_{11}}{blmd_1} - a_{38}x_3 \frac{x_{12}}{blmd_2} \right. \\ \left. + a_{39} \frac{x_{15}}{bsgm_2} - a_{40} \frac{x_{10}}{blmd_0} \frac{x_{12}}{blmd_2} - a_{10}x_2 \frac{x_{12}}{blmd_2} - a_{41}x_8 \frac{x_{12}}{blmd_2} \right] \end{aligned} \quad (3.61)$$

$$\frac{dx_{13}}{dt} = bsgm_0 \left[a_{38}x_3 \frac{x_{10}}{blmd_0} - a_{39} \frac{x_{13}}{bsgm_0} \right] \quad (3.62)$$

$$\frac{dx_{14}}{dt} = bsgm_1 \left[a_{38} x_3 \frac{x_{11}}{blmd_1} - a_{39} \frac{x_{14}}{bsgm_1} \right] \quad (3.63)$$

$$\frac{dx_{15}}{dt} = bsgm_2 \left[a_{38} x_3 \frac{x_{12}}{blmd_2} - a_{39} \frac{x_{15}}{bsgm_2} \right] \quad (3.64)$$

$$\frac{dx_{16}}{dt} = bmu_0 \left[a_{42} \left(\frac{x_{10}}{blmd_0} \right)^2 + a_{10} x_2 \frac{x_{10}}{blmd_0} + a_{41} x_8 \frac{x_{10}}{blmd_0} \right] \quad (3.65)$$

$$\frac{dx_{17}}{dt} = bmu_1 \left[a_{40} \frac{x_{10}}{blmd_0} \frac{x_{11}}{blmd_1} + a_{10} x_2 \frac{x_{11}}{blmd_1} + a_{41} x_8 \frac{x_{11}}{blmd_1} \right] \quad (3.66)$$

$$\frac{dx_{18}}{dt} = bmu_2 \left[a_{40} \frac{x_{10}}{blmd_0} \frac{x_{12}}{blmd_2} + a_{40} \left(\frac{x_{11}}{blmd_1} \right)^2 + a_{10} x_2 \frac{x_{12}}{blmd_2} + a_{41} x_8 \frac{x_{12}}{blmd_2} \right] \quad (3.67)$$

3.5 Validation of the Bimolecular NMRP of Styrene Model with Data

Most of the studies on NMRP of styrene show a disagreement between experimental data and theory. In fact, the theory discrepancy may be due to inaccurate kinetic rate constants or to missing side reactions that are not accounted for in the kinetic models.

The first possibility of the model discrepancy has been addressed in section 3.2.2.1 upon adding two side reactions. Next, we will attempt an optimal parameter estimation.

A wide variation of the rate constants is reported in open literature. In this study, an extensive search in literature has been done in order to find the most reliable kinetic rates (Veregin et al., 1993; Greszta et al., 1996; Dhib et al., 2000; Bonilla et al., 2002; Zhang et al., 2002 and Belincanta-Ximenes et al., 2007). A parameter estimation procedure was accomplished to adjust the kinetic rates. The kinetic rates found in the literature have been used as the initial estimates to start the parameter estimation procedure for the improving the model performance. The kinetic rate constants are written according to Arrhenius equation (Avery, 1974), and they are listed in Table 3.7.

3.5.1 Parameter Estimation

Parameter estimation was performed for the bimolecular NMRP of styrene process. Once a mathematical model has been developed for a polymerization system, a common approach is to compute the values of the model parameters so that the model can give an acceptable prediction of real data. In this work, experimental conversion C and polydispersity index PDI values were collected from literature (Roa-Luna et al., 2007). The values of the parameters A and E in the Arrhenius equation were estimated by minimizing the errors between the theoretical values and experimental values of styrene conversion and the polymer polydispersity index. The minimization function is expressed as follows:

$$\min_z \quad J(z) = \sum_{i=1}^N w_1 (C_{mi}(t, z) / C_{di} - 1)^2 + w_2 (PDI_{mi}(t, z) / PDI_{di} - 1)^2 \quad (3.68)$$

where $C_{mi}(t, z) = 1 - x_2(t) / x_2(0)$ is the monomer conversion.

subject to the dimensionless kinetic model (3.50) to (3.67) which is rewritten in vector form:

$$\dot{x}(t) = f(x, t, z) \quad (3.69)$$

$$x(0) = x_0 \quad (3.70)$$

where x is the state vector.

$$x = [x_1, x_2, x_3, x_4, x_5, x_6, x_7, x_8, x_9, x_{10}, x_{11}, x_{12}, x_{13}, x_{14}, x_{15}, x_{16}, x_{17}, x_{18}]^T$$

and z is the vector of parameters to estimate:

$$z = [A_{da}, E_{da}, A_a, E_a, A_{decomp}, E_{decomp}, A_{dal}, E_{dal}, A_{a1}, E_{a1}, A_{da2}, E_{da2}, A_{a2}, E_{a2}, A_{fM}, E_{fM}, A_{dim}, E_{dim}, A_{ia}, E_{ia}]^T \quad (3.71)$$

The symbols A and E are the kinetic parameters in the Arrhenius equation.

$$k = A \exp(-E / RT) \quad (3.72)$$

Here N is number of data, C_{mi} represents the theoretical monomer conversion, C_{di} is the experimental data of monomer conversion; PDI_{mi} is the theoretical values and PDI_{di} is the experimental data of polydispersity index, respectively. Finally, w_1 and w_2 denote weight factors used to bring the conversion and polydispersity index to the same scale. In this case, $w_1 = w_2 = 1$ since conversion and polydispersity index are scaled to be equally important.

The conversion C and polydispersity index PDI values were determined by numerical integration of the dimensionless model. Standard Matlab routines for static optimization and numerical integration were used. The optimal estimates of each parameter A and E are shown in the fourth column of Table 3.7, whereas the kinetic rate values listed in the second column are from the literature.

It is important to keep in mind that $(k_p, k_{p1}, k_{fd}, k_d, k_{PR}, k_{h3}, k_t)$ were not included in this parameter estimation procedure. Only the parameter subset $(k_{da}, k_a, k_{decomp}, k_{dal}, k_{a1}, k_{da2}, k_{a2}, k_{fM}, k_{dim}, k_{ia})$ was updated in this case.

In this study, various kinetic rates used for the dormant living exchange reversible reactions (monomeric, dimeric and polymeric alkoxyamine) were represented by $(k_{a1}, k_{dal}, k_{a2}, k_{da2}, k_a, k_{da})$, respectively. This modification is different from previous studies done by Bonilla et al. (2002) and Belincanta-Ximenes et al. (2007), where they only had dormant living exchange reversible reactions (monomeric and polymeric alkoxyamine) with kinetic rates of the activation k_a and deactivation k_{da} had the same numerical values.

Table 3.7: Kinetic rate constants for bimolecular NMRP of styrene

Variable/ Units	Kinetic rate expressions	Reference	Kinetic rate expressions	Reference
k_d min^{-1}	$1.02 \times 10^{17} \exp\left(-\frac{30000}{RT}\right)$	Zhang and Ray, 2002	$1.02 \times 10^{17} \exp\left(-\frac{30000}{RT}\right)$	Zhang and Ray, 2002
k_{PR} $L \cdot \text{mol}^{-1} \text{min}^{-1}$	6.0	Veregin et al.1993	6.0	Veregin et al.1993 $L \cdot \text{mol}^{-1} \text{min}^{-1}$
k_{dim} $L \cdot \text{mol}^{-1} \text{min}^{-1}$	$1.134 \times 10^4 \exp\left(-\frac{16185.1}{RT}\right)$	Belincanta-Ximenes et al.,2007	$753.89 \exp\left(-\frac{2.522 \times 10^4}{RT}\right)$	This study $L \cdot \text{mol}^{-1} \text{min}^{-1}$
k_{ia} $L \cdot \text{mol}^{-1} \text{min}^{-1}$	$3.815 \times 10^{14} \exp\left(-\frac{36598.55}{RT}\right)$	Belincanta-Ximenes et al.,2007	$5.786 \times 10^8 \exp\left(-\frac{3.469 \times 10^4}{RT}\right)$	This study $L \cdot \text{mol}^{-1} \text{min}^{-1}$
k_{p1} $L^2 \cdot \text{mol}^{-2} \text{min}^{-1}$	$1.314 \times 10^7 \exp\left(-\frac{27440}{RT}\right)$	Dhib et al., 2000	$1.314 \times 10^5 \exp\left(-\frac{1.0976 \times 10^3}{RT}\right)$	This study $L^2 \cdot \text{mol}^{-2} \text{min}^{-1}$
k_p $L \cdot \text{mol}^{-1} \text{min}^{-1}$	$2.560 \times 10^9 \exp\left(-\frac{7769.17}{RT}\right)$	Zhang and Ray, 2002	$1.302 \times 10^9 \exp\left(-\frac{7.75923 \times 10^3}{RT}\right)$	Dhib et al., 2000 $L \cdot \text{mol}^{-1} \text{min}^{-1}$
k_{da} $L \cdot \text{mol}^{-1} \text{min}^{-1}$	$3.018 \times 10^{11} \exp\left(-\frac{3722}{RT}\right)$	Zhang and Ray, 2002	$6.437 \times 10^9 \exp\left(-\frac{3.423 \times 10^3}{RT}\right)$	This study $L \cdot \text{mol}^{-1} \text{min}^{-1}$
k_a min^{-1}	$1.2 \times 10^{15} \exp\left(-\frac{29683}{RT}\right)$	Zhang and Ray, 2002	$2.166 \times 10^{13} \exp\left(-\frac{29136.83}{RT}\right)$	This study min^{-1}
k_{dal}	N/A		$4.079 \times 10^9 \exp\left(-\frac{3.963 \times 10^3}{RT}\right)$	This study $L \cdot \text{mol}^{-1} \text{min}^{-1}$

...continue

Table 3.7: (continued)

k_{a1}	N/A		$2.002 \times 10^{13} \exp\left(-\frac{25815.30}{RT}\right)$	This study min^{-1}
k_{da2}	N/A		$4.12 \times 10^9 \exp\left(-\frac{4.119 \times 10^3}{RT}\right)$	This study $L \cdot \text{mol}^{-1} \text{min}^{-1}$
k_{a2}	N/A		$2.106 \times 10^{13} \exp\left(-\frac{25539.25}{RT}\right)$	This study min^{-1}
k_{decomp} min^{-1}	$3.420 \times 10^{16} \exp\left(-\frac{36639.6}{RT}\right)$	Zhang and Ray, 2002	$4.418 \times 10^{14} \exp\left(-\frac{40263.25}{RT}\right)$	This study min^{-1}
k_{h3} $L \cdot \text{mol}^{-1} \text{min}^{-1}$	0.06	Bonilla et al., 2002	0.06	Bonilla et al., 2002 $L \cdot \text{mol}^{-1} \text{min}^{-1}$
k_t $L \cdot \text{mol}^{-1} \text{min}^{-1}$	$1.201 \times 10^{12} \exp\left(-\frac{3081.84}{RT}\right)$	Zhang and Ray, 2002	$4.92 \times 10^{11} \exp\left(-\frac{3471.29}{RT}\right)$	Dhib et al., 2000 $L \cdot \text{mol}^{-1} \text{min}^{-1}$
k_{fM} $L \cdot \text{mol}^{-1} \text{min}^{-1}$	$5.626 \times 10^8 \exp\left(-\frac{13372}{RT}\right)$	Zhang and Ray, 2001	$1.06 \times 10^9 \exp\left(-\frac{1.313 \times 10^4}{RT}\right)$	This study $L \cdot \text{mol}^{-1} \text{min}^{-1}$
k_{fD} $L \cdot \text{mol}^{-1} \text{min}^{-1}$	50	Greszta and Matyjaszewski, 1996	$9.376 \times 10^3 \exp\left(-\frac{3343}{RT}\right)$	This study $L \cdot \text{mol}^{-1} \text{min}^{-1}$

Note: T (K) and R ($\text{cal mol}^{-1} \text{K}^{-1}$)

The experimental data were collected from literature (Roa-Luna et al, 2007) for bimolecular NMRP of styrene for the molar ratios of [TEMPO]/[BPO] of 0.9, 1.1 and 1.2 at 120°C, and also [TEMPO]/[BPO] molar ratios of 1.1 and 1.3 at 130°C.

The data collected with a $[\text{TEMPO}]/[\text{BPO}]$ molar ratio of 1.1 at 120°C was selected for the parameter estimation. The results in Figure 3.6 demonstrate almost a very good fit of the model to the data at time interval less than 20 hours for the monomer conversion. However, the model appears to over predict the data at times over 20 hours. This might be due to the diffusion control reaction condition prevailing in the reactor at high conversions.

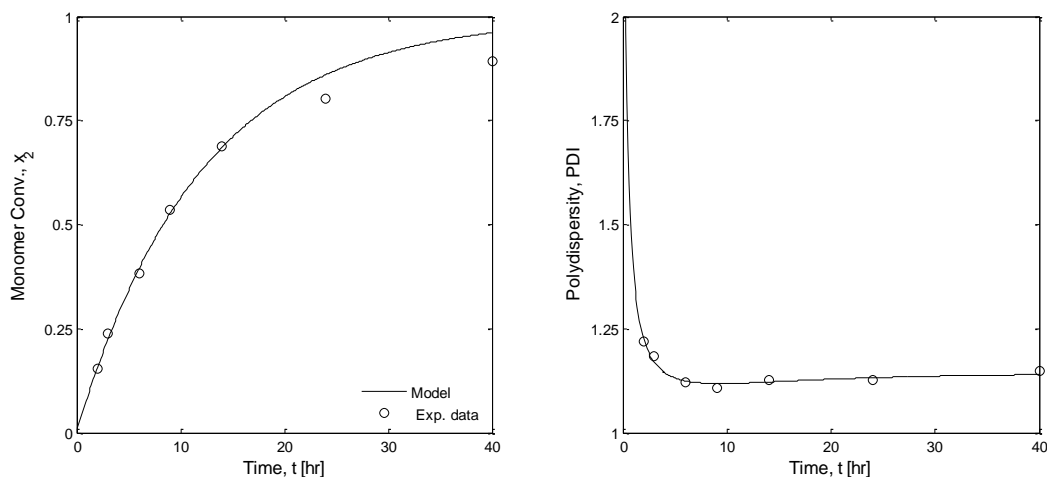


Figure 3.6: Model predictions (optimal estimates) for ratio $[\text{TEMPO}]/[\text{BPO}]=1.1$ and $T=120^\circ\text{C}$ (Source of data: Roa-Luna et al., 2007)

3.5.2 Comparison of Model Predictions with Data

It is primordial to examine and validate the predictions of the bimolecular NMRP kinetic model at different $[\text{TEMPO}]/[\text{BPO}]$ molar ratios and at different reaction temperatures. Therefore, simulation runs were done using the experimental data collected from literature (Roa-Luna et al, 2007) for bimolecular NMRP of styrene for molar ratios of $[\text{TEMPO}]/[\text{BPO}]$ of 0.9 and 1.2 at 120°C , and also molar ratios of 1.1 and 1.3 at 130°C .

Figure 3.7 shows plots of monomer conversion and polydispersity versus time for molar ratios of $[\text{TEMPO}]/[\text{BPO}]$ 1.2 at 120°C . Very good agreement was obtained between the model predictions and the data for the monomer conversion and good agreement for polydispersity. Published data on styrene controlled polymerization (Veregin et al., 1993; Georges et al., 1994; Fukuda et al., 1996; Greszta et al., 1996; Veregin et al., 1996; Butte et al., 1999; Zhang et al.,

2002; Bonilla et al., 2002; Roa-Luna et al., 2007; Belincanta-Ximenes et al., 2007; Nabifar et al., 2008 and Roa-Luna et al., 2008) show experimental evidence of large polydispersity index at low conversions, but the PDI stays close to almost 1.1 as the conversion increases. This result is similar to the ones predicted by the model in our case study.

Simulation tests were done using the experimental data for [TEMPO]/[BPO] ratio 0.9 at 120°C. In this case, Figure 3.8 shows that the model does not give good prediction of the data of the monomer conversion. However, the polydispersity plot predicts the data pretty well.

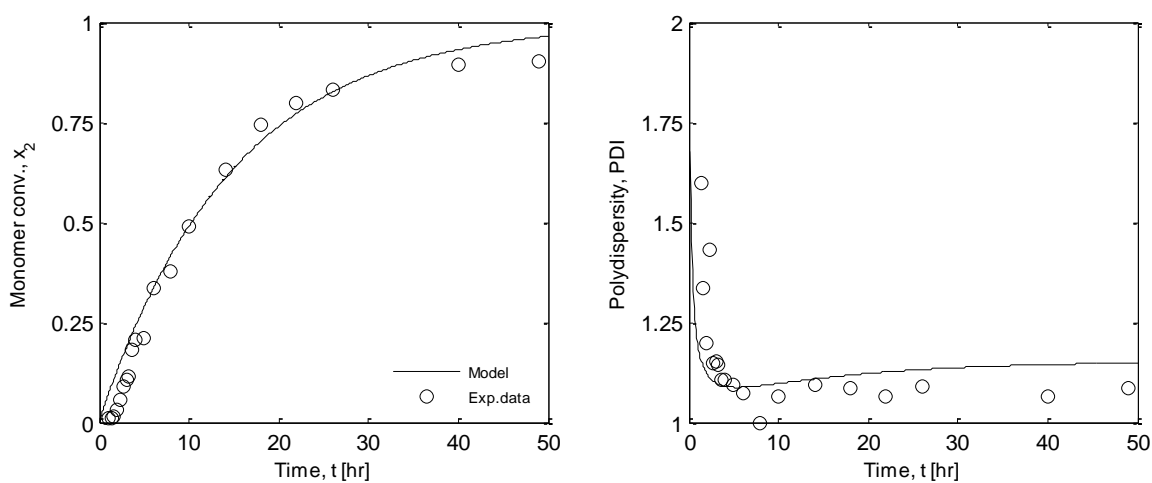


Figure 3.7: Model predictions for ratio [TEMPO]/[BPO]=1.2 and T=120°C
(Source of data: Roa-Luna et al., 2007)

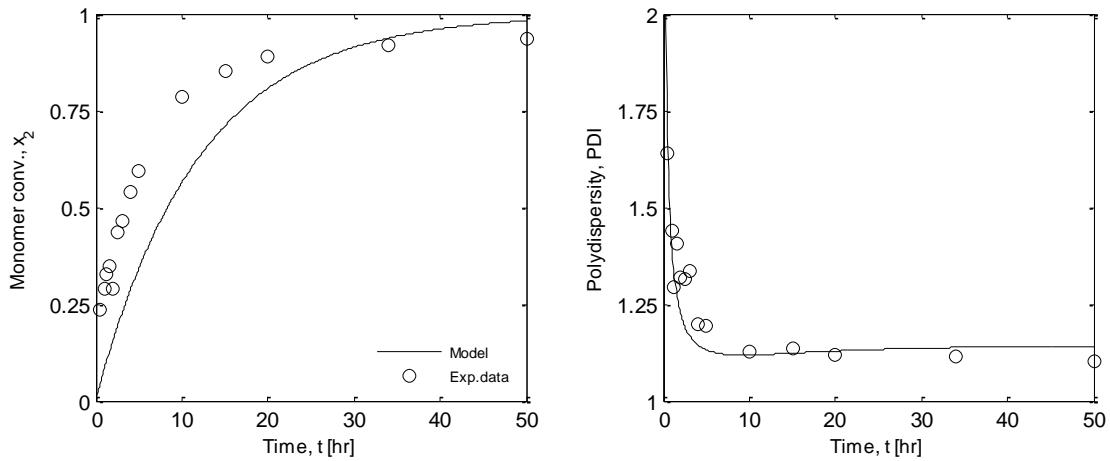


Figure 3.8: Model predictions for ratio $[\text{TEMPO}]/[\text{BPO}]=0.9$ and $T=120^{\circ}\text{C}$
(Source of data: Roa-Luna et al., 2007)

Plots in Figure 3.9 and 3.10 compare model prediction with data at 130°C and $[\text{TEMPO}]/[\text{BPO}]$ ratio of 1.1 and 1.3, respectively. For the first case, good agreement is obtained between the model prediction and the data of the monomer conversion especially for data up to 0.80 conversion. But the model predicts slightly higher values of the polydispersity data. With $[\text{TEMPO}]/[\text{BPO}]$ ratio of 1.3, almost perfect match is obtained between the experimental data and the model prediction for the polydispersity and fairly good match for the monomer conversion.

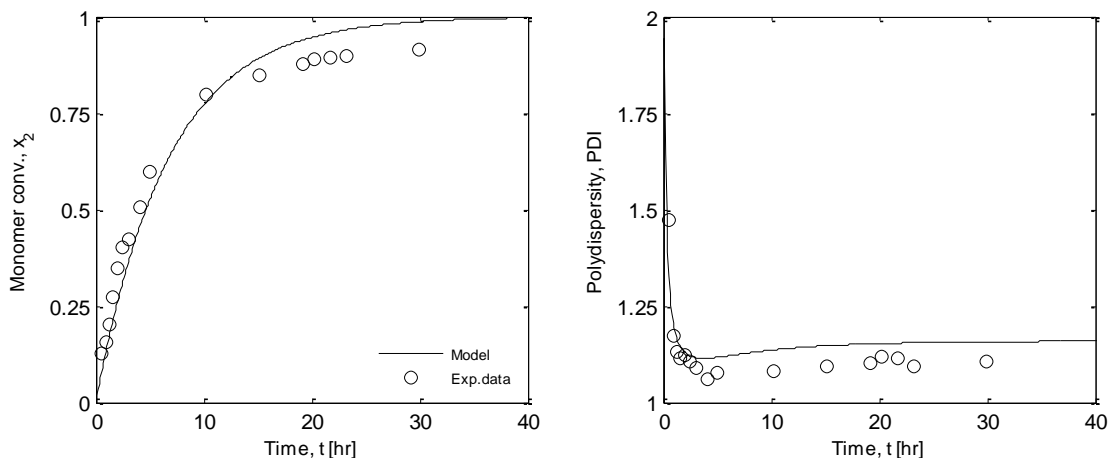


Figure 3.9: Model predictions for ratio $[\text{TEMPO}]/[\text{BPO}]=1.1$ and $T=130^\circ\text{C}$
(Source of data: Roa-Luna et al., 2007)

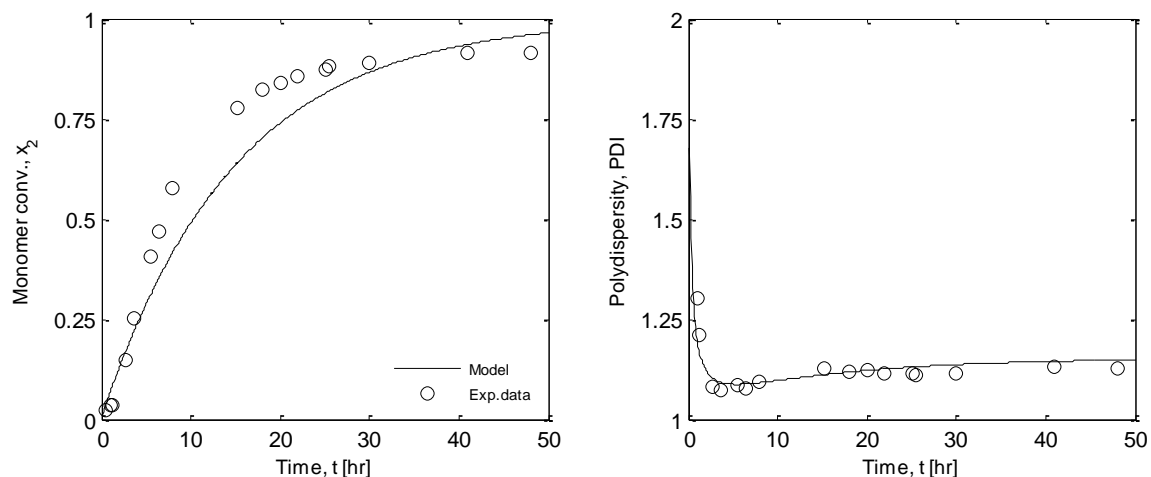


Figure 3.10: Model predictions for ratio $[\text{TEMPO}]/[\text{BPO}]=1.3$ and $T=130^\circ\text{C}$
(Source of data: Roa-Luna et al., 2007)

In overall, the model predicts pretty well of bimolecular NMRP at 120 and 130°C and $[\text{TEMPO}]/[\text{BPO}]$ ratio ranging from 0.9 to 1.3.

Now, it is important to analyze the effects of temperature and $[\text{TEMPO}]/[\text{BPO}]$ ratios on the polymerization rate. It is clear from the conversion plots (Figures 3.6 to 3.9) that the same conversion can be achieved in less time at higher temperature. But, the model predicts almost the

same values of polydispersity 1.1 and 1.25 as temperature goes from 120 to 130°C, which indicates that the effect of temperature is not important on polydispersity. But keeping the temperature invariant at 120°C, there is a significant effect of the [TEMPO]/[BPO] ratio on the conversion. For example, at 120°C, when [TEMPO]/[BPO] ratio is 0.9 the free radicals cannot all be trapped by TEMPO leading to a decrease in dormant radical concentration in comparison to ratio 1.1. Propagation occurs mainly as in the regular radical polymerization for [TEMPO]/[BPO] is 0.9, resulting in an increase in dead polymer concentration compared to [TEMPO]/[BPO] is 1.1 or 1.2.

Now looking at the polydispersity plots in Figure 3.6 and Figure 3.8 at 120°C, clearly, low PDI is obtained at the beginning of the polymerization when the [TEMPO]/[BPO] ratio of 1.1 and a high PDI value with a ratio of 0.9. Thus, decreasing the concentration of TEMPO brings the polymerization system close to regular polymerization in the initial reaction period.

Chapter 4: Bimolecular NMRP of Styrene in CSTR Reactor

In this chapter we investigate the steady state bifurcation behavior of the styrene NMRP kinetic model in a CSTR reactor. Continuous reactors are extensively used in free radical polymerization. These reactors, once operating at steady state, will produce a consistent product at low manufacturing cost. As long as steady state can be maintained, the polymer produced will be consistent over a long period of time. The steady state behavior of a continuous reactor is expected to have two segments: one stable and one unstable. Occurrence of unstable steady state behavior affects the quality of the polymer produced and as a result a closed loop control scheme is necessary. Otherwise, less control is expected when the operating region is located in the stable steady state segment.

4.1 Literature Review of the Steady State Analysis of the Continuous Stirred Tank Reactor (CSTR) Polymerization Reactors

There is still much research work to be done on CRP polymerization processes, before they can become an alternative commercial importance. In fact, most of the published work on the CRP reactions was carried out in batch reactors under isothermal conditions. Jaisinghani and Ray (1977) studied bulk homopolymerization of methyl methacrylate (MMA) and styrene in a CSTR. They determined the influence of operating conditions on the steady state and dynamic behavior of the reactor.

Schmidt and Ray (1981) showed the existence of steady state multiplicity behavior of an isothermal MMA polymerization reactor. They attributed steady state multiplicity to the strong occurrence of gel effect of the polymerization. Also, Hamer et al. (1981) demonstrated the presence of stable limit cycles in continuous homopolymerizations and copolymerizations of MMA and vinyl acetate (VA).

Kim and Choi (1988) analyzed the steady state behavior of styrene polymerization in CSTR with bifunctional initiators and it was compared with polymerization with monofunctional initiators. The steady state reactor model analysis revealed five regions of steady state behavior within the parameter space using the reactor residence time as the bifurcation parameter.

Russo and Bequette (1992) investigated the non-linear behavior analysis of a living free radical polymerization (LFRP) process. In their work, they demonstrated that cooling jacket dynamics cannot be neglected because it may have a significant impact on the non-linear behavior of the whole system. In a subsequent work, Russo and Bequette (1998) employed steady state multiplicity analysis to study the operating range of a jacketed exothermic styrene polymerization CSTR.

Filho et al. (1994) analyzed three systems: vinylacetate, styrene and MMA polymerization. A generic model described the dynamic behavior of continuous free-radical solution polymerizations and showed that most reactors can present as many as five different steady state solutions, regardless of the particular chemical system analyzed. Later, that work was extended by Melo et al. (2001) to show that self-sustained oscillatory responses may also be considered to be generic reactor responses.

Zhang and Ray (2001) proposed a model for the RAFT polymerization scheme and corroborated their results with experimental data obtained for MMA RAFT polymerization. That paper was the first attempt to study the effect of the reactor type on Living Free Radical Polymerization (LFRP) processes. That work analyzes the behavior of variables such as molecular weight and polydispersity index in a single CSTR, a series of CSTRs, and semibatch reactors. Later, Zhang and Ray (2002) demonstrated a comprehensive kinetic model for batch, semibatch, and continuous tank reactors. The study was conducted for both ATRP and NMRP. They reported that the residence time distribution in CSTR has a significant effect on the development of chain architecture.

Schork and Smulders (2004) discussed the polydispersity of an ideal RAFT polymerization and an ideal reversible termination polymerization (ATRP or NMRP) carried out in a single homogeneous CSTR. In addition, they studied the polydispersity of an ideal living radical polymerization carried out in a CSTR train. Their final conclusion was for both RAFT and

reversible termination living radical polymerization in a single CSTR, the molecular weight distribution reverts to that expected for true living radical polymerization. Besides, for a CSTR, the polydispersity approaches 2, rather than the value of unity predicted for a batch reactor, while for a CSTR train, the polydispersity decreases from 2 with an increase in the number of reactors.

In addition, Lemoine-Nava et al. (2006) studied the non-linear behavior of NMRP of styrene taking place in a single continuously stirred tank reactor. Typical hysteresis behavior was found for this reactor. Input multiplicities, disjoint bifurcations and isola behavior were found.

In this work, the steady state bifurcation analysis was done to identify the right operating region to produce polymer with the desired characteristics using bimolecular NMRP of styrene in single CSTR reactor.

4.2 Bimolecular NMRP of Styrene in a CSTR Reactor

4.2.1 Continuous Stirred Tank Reactor (CSTR) Design

In this section, a jacketed lab-scale continuous stirred tank reactor has designed in order to study the behavior of our model. Figure 4.1 shows the schematic of the CSTR considered in this work.

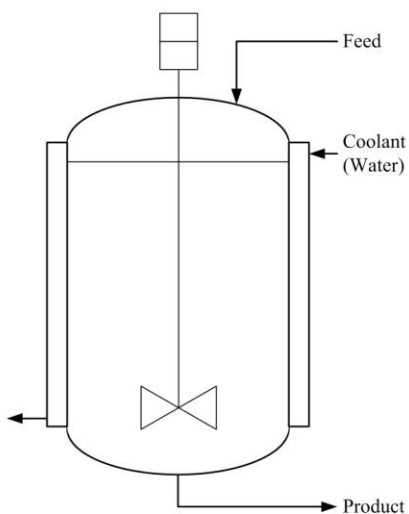


Figure 4.1: Schematic diagram of a jacketed CSTR

First, the volume of the reactor assumed to be (10 L). Furthermore, in order to calculate the dimensions of the reactor, the aspect ratio (H/D) needed to be chosen, as shown in Eq. (4.1)

$$H / D_{in} = 2 \quad (4.1)$$

At this point, it is worthwhile to explain why the aspect ratio (H/D) between 1 and 2 are frequently used for reactors. The first reason is the capital cost, the weight of material required to build a reactor of a fixed volume is minimized using an aspect ratio of ~1. The second consideration is mixing; as it becomes difficult to achieve good mixing if the aspect ratio (H/D) increases. (Luyben, 2007; Dou et al., 2009).

The following steps are used to calculate the dimensions of the reactor which are explained further below.

$$V_{in} = V_{in}(cylinder) + V_{in}(sphere) / 2 \quad (4.2)$$

$$A_{in} = A_{in}(cylinder) + A_{in}(sphere) / 2 \quad (4.3)$$

The jacketed area required represented by the first term on the right hand side of Eq. (4.3). The reactor dimensions are listed in Table 4.1.

Table 4.1: Reactor dimensions

Definitions	Variables/units	Values
Inner diameter	$D_{in} (m)$	0.176
Outer diameter	$D_{out} (m)$	0.186
Height	$H (m)$	0.352
Total inner area	$A_{in} (m^2)$	0.243
Jacketed area	$A (m^2)$	0.195
Inner volume	$V_{in} (L)$	10

4.2.2 Kinetic Model

In this part, a mathematical model of bimolecular NMRP of styrene in CSTR is discussed. It is important to keep in mind that the differential equations Eqs. (4.4) to (4.12) of the reaction species in the reactor and the differential equations for the moments Eqs. (4.16) to (4.24) are based on the reaction mechanism presented previously in section 3.2.2.2. In addition, energy balances are given by Eqs. (4.22) and (4.23) for the reactor and the jacket temperature, respectively, (Verazaluce-Garcia et al, 2000; Fogler, 1999; Bird, 2007).

The mathematical model was developed by employing the following assumptions and approximations: (i) perfect mixing, (ii) constant physical properties as well as no gel effect correlations included. Clearly, below is the set of ordinary differential model equations:

$$\frac{d[I]}{dt} = -k_d[I] - k_{PR}[I][NO_x^\bullet] + \frac{(I_f - I)}{\theta} \quad (4.4)$$

$$\begin{aligned} \frac{d[M]}{dt} = & -2fk_d[I] - k_{PR}[I][NO_x^\bullet] - 2k_{dim}[M]^2 - k_{ia}[M][D] - k_{p1}[M]([D^\bullet] + [M^\bullet]) \\ & - k_p[M][\lambda_0] + k_{decomp}[MNO_x] - k_{fM}[M][\lambda_0] + \frac{(M_f - M)}{\theta} \end{aligned} \quad (4.5)$$

$$\begin{aligned} \frac{d[NO_x^\bullet]}{dt} = & -k_{PR}[NO_x^\bullet][I] - k_{dal}[NO_x^\bullet][M^\bullet] + k_{a1}[MNO_x] - k_{da2}[D^\bullet][NO_x^\bullet] + k_{a2}[DNO_x] \\ & - k_{da}[\lambda_0][NO_x^\bullet] + k_a[\delta_0] - k_{h3}[D][NO_x^\bullet] + \frac{(NO_x^\bullet - NO_x)}{\theta} \end{aligned} \quad (4.6)$$

$$\frac{d[M^\bullet]}{dt} = +k_{ia}[M][D] - k_{p1}[M][M^\bullet] - k_{dal}[NO_x^\bullet][M^\bullet] + k_{a1}[MNO_x] + k_{fM}[M][\lambda_0] - \frac{M^\bullet}{\theta} \quad (4.7)$$

$$\begin{aligned} \frac{d[D^\bullet]}{dt} = & +k_{ia}[M][D] - k_{p1}[M][D^\bullet] - k_{da2}[D^\bullet][NO_x^\bullet] + k_{a2}[DNO_x] + k_{h3}[NO_x^\bullet][D] \\ & + k_{fD}[D][\lambda_0] - \frac{D^\bullet}{\theta} \end{aligned} \quad (4.8)$$

$$\frac{d[HNO_x]}{dt} = +k_{decomp}[MNO_x] + k_{h3}[NO_x^\bullet][D] - \frac{HNO_x}{\theta} \quad (4.9)$$

$$\frac{d[MNO_x]}{dt} = +k_{dal}[NO_x^\bullet][M^\bullet] - k_{a1}[MNO_x] - k_{decomp}[MNO_x] - \frac{MNO_x}{\theta} \quad (4.10)$$

$$\frac{d[D]}{dt} = +k_{dim}[M]^2 - k_{ia}[D][M] - k_{h3}[D][NO_x^\bullet] - k_{fd}[\lambda_0][D] - \frac{D}{\theta} \quad (4.11)$$

$$\frac{d[DNO_x]}{dt} = +k_{da2}[NO_x^\bullet][D^\bullet] - k_{a2}[DNO_x] - \frac{DNO_x}{\theta} \quad (4.12)$$

The method of moments is used to describe the characteristics of the polymer. There are three polymer populations in this system: living polymer radicals, dead polymer chains and dormant species. The i^{th} moments for living radical, dead and dormant species are defined by Eqs. (3.6), (3.7), and (3.38), respectively.

First, the molar balance equations for polymer molecules of the three types are derived. Then application of the method of moments leads to Eqs. (4.13) to (4.21) as follows:

Live polymer

$$\begin{aligned} \frac{d(\lambda_0)}{dt} &= 2fk_d[I] + k_{PR}[I][NO_x^\bullet] + k_{p1}[M]([M^\bullet] + [D^\bullet]) - k_{da}[NO_x^\bullet][\lambda_0] + k_a[\delta_0] \\ &- k_t[\lambda_0]^2 - k_{fM}[\lambda_0][M] - k_{fD}[D][\lambda_0] - \frac{\lambda_0}{\theta} \end{aligned} \quad (4.13)$$

$$\begin{aligned} \frac{d(\lambda_1)}{dt} &= 2fk_d[I] + k_{PR}[I][NO_x^\bullet] + k_{p1}[M]([M^\bullet] + [D^\bullet]) + k_p[M][\lambda_0] - k_{da}[NO_x^\bullet][\lambda_1] + k_a[\delta_1] \\ &- k_t[\lambda_0][\lambda_1] - k_{fM}[\lambda_1][M] - k_{fD}[D][\lambda_1] - \frac{\lambda_1}{\theta} \end{aligned} \quad (4.14)$$

$$\begin{aligned} \frac{d(\lambda_2)}{dt} &= 2fk_d[I] + k_{PR}[I][NO_x^\bullet] + k_{p1}[M]([M^\bullet] + [D^\bullet]) + k_p[M](\lambda_0 + 2[\lambda_1]) - k_{da}[NO_x^\bullet][\lambda_2] \\ &+ k_a[\delta_2] - k_t[\lambda_0][\lambda_2] - k_{fM}[\lambda_2][M] - k_{fD}[D][\lambda_2] - \frac{\lambda_2}{\theta} \end{aligned} \quad (4.15)$$

Dormant polymer

$$\frac{d(\delta_0)}{dt} = +k_{da}[NO_x^\bullet][\lambda_0] - k_a[\delta_0] - \frac{\delta_0}{\theta} \quad (4.16)$$

$$\frac{d(\delta_1)}{dt} = +k_{da}[NO_x^\bullet][\lambda_1] - k_a[\delta_1] - \frac{\delta_1}{\theta} \quad (4.17)$$

$$\frac{d(\delta_2)}{dt} = +k_{da}[NO_x^\bullet][\lambda_2] - k_a[\delta_2] - \frac{\delta_2}{\theta} \quad (4.18)$$

Dead polymer

$$\frac{d(\mu_0)}{dt} = +\frac{1}{2}k_t[\lambda_0]^2 + k_{fM}[\lambda_0][M] + k_{fD}[\lambda_0][D] - \frac{\mu_0}{\theta} \quad (4.19)$$

$$\frac{d(\mu_1)}{dt} = +k_t[\lambda_0][\lambda_1] + k_{fM}[\lambda_1][M] + k_{fD}[\lambda_1][D] - \frac{\mu_1}{\theta} \quad (4.20)$$

$$\frac{d(\mu_2)}{dt} = +k_t([\lambda_0][\lambda_2] + [\lambda_1]^2) + k_{fM}[\lambda_2][M] + k_{fD}[\lambda_2][D] - \frac{\mu_2}{\theta} \quad (4.21)$$

Energy equations

$$\frac{dT}{dt} = \frac{(-\Delta H_R)k_p[M]([M^\bullet] + [R_{in}] + [D^\bullet] + [\lambda_0])}{\rho_m CP_m} - \frac{UA(T - T_j)}{\rho_m CP_m V} + \frac{(T_f - T)}{\theta} \quad (4.22)$$

$$\frac{dT_j}{dt} = \frac{Q_w(T_{fj} - T_j)}{V_j} + \frac{UA(T - T_j)}{\rho_w CP_w V_j} \quad (4.23)$$

4.3 Dimensionless Form of the Bimolecular NMRP of Styrene Kinetic Model in CSTR

In order to avoid numerical problems related to the stiffness of the differential equations, all the differential equations above describing the kinetic behavior and the molecular weight development were transformed into dimensionless differential equations. This is a common practice in chemical and polymer reaction engineering.

The reader is referred to Table 4.2 for the dimensionless expressions and the scaling factors. Other model constants are shown in Table 4.3.

Table 4.2: Dimensionless variables for CSTR

$x_1 = \frac{I_f - I}{I_f}$	$x_2 = \frac{M_f - M}{M_f}$	$x_3 = \frac{NO_{xf}^{\bullet} - NO_x^{\bullet}}{NO_{xf}^{\bullet}}$	$x_4 = \frac{M^{\bullet}}{M_0^{\bullet}}$
$x_5 = \frac{D^{\bullet}}{D_0^{\bullet}}$	$x_6 = \frac{HNO_x}{HNO_{x0}}$	$x_7 = \frac{MNO_x}{MNO_{x0}}$	$x_8 = \frac{D}{D_0}$
$x_9 = \frac{DNO_x}{DNO_{x0}}$	$x_{10} = \frac{\lambda_0 blmd_0}{M_f}$	$x_{11} = \frac{\lambda_1 blmd_1}{M_f}$	$x_{12} = \frac{\lambda_2 blmd_2}{M_f}$
$x_{13} = \frac{\delta_0 bsgm_0}{M_f}$	$x_{14} = \frac{\delta_1 bsgm_1}{M_f}$	$x_{15} = \frac{\delta_2 bsgm_2}{M_f}$	$x_{16} = \frac{\mu_0 bmu_0}{M_f}$
$x_{17} = \frac{\mu_1 bmu_1}{M_f}$	$x_{18} = \frac{\mu_2 bmu_2}{M_f}$	$x_{19} = \frac{T - T_0}{T_0}$	$x_{20} = \frac{T_j - T_{j0}}{T_{j0}}$
Scaling factors			
$blmd_0$	$blmd_1$	$blmd_2$	
$bsgm_0$	$bsgm_1$	$bsgm_2$	
bmu_0	bmu_1	bmu_2	

Table 4.3: Simplifying expressions in the dimensionless CSTR model

$a_0 = k_d \theta$	$a_1 = k_{PR} NO_{xf} \theta$	$a_2 = \frac{2fk_d I_f \theta}{M_f}$
$a_3 = \frac{k_{PR} I_f NO_{xf} \theta}{M_f}$	$a_4 = 2k_{dim} M_f \theta$	$a_5 = k_{ia} D_0 \theta$
$a_6 = k_{p1} M_0 \theta$	$a_7 = k_{p1} D_0 \theta$	$a_8 = k_p M_f \theta$
$a_9 = \frac{k_{decomp} MNO_{x0} \theta}{M_f}$	$a_{10} = k_{fM} M_f \theta$	$a_{11} = k_{PR} I_f \theta$
$a_{12} = k_{da1} M_0 \theta$	$a_{13} = \frac{k_{a1} MNO_{x0} \theta}{NO_{xf}}$	$a_{14} = k_{da2} D_0 \theta$
$a_{15} = \frac{k_{a2} DNO_{x0} \theta}{NO_{xf}}$	$a_{16} = k_{da} M_f \theta$	$a_{17} = \frac{k_a M_f \theta}{NO_{xf}}$
$a_{18} = k_{h3} D_0 \theta$	$a_{19} = \frac{k_{ia} M_f D_0 \theta}{M_0}$	$a_{20} = k_{p1} M_f \theta$
$a_{21} = k_{da1} NO_{xf} \theta$	$a_{22} = \frac{k_{a1} MNO_{x0} \theta}{M_0}$	$a_{23} = \frac{k_{fM} M_f^2 \theta}{M_0}$
$a_{24} = \frac{k_{ia} M_f D_0 \theta}{D_0}$	$a_{25} = k_{da2} NO_{xf} \theta$	$a_{26} = \frac{k_{a2} DNO_{x0} \theta}{D_0}$
$a_{27} = \frac{k_{h3} D_0 NO_{xf} \theta}{D_0}$	$a_{28} = \frac{k_{fD} M_f D_0 \theta}{D_0}$	$a_{29} = \frac{k_{decomp} MNO_{x0} \theta}{HNO_{x0}}$
$a_{30} = \frac{k_{h3} D_0 NO_{xf} \theta}{HNO_{x0}}$	$a_{31} = \frac{k_{da1} M_0 NO_{xf} \theta}{MNO_{x0}}$	$a_{32} = k_{a1} \theta$

$a_{33} = k_{decomp}\theta$	$a_{34} = \frac{k_{dim}M_f^2\theta}{D_0}$	$a_{35} = k_{ia}M_f\theta$
$a_{36} = k_{h3}NO_{xf}^*\theta$	$a_{37} = k_{jD}M_f\theta$	$a_{38} = k_{da}NO_{xf}^*\theta$
$a_{39} = k_a\theta$	$a_{40} = k_tM_f\theta$	$a_{41} = k_{jD}D_0\theta$
$a_{42} = \frac{k_tM_f\theta}{2}$	$a_{43} = \frac{k_{da2}D_0^*NO_{xf}^*\theta}{DNO_{x0}}$	$a_{44} = k_{a2}\theta$
$a_{45} = \frac{(-\Delta H_R)k_pM_fM_0^*\theta}{\rho_m CP_m T_0}$	$a_{46} = \frac{(-\Delta H_R)k_pM_fD_0^*\theta}{\rho_m CP_m T_0}$	$a_{47} = \frac{(-\Delta H_R)k_pM_f^2\theta}{\rho_m CP_m T_0}$
$a_{48} = \frac{(-\Delta H_R)2fk_pk_dI_f\theta}{k_1\rho_m CP_m T_0}$	$a_{49} = \frac{(-\Delta H_R)k_pk_{PR}I_fNO_{xf}^*\theta}{k_1\rho_m CP_m T_0}$	$a_{50} = \frac{UA\theta}{\rho_m CP_m V}$
$a_{51} = \frac{UA\theta T_{j0}}{\rho_m CP_m VT_0}$	$a_{52} = \frac{Q_w\theta}{V_j}$	$a_{53} = \frac{UA\theta T_0}{\rho_w CP_w V_j T_{j0}}$
$a_{54} = \frac{UA\theta}{\rho_w CP_w V_j}$	$a_{55} = \frac{T_f - T_0}{T_0}$	$a_{56} = \frac{T_{fj} - T_{j0}}{T_{j0}}$

Using the dimensionless expressions, the scaling factors and the model constants; the kinetic model in dimensionless form is given below:

$$\frac{dx_1}{dt} = a_0(1-x_1) + a_1(1-x_1)(1-x_3) - x_1 \quad (4.24)$$

$$\begin{aligned} \frac{dx_2}{dt} = & a_2(1-x_1) + a_3(1-x_1)(1-x_3) + a_4(1-x_2)^2 + a_5(1-x_2)x_8 + a_6(1-x_2)x_4 + a_7(1-x_2)x_5 \\ & + a_8(1-x_2)\frac{x_{10}}{blmd_0} - a_9x_7 + a_{10}(1-x_2)\frac{x_{10}}{blmd_0} - x_2 \end{aligned} \quad (4.25)$$

$$\begin{aligned} \frac{dx_3}{dt} = & a_{11}(1-x_1)(1-x_3) + a_{12}(1-x_3)x_4 - a_{13}x_7 + a_{14}(1-x_3)x_5 - a_{15}x_9 + a_{16}(1-x_3)\frac{x_{10}}{blmd_0} \\ & - a_{17}\frac{x_{13}}{bsgm_0} + a_{18}(1-x_3)x_8 - x_3 \end{aligned} \quad (4.26)$$

$$\frac{dx_4}{dt} = a_{19}(1-x_2)x_8 - a_{20}(1-x_2)x_4 - a_{21}(1-x_3)x_4 + a_{22}x_7 + a_{23}(1-x_2)\frac{x_{10}}{blmd_0} - x_4 \quad (4.27)$$

$$\frac{dx_5}{dt} = a_{24}(1-x_2)x_8 - a_{20}(1-x_2)x_5 - a_{25}(1-x_3)x_5 + a_{26}x_9 + a_{27}(1-x_3)x_8 + a_{28}x_8\frac{x_{10}}{blmd_0} - x_5 \quad (4.28)$$

$$\frac{dx_6}{dt} = a_{29}x_7 + a_{30}(1-x_3)x_8 - x_6 \quad (4.29)$$

$$\frac{dx_7}{dt} = a_{31}(1-x_3)x_4 - a_{32}x_7 - a_{33}x_7 - x_7 \quad (4.30)$$

$$\frac{dx_8}{dt} = a_{34}(1-x_2)^2 - a_{35}(1-x_2)x_8 - a_{36}(1-x_3)x_8 - a_{37}x_8\frac{x_{10}}{blmd_0} - x_8 \quad (4.31)$$

$$\frac{dx_9}{dt} = a_{43}(1-x_3)x_5 - a_{44}x_9 - x_9 \quad (4.32)$$

$$\begin{aligned} \frac{dx_{10}}{dt} = & blmd_0 \left[a_2(1-x_1) + a_3(1-x_1)(1-x_3) + a_6(1-x_2)x_4 + a_7(1-x_2)x_5 - a_{38}(1-x_3)\frac{x_{10}}{blmd_0} \right. \\ & \left. + a_{39}\frac{x_{13}}{bsgm_0} - a_{40}\left(\frac{x_{10}}{blmd_0}\right)^2 - a_{10}(1-x_2)\frac{x_{10}}{blmd_0} - a_{41}x_8\frac{x_{10}}{blmd_0} \right] - x_{10} \end{aligned} \quad (4.33)$$

$$\frac{dx_{11}}{dt} = blmd_1 \left[a_2(1-x_1) + a_3(1-x_1)(1-x_3) + a_6(1-x_2)x_4 + a_7(1-x_2)x_5 + a_8(1-x_2)\frac{x_{10}}{blmd_0} \right]$$

$$-a_{38}(1-x_3)\frac{x_{11}}{blmd_1} + a_{39}\frac{x_{14}}{bsgm_1} - a_{40}\frac{x_{10}}{blmd_0}\frac{x_{11}}{blmd_1} - a_{10}(1-x_2)\frac{x_{11}}{blmd_1} - a_{41}x_8\frac{x_{11}}{blmd_1} \Big] - x_{11} \quad (4.34)$$

$$\begin{aligned} \frac{dx_{12}}{dt} = & blmd_2 \left[a_2(1-x_1) + a_3(1-x_1)(1-x_3) + a_6(1-x_2)x_4 + a_7(1-x_2)x_5 + a_8(1-x_2)\frac{x_{10}}{blmd_0} \right. \\ & + 2a_8(1-x_2)\frac{x_{11}}{blmd_1} - a_{38}(1-x_3)\frac{x_{12}}{blmd_2} + a_{39}\frac{x_{15}}{bsgm_2} - a_{40}\frac{x_{10}}{blmd_0}\frac{x_{12}}{blmd_2} - a_{10}(1-x_2)\frac{x_{12}}{blmd_2} \\ & \left. - a_{41}x_8\frac{x_{12}}{blmd_2} \right] - x_{12} \quad (4.35) \end{aligned}$$

$$\frac{dx_{13}}{dt} = bsgm_0 \left[a_{38}(1-x_3)\frac{x_{10}}{blmd_0} - a_{39}\frac{x_{13}}{bsgm_0} \right] - x_{13} \quad (4.36)$$

$$\frac{dx_{14}}{dt} = bsgm_1 \left[a_{38}(1-x_3)\frac{x_{11}}{blmd_1} - a_{39}\frac{x_{14}}{bsgm_1} \right] - x_{14} \quad (4.37)$$

$$\frac{dx_{15}}{dt} = bsgm_2 \left[a_{38}(1-x_3)\frac{x_{12}}{blmd_2} - a_{39}\frac{x_{15}}{bsgm_2} \right] - x_{15} \quad (4.38)$$

$$\frac{dx_{16}}{dt} = bmu_0 \left[a_{42}\left(\frac{x_{10}}{blmd_0}\right)^2 + a_{10}(1-x_2)\frac{x_{10}}{blmd_0} + a_{41}x_8\frac{x_{10}}{blmd_0} \right] - x_{16} \quad (4.39)$$

$$\frac{dx_{17}}{dt} = bmu_1 \left[a_{40}\frac{x_{10}}{blmd_0}\frac{x_{11}}{blmd_1} + a_{10}(1-x_2)\frac{x_{11}}{blmd_1} + a_{41}x_8\frac{x_{11}}{blmd_1} \right] - x_{17} \quad (4.40)$$

$$\frac{dx_{18}}{dt} = bmu_2 \left[a_{40}\frac{x_{10}}{blmd_0}\frac{x_{12}}{blmd_2} + a_{40}\left(\frac{x_{11}}{blmd_1}\right)^2 + a_{10}(1-x_2)\frac{x_{12}}{blmd_2} + a_{41}x_8\frac{x_{12}}{blmd_2} \right] - x_{18} \quad (4.41)$$

$$\frac{dx_{19}}{dt} = a_{55} - x_{19} + a_{45}(1 - x_2)x_4 + a_{46}(1 - x_2)x_5 + a_{47}(1 - x_2)\frac{x_{10}}{blmd_0} + a_{48}(1 - x_1) + a_{49}(1 - x_1) - a_{50}(1 + x_{19}) + a_{51}(1 + x_{20}) \quad (4.42)$$

$$\frac{dx_{20}}{dt} = a_{52}(a_{56} - x_{20}) + a_{53}(1 + x_{19}) + a_{54}(1 + x_{20}) \quad (4.43)$$

4.4 Steady State Bifurcation Analysis

Next will be discussed the nonlinear behavior of the bimolecular nitroxide mediated radical polymerization of styrene (NMRP) taking place in a continuous stirred tank reactor (CSTR). The cooling water flow rate, feed stream temperature, residence time, initiator feed stream concentration and controller feed stream concentration were chosen as the bifurcation parameters.

4.4.1 Numerical Algorithm

In this study, bifurcation analysis was performed using Matcont, which is Matlab continuation package. Matcont is a Graphical User Interface (GUI) for the interactive numerical study of parameterized nonlinear ODEs. It allows the computation of curves of equilibria, limit points, Hopf points, branch points of equilibria, limit cycles, and branch point bifurcation points of limit cycles, and homoclinic orbits. Matcont can start these computations from equilibria or periodic orbits computed by time integration and it can monitor user-defined functions and locate their roots along computed curves. Also, it can compute all necessary derivatives by finite differences, from file or by using the symbolic toolbox of Matlab (Dhooge et al., 2003).

Briefly, a system of nonlinear ordinary differential equations is given below:

$$\frac{dx}{dt} = f(x, u) \quad (4.44)$$

where $x \in R^n$ is the vector of the state variables, $u \in R^m$ is the vector of process inputs, and $f \in R^n$ is the vector of nonlinear functions. If x^* is an equilibrium point or steady state of this system for a given set of inputs u^* , then:

$$\left. \frac{dx}{dt} \right|_{x^*, u^*} = f(x^*, u^*) = 0 \quad (4.45)$$

In order to analyze the behavior of this type, it is often useful to compute branches of equilibria, Hopf points, limit points etc., if an appropriate number of parameters are available (Melo et al., 2001; Dhooze et al., 2006).

In addition to the bifurcation diagrams, Matcont also computes the system eigenvalues at the satisfied equilibrium points. In general, if the real part of all the eigenvalues are strictly negative, the steady state is identified as stable. The supremum “sup” is defined to be the smallest real number that is greater than or equal to every number in the partially ordered set. Then for stability condition:

$$\sup(\text{eig}(\frac{\partial f}{\partial x}(x^*, u^*))) < 0 \quad (4.46)$$

Now, if the real part of at least one eigenvalue is not negative, the steady state is identified as unstable. Then, for instability condition:

$$\sup(\text{eig}(\frac{\partial f}{\partial x}(x^*, u^*))) > 0 \quad (4.47)$$

In all Figures presented in this section, the stable solution branches are plotted with solid lines (—) and the unstable solution branches with dashed lines (---). The points at which the stable and unstable branches meet are known as limit points. In general, stability interchange takes place at turning points, which are the limit points. These are points where one of the eigenvalues of the linearized Jacobian matrix at steady state conditions moves from one side of the complex diagram to the other one on the real axis as it can be seen in Eq. (4.49) At these points, the

number of different steady state solution generally changes and so do their stability characteristics (Pinto 1995). Then for limit point condition is:

$$\sup(\text{eig}(\frac{\partial f}{\partial x}(x^*, u^*))) = 0 \quad (4.48)$$

where the linearized Jacobian matrix evaluated at steady state conditions is given by :

$$\frac{\partial f}{\partial x}(x^*, u^*) = \left[\begin{array}{ccc} \frac{\partial f_1}{\partial x_1} & \dots & \frac{\partial f_1}{\partial x_n} \\ \vdots & \ddots & \vdots \\ \frac{\partial f_n}{\partial x_1} & \dots & \frac{\partial f_n}{\partial x_n} \end{array} \right]_{x^*, u^*} \quad (4.49)$$

4.5 Result Analysis

For a good presentation of a general framework for the nonlinear behavior of continuous bimolecular NMRP of styrene, some important practical issues should be mentioned first. In practice, due to operational difficulties that arise as a consequence of the onset of gel effect, it is not advisable to allow the reaction to achieve monomer conversions in excess of 55% (Kiparissides, 1996). It is important to note that the mathematical models presented in chapters 3 and 4 do not consider the gel effect since there is currently not a good enough understanding of the diffusion controlled effects in living free radical polymerization systems. Therefore, the model solutions in the high conversion region are subject to certain degree of uncertainty.

All of the figures presented here were plotted in such a way that the full behavior of the mathematical model could be observed. In other words, the plotting range was made as wide as possible to capture a complete picture of the process behavior. Therefore, in certain situations, the continuation package produces results that, while mathematically acceptable, are not physically feasible. It is also important to keep in mind that finding the right operating region was highly challenging. Many times, interesting hysteresis behavior of the model was found in unrealistic operating regions. The interested reader is referred to Figure C.1 in Appendix C for one such example. Here, it is clear that the system has input and output multiplicity but in very low feed stream temperature which is acceptable mathematically but not in practice. Similar observation has been found for Figure C.2 when the system operated at 15 min residence time.

The set of reactor operating conditions at the nominal operating point, as well as the physical properties of the reaction mixture are listed in Table 4.4. The list of cases covered in this work showing primary and secondary bifurcation parameters can be found in Table 4.5.

Table 4.4: Reactor operating conditions and physical properties

Parameters	Values	Units
Monomer feed stream concentration	8.377	mol/L
Nitroxide radical (TEMPO) feed stream concentration	0.0432	mol/L
Initiator feed stream concentration (BPO)	0.036	mol/L
Feed stream temperature	403.15	K
Cooling water flow rate	0.022	L/s
Cooling water feed temperature	293.15	K
Reactor volume	10	L
Cooling jacket volume	1	L
Jacket heat transfer coefficient	80.228	J/m ² sK
Jacketed heat transfer area	0.195	m ²
Heat of polymerization ($-\Delta H_R$)	68040	J/mol
Heat capacity of reaction mixture	1647.27	J/(kg K)
Heat capacity of coolant	4045.7	J/(kg K)
Density of reaction mixture	0.952	kg/L
Density of cooling water	1	kg/L

Table 4.5: Selection of bifurcation parameters

Main bifurcation parameters	Secondary bifurcation parameters	Figure numbers
Coolant flow rate	Feed stream temperature	Figure (4.2)
	Residence time	Figure (4.3)
	[TEMPO]/[BPO] ratio	Figure (4.4)
Feed stream temperature	Coolant flow rate	Figure (4.5)
	Residence time	Figure (4.6)
	[TEMPO]/[BPO] ratio	Figure (4.7)
Residence time	Feed stream temperature	Figure (4.8)
	Coolant flow rate	Figure (4.9)
	[TEMPO]/[BPO] ratio	Figure (4.10)
Initiator feed stream concentration	Feed stream temperature	Figure (4.11)
	Coolant flow rate	Figure (4.12)
	Residence time	Figure (4.13)
TEMPO feed stream concentration	Feed stream temperature	Figure (4.14)
	Coolant flow rate	Figure (4.15)
	Residence time	Figure (4.16)

4.5.1 The Effect of Coolant Flow Rate as a Main Bifurcation Parameter

The steady state bifurcation behavior of the bimolecular styrene NMRP model was analyzed with coolant flow rate as the main bifurcation parameter and the feed stream temperature, residence time, and [TEMPO]/[BPO] ratio, respectively, as secondary bifurcation parameters.

The steady state bifurcation behavior is shown in Figure 4.2, with the coolant flow rate as the main bifurcation parameter and the feed stream temperature as the secondary parameter. The reactor shows typical hysteresis behavior for the monomer conversion and reactor temperature. In addition, both input and output multiplicities are observed for the TEMPO conversion, molecular weights, polydispersity index (PDI), and jacket temperature.

As mentioned before from a practical perspective, the most interesting conversion regions is the medium conversion region. It is clear from analyzing the monomer conversion profile in Figure 4.2 that, in this region, the reactor operates at open-loop unstable steady state conditions. As reported in previous work done by Russo and Bequette (1992), in such systems this behavior could lead to process control difficulties.

The steady state profiles of the TEMPO conversion, PDI, molecular weights, respectively, exhibit interesting bifurcation behavior unlike the profiles of the initiators and monomers. These profiles show significant changes depending on the magnitude of the coolant flow rate. For example, the number averaged molecular weight (NAMW) first increased with increasing coolant flow rate. However, a significant decreasing trend in NAMW was observed after a certain flow rate threshold was attained. This behavior can have a significant impact on the operation of the reactor in an industrial setting. The steady state behavior of these variables for jacketed continuous stirred tank reactors has not been widely studied in the literature. Comparing our results with the previous work done by Roberto et al. (2006) on the unimolecular styrene nitroxide mediated radical polymerization in CSTR, clearly their system has similar behavior for molecular weights. However, when Russo and Bequette (1998) analyzed their work on the steady state multiplicity features of styrene polymerization in continuous stirred tank reactor, they reported that the behavior of the molecular weights was considerably different from the one found in our work, because in the latter no closed trajectories were found.

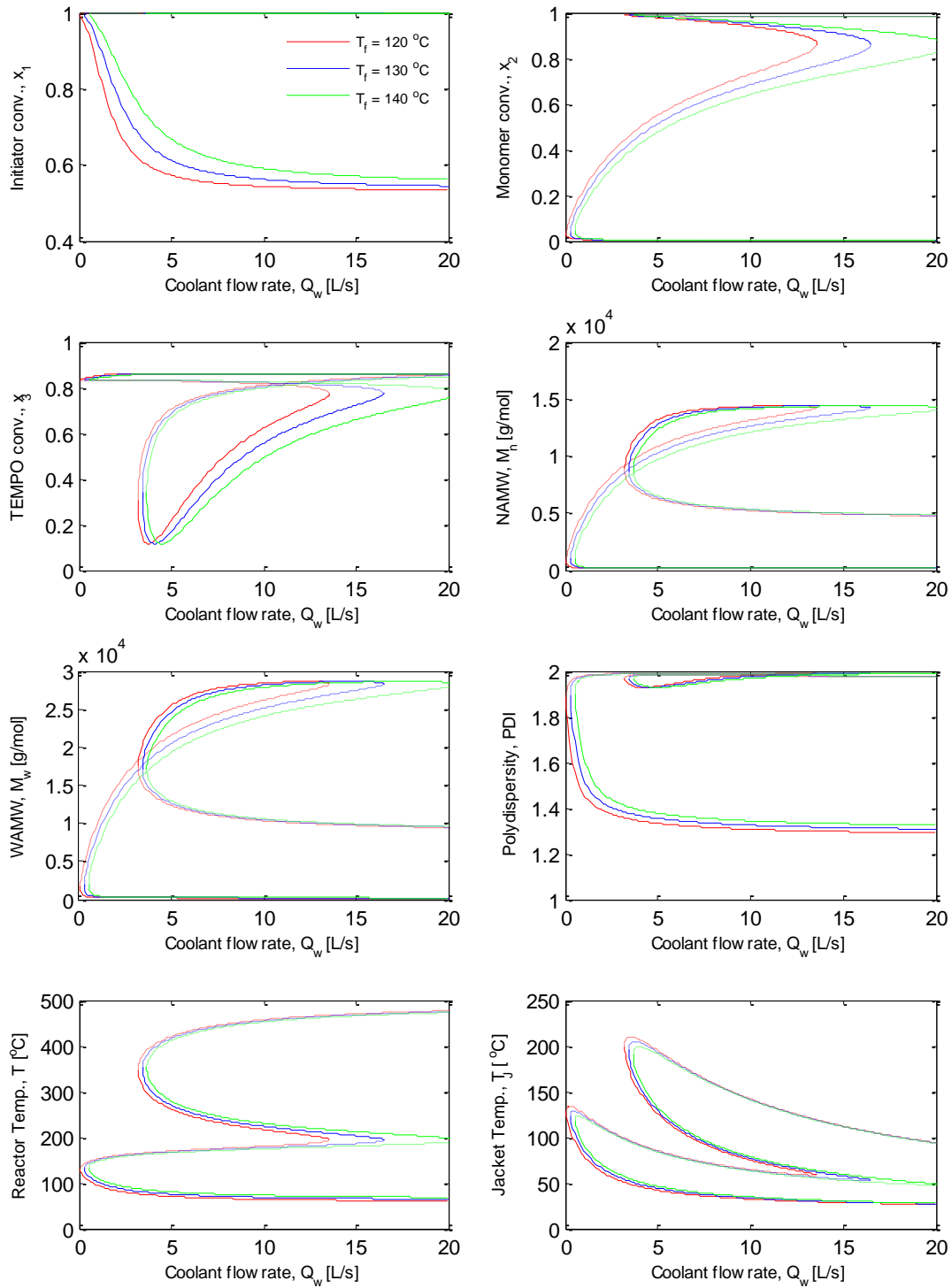


Figure 4.2: Bifurcation diagrams with coolant flow rate as the main bifurcation parameter and feed stream temperature as the secondary bifurcation parameter. The stable solutions are plotted with solid lines (—) and the unstable solutions with dashed lines (---)

Referring to Figure 4.2, the PDI has values between 1.3 and 2. For living radical polymerizations, polydispersities must not be higher than 1.4 to 1.6, so the reactions can be considered as living reactions. Looking at the PDI profile in Figure 4.2, it can be seen that manipulating the feed stream temperature in the region belonging to medium conversion conditions will never take the PDI below 1.9.

Practical results can be found by analyzing the plots for reactor temperature and the jacket temperature; it is possible to see that the (most interesting) medium conversion branch appears when both the reactor temperature and the jacket temperature present input and output multiplicities. Also, it is interesting to note that if the feed stream temperature increases, the monomer conversion within the reactor decreases, as well as the conversion of TEMPO, leading to higher rates of propagation and, thus, a higher heat generation, making the heat transfer duty of the reactor insufficient. Furthermore, when the feed stream temperature increases, the number and weight average molecular weight decreases. In fact, the PDI, reactor temperature as well as the jacket temperature did not change their behavior by increasing the feed stream temperature.

There are some good reasons for studying the steady state behavior of the reactor with the feed stream temperature in the range of 120 to 140°C. In one hand, living radical polymerization takes place only at temperatures around 120°C and higher so that 120°C is the lower limit. On the other hand; choosing 140°C to be the upper limit has some reasons; first, when a higher feed stream temperature embeds into the process stream a considerably higher thermal load and heat transfer difficulties arise. Second, this increment in the feed stream temperature will lead to an increase in the reaction rates, including the propagation step, giving rise to a higher release of heat. Third, operating under high temperature regions causes high viscosity problems, even if this problem did not arise, the limitation could be that the conversions and PDI are reached at very high reactor temperature regions (above 180°C). This PDI belongs to regions where the molecular weights are quite low, thus limiting the applicability range of the process for different polymer qualities. Finally, at such regions, the cooling water on the jacket side becomes heated quickly, getting prone to evaporate, bringing complications to the heat exchange system due to the phase change (Roberto et al., 2006).

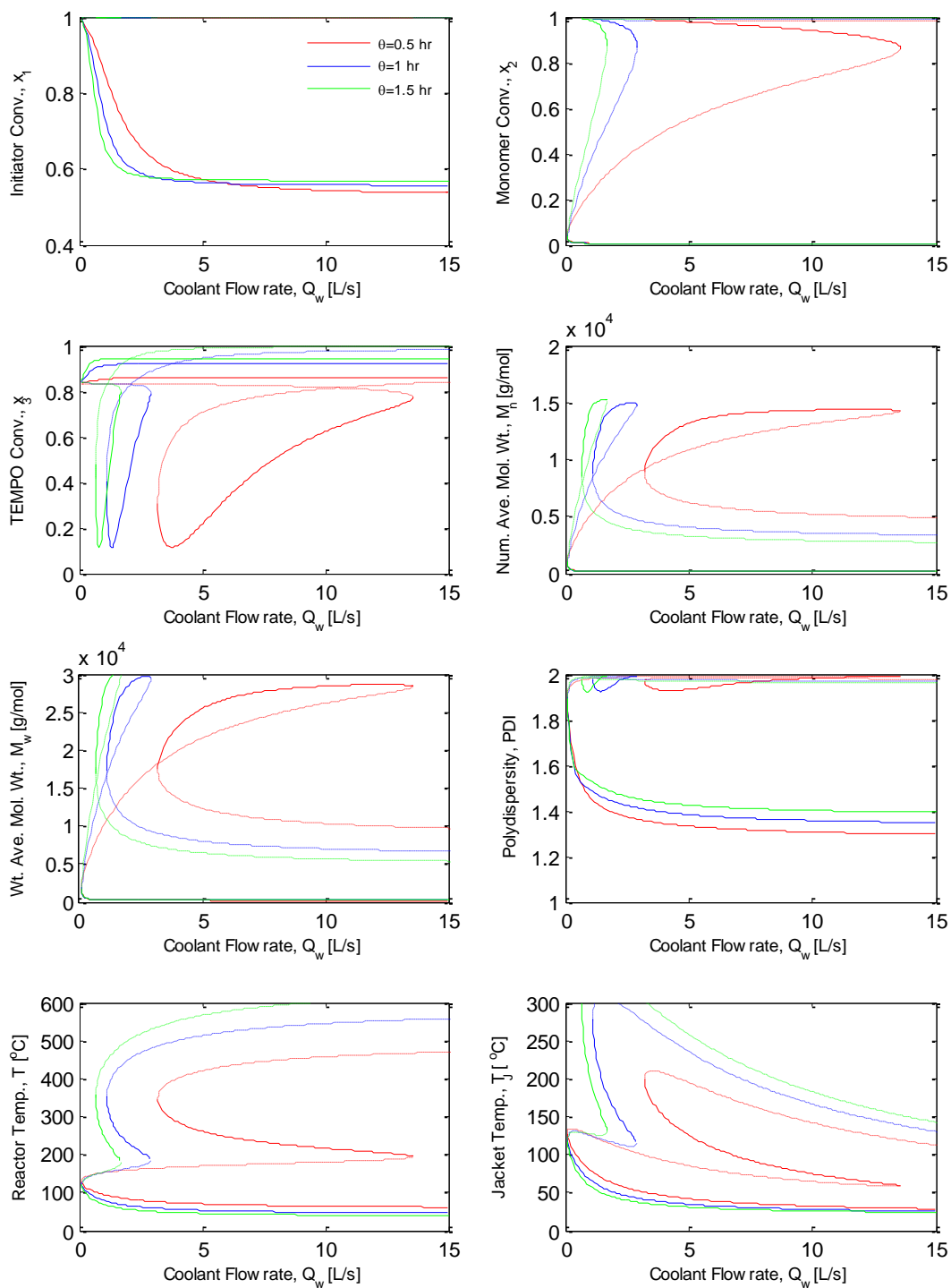


Figure 4.3: Bifurcation diagrams with coolant flow rate as the main bifurcation parameter and residence time as the secondary bifurcation parameter. The stable solutions are plotted with solid lines (—) and the unstable solutions with dashed lines (---)

Figure 4.3 shows the steady state bifurcation behavior when the coolant flow rate is the main bifurcation parameter and the residence time is the secondary parameter. In this case, the reactor operating condition shows the typical hysteresis behavior for the monomer conversion and reactor temperature. In contrast, both input and output multiplicities are observed for the TEMPO conversion, molecular weights, PDI, and jacket temperature.

The steady state profile shows that increasing the residence time does not affect the initiator conversion significantly since the profiles are essentially overlapping. Looking at the monomer conversion profile, it can be seen that, in this case, a wide range of conversions from 0.1 to 0.9 can be obtained from the mid-branch of the diagram, where the steady states are open-loop unstable. Similar to the results obtained in Figure 4.2, the profiles of the TEMPO conversion, molecular weight, and PDI show both increasing and decreasing trends. In addition, each of these profiles are self-intersecting curves, i.e., they intersect themselves at different points. For the TEMPO conversion profile, wide range of conversions from 0.2 to 0.8 can be obtained in which both open-loop stable and unstable segments exist.

Furthermore, the highest values for the number and weight average molecular weights appear to be reached at the second intermediate conversion stable branch of the steady state curves. However, lower molecular weights values around 1×10^4 g/mol can be achieved on the high monomer conversion branch. In this case, high PDI values, close to 2, were again found.

It is useful to identify the 'best' operating region from the bifurcation diagram. One can admit that 0.5 hr residence time is the best value because it gives a wider range for the coolant flow rate as it is clear in all plots. Furthermore, the medium conversion branch has a wide range, for this segment the number and weight average molecular weights can reach its highest values as well as acceptable reactor and jacket temperatures, but a quite high PDI values found for this branch. Obviously, the high conversion branches are not considered in this analysis because the reactor temperature conditions are not physically realizable.

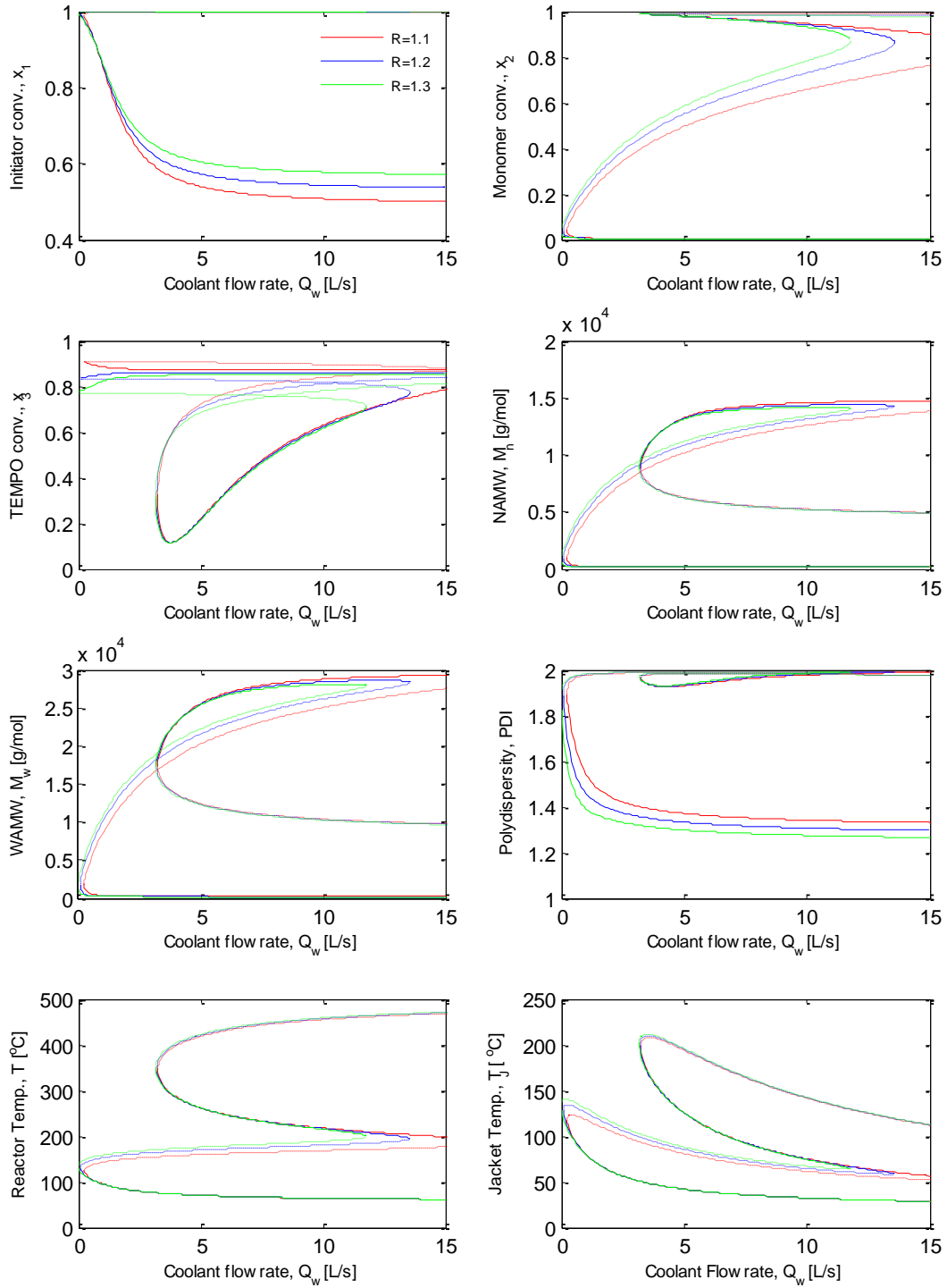


Figure 4.4: Bifurcation diagrams with coolant flow rate as the main bifurcation parameter and ratio $R=[\text{TEMPO}]/[\text{BPO}]$ as the secondary bifurcation parameter. The stable solutions are plotted with solid lines (—) and the unstable solutions with dashed lines (---)

Figure 4.4 shows the steady state bifurcation behavior when the coolant flow rate is the main bifurcation parameter and $[\text{TEMPO}]/[\text{BPO}]$ ratio is the secondary parameter. Again, similar hysteresis behavior for the monomer conversion and reactor temperature were observed; whereas the TEMPO conversion, molecular weights, PDI, and jacket temperature demonstrate both input and output multiplicities. Furthermore, visible self-intersecting curves behavior appears for TEMPO conversion, molecular weights and PDI.

Without a doubt, increasing the $[\text{TEMPO}]/[\text{BPO}]$ ratio did not affect the behavior of the system especially for the reactor and jacket temperatures; while a slight difference appeared in the second segment of the monomer conversion plot as it increases by increasing the $[\text{TEMPO}]/[\text{BPO}]$ ratio. Here the initiator has got a high conversion in the first segment. Obviously, the unstable segment of the monomer conversion plot starts from 0.1 to 0.8, whereas the TEMPO conversion self-intersecting curves is in the range from 0.1 to 0.8 which has both the stable and unstable segments.

Looking at the number and weight average molecular weight profiles, for the number average molecular weight the self-intersecting curves is from 1×10^4 to 1.5×10^4 (g/mol) whereas the weight average molecular weight self-intersecting curves range from 2×10^4 to 3×10^4 (g/mol). For both plots, low values of number and weight average molecular weight can be achieved as the monomer conversion increases. Furthermore, for the molecular weights lines overlap at the high monomer conversion segments, this indicates that the selected nominal value of $[\text{TEMPO}]/[\text{BPO}]$ ratio to be 1.2 is logical. Furthermore, to be more realistic the operating region has been inspected, one need to look at the medium conversion line in all of the plots, although it represents the unstable steady state but all the operating conditions are applicable in the real process accept the high values of PDI which has the value of 1.9 to 2.

4.5.2 The Effect of Feed Stream Temperature as a Main Bifurcation Parameter

In this part, we will analyze the behavior of our model when the feed stream temperature is the main bifurcation parameter and secondary parameters are coolant flow rate, residence time and $[\text{TEMPO}]/[\text{BPO}]$ ratio, respectively.

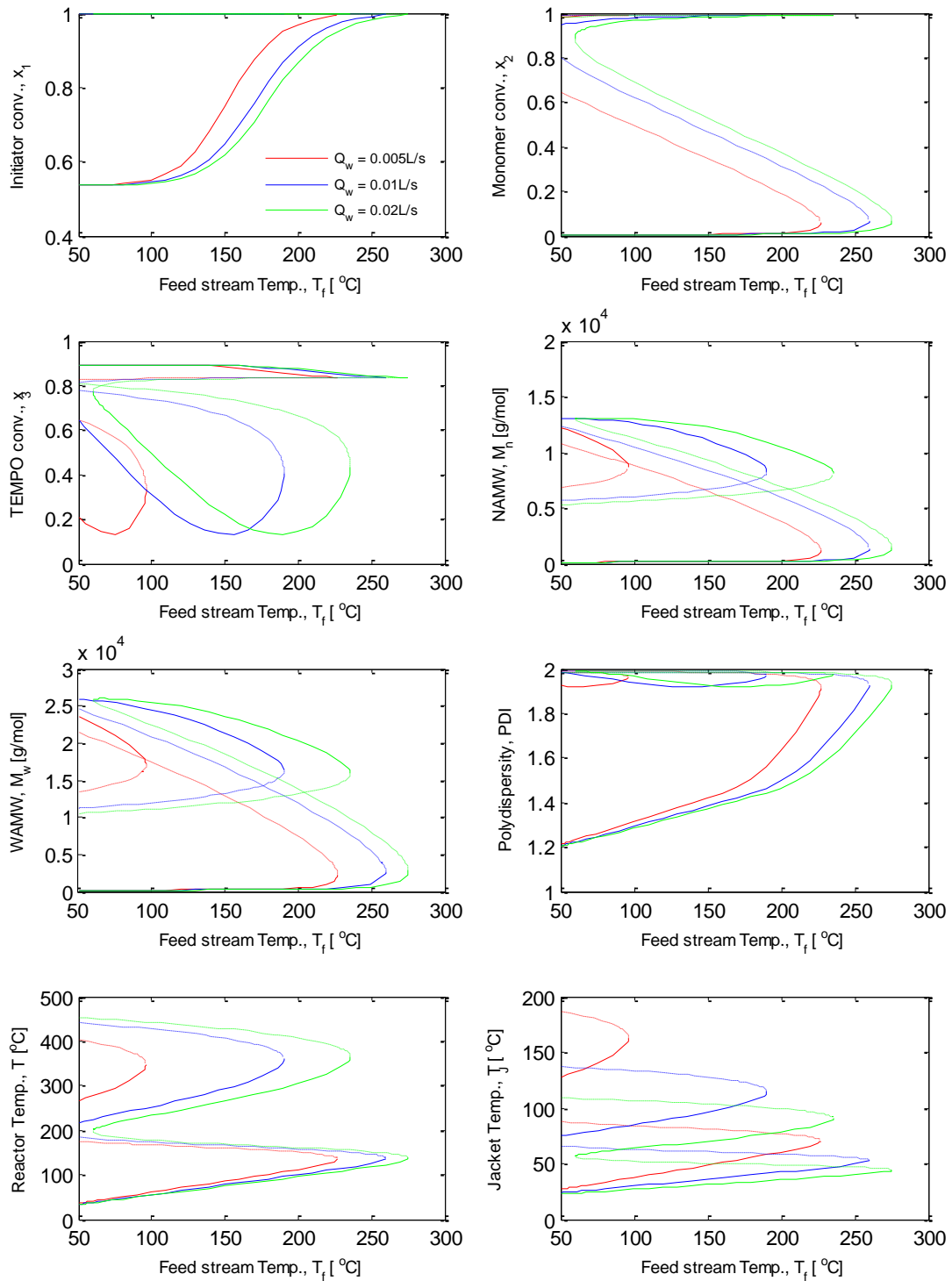


Figure 4.5: Bifurcation diagrams with feed stream temperature as the main bifurcation parameter and coolant flow rate as the secondary bifurcation parameter. The stable solutions are plotted with solid lines (—) and the unstable solutions with dashed lines (---)

Figure 4.5 shows the steady state bifurcation behavior of the CSTR when the feed stream temperature is the main bifurcation parameter and coolant flow rate is the secondary parameter. In this case, the monomer conversion increases by increasing the coolant flow rate. The system again has the typical hysteresis behavior for the monomer conversion and reactor temperature while the TEMPO conversion, molecular weights, PDI, and jacket temperature show both input and output multiplicities just as in the previous cases.

From an operational perspective, at this point, it is worth mentioning that the most reasonable operating range was plotted. Focusing on the monomer conversion plot, at high coolant flow rates, the system displays four segments, but when the coolant flow rate decreases to the value of 0.005L/s, the system displays only two segments whereas the other segments are in the 0-like disjoint region.

Russo and Bequette (1998) reported that when a continuation diagram passes through regions where the distinguished parameter takes unfeasible values in this case. It is said that the diagram has a 0-disjoint bifurcation. For better clarification, the reader is referred to Figure C.1 where the behavior of the model is plotted in the disjoint region. From this figure one can see the full profile of the model but we admit that it is impractical to run the process under such low temperature. However, at the higher coolant flow rate, 0.02L/s, it is clear to see that all the segments of the model appear in the feasible range.

As in the prior cases, the initiator conversion reaches high conversion from the beginning, while the TEMPO conversion exhibits self-intersecting curves ranging from 0.2 to 0.8. Now when analyzing the molecular weights and the PDI profiles, it can be seen that the values of the molecular weights are acceptable but the PDI has got a quite high values for the medium monomer conversion.

Looking at the reactor and jacket temperature plots, the 0-like disjoint region is clear here also as well as increasing the coolant flow rate helped to shift from the unfeasible region to the feasible region. Furthermore, for the medium monomer conversion, both the reactor and jacket temperatures have got acceptable values because it is always preferable to work when the reactor

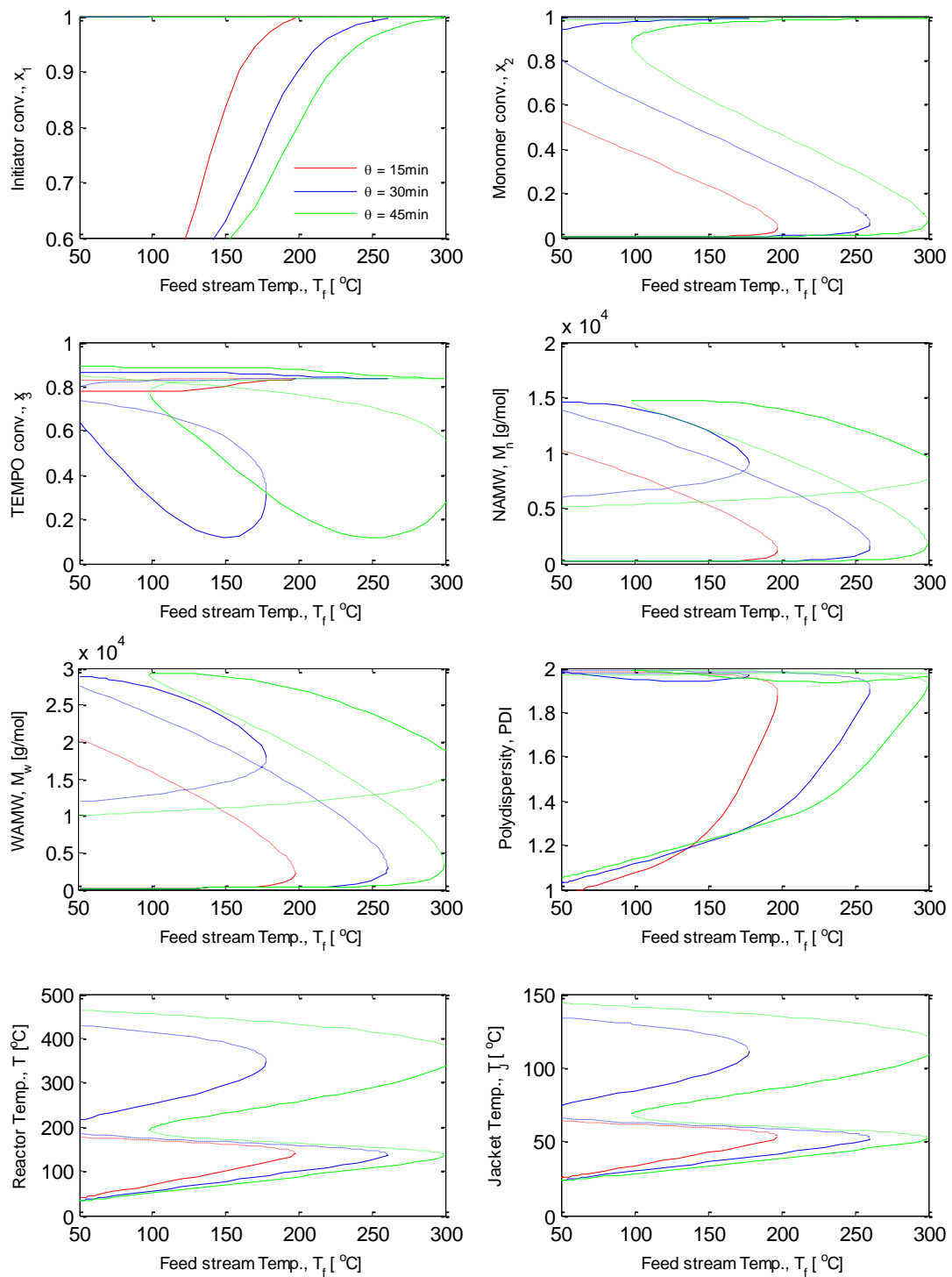


Figure 4.6: Bifurcation diagrams with feed stream temperature as the main bifurcation parameter and residence time as the secondary bifurcation parameter. The stable solutions are plotted with solid lines (—) and the unstable solutions with dashed lines (---)

temperature is less than 180 °C and jacket temperature less than 100 °C since coolant fluid used here is water so we have to avoid phase changing (evaporation) which could cause operating problems.

Looking at the steady state bifurcation behavior when the feed stream temperature is the main bifurcation parameter and residence time is the secondary parameter shown in Figure 4.6. Here it is important to pay attention to the residence time range. Obviously, when the residence time is 15 min, the model show only two segments and again the other segments are in the 0-like disjoint region, see Figure C.2 for more details. It is clear that when the residence time increases the gap between the medium and the high conversion branches increases, displacing the medium conversion branch to regions where the feed temperature is more realistic for practical purposes.

As in the previous case, the NMRP of styrene model exhibit hysteresis behavior for the monomer conversion and reactor temperature whereas both input and output multiplicities is the behavior for the TEMPO conversion, molecular weights, PDI, and the jacket temperature; however, in this case the TEMPO conversion, molecular weights and PDI exhibits self-intersecting curves. Although the input and output multiplicities is the behavior for the number and weight average molecular weights, both have achieved acceptable values. Again here the PDI has values above 1.9.

Moreover, it is interesting to note that for the right operating region where the medium monomer conversion occurs; it is clear to see from analyzing the monomer conversion plot that the medium conversion exhibit unstable steady state behavior in the range of 0.1 to 0.8. The reactor and jacket temperatures show acceptable values for the second segment because the maximum value for the reactor temperature is about 180°C and the jacket temperature for the same segment has a value less than 75°C.

In the last part of this section, the steady state bifurcation behavior when the feed stream temperature is the main bifurcation parameter and [TEMPO]/[BPO] ratio is the secondary parameter has been analyzed as shown in Figure 4.7. Here it is possible to say that increasing the [TEMPO]/[BPO] ratio did not affect the performance of the model. In this case the model has hysteresis behavior for the monomer conversion, jacket and reactor temperatures whereas the

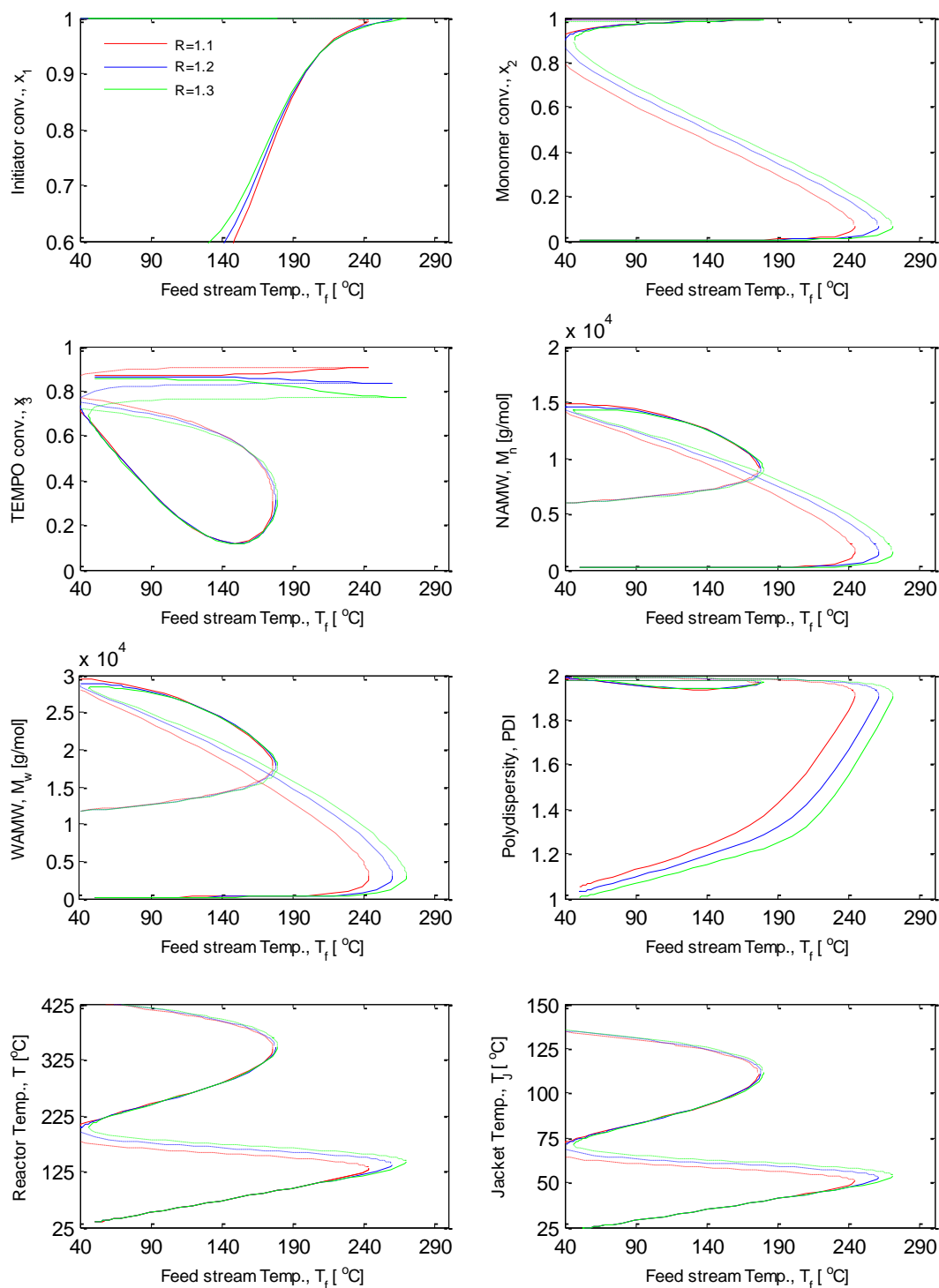


Figure 4.7: Bifurcation diagrams with feed stream temperature as the main bifurcation parameter and ratio $R = [\text{TEMPO}]/[\text{BPO}]$ as the secondary bifurcation parameter. The stable solutions are plotted with solid lines (—) and the unstable solutions with dashed lines (---)

TEMPO conversion, molecular weights and PDI demonstrate input and output multiplicities as well as self-intersecting curves. Also, in the initiator conversion plot all the lines are overlapping and have got to the high conversion fast.

Looking at the monomer conversion profile, one can report that at the lower [TEMPO]/[BPO] ratio the monomer conversion is less than the other ratios and by increasing the [TEMPO]/[BPO] ratio the system moved slightly to better operating region which indicates that for lower [TEMPO]/[BPO] ratio such as 0.9 or even less, the system will definitely shift back to the 0-like disjoint region. However, increasing the [TEMPO]/[BPO] ratio did not affect the behavior of TEMPO conversion, molecular weights, PDI, as well as the reactor and jacket temperatures.

The number average molecular weight has values between 0.25×10^4 to 1.5×10^4 (g/mol) for the second segment, but lower values can be reached in the last segment that which represents the high monomer conversion branch. Same situation holds for the weight average molecular weight with values between 0.25×10^4 to 3×10^4 (g/mol) for the second segment whereas lower values (around 1.25×10^4 g/mol) can be achieved for the last segment. In this case, again the same noticeable high value for the PDI appears.

4.5.3 The Effect of Residence Time as a Main Bifurcation Parameter

Interesting results appears when using the residence time as main bifurcation parameter and secondary parameters are feed stream temperature, coolant flow rate and [TEMPO]/[BPO] ratio, respectively. Looking at the steady state bifurcation behavior of the model in Figure 4.8 when the residence time is the main bifurcation parameter and the feed stream temperature is the secondary parameter, one can tell that the monomer conversion, molecular weights, reactor and jacket temperature show typical hysteresis behavior whereas the plots of TEMPO conversion and PDI show input and output multiplicities as well as self-intersecting curves.

Obviously, increasing the feed stream temperature did not affect the behavior of the system especially for the initiator conversion; however, at feed stream temperature 120°C there is wider residence time range for all the plots. Moreover, increasing the feed stream temperature value

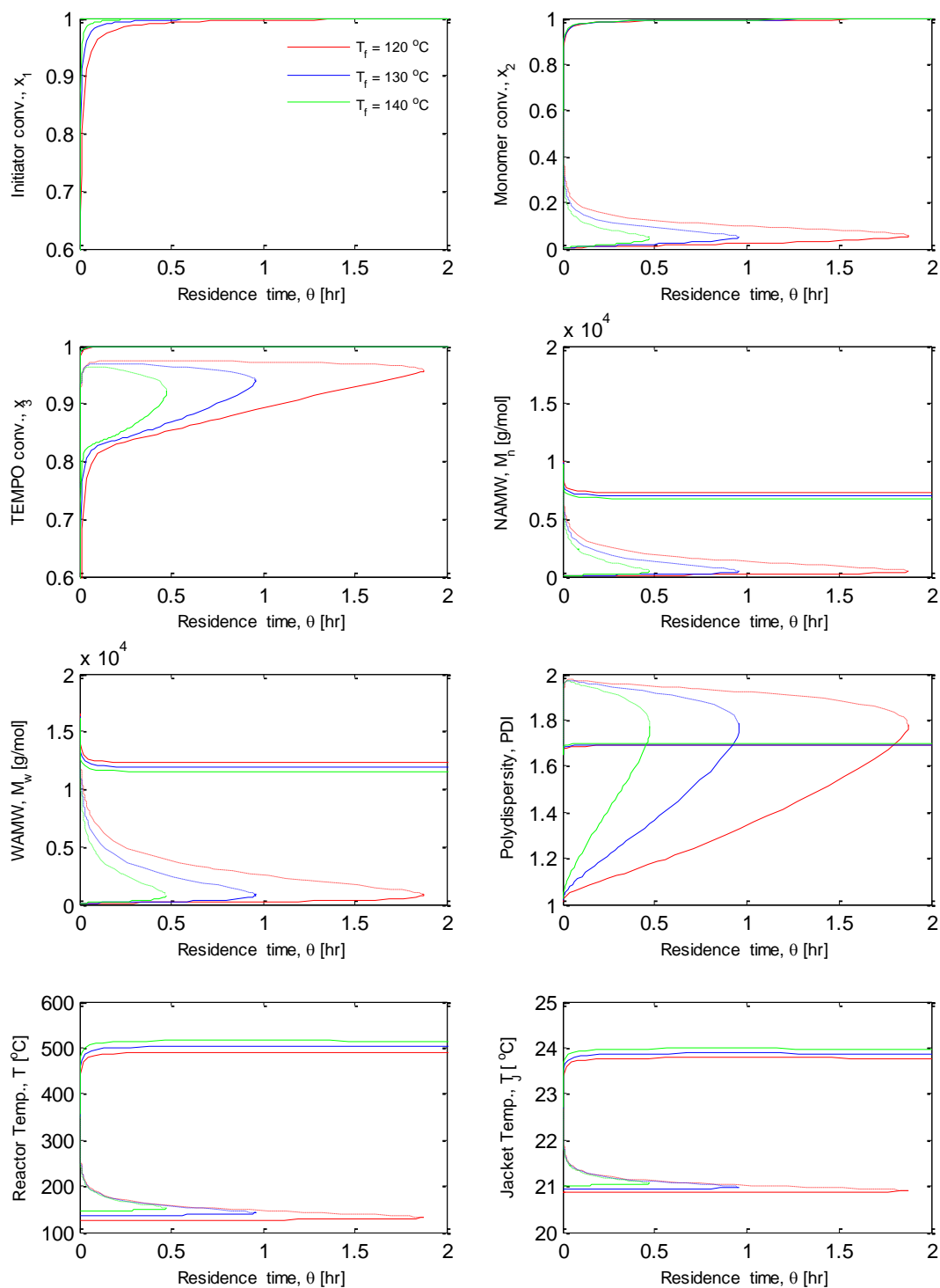


Figure 4.8: Bifurcation diagrams with residence time as the main bifurcation parameter and feed stream temperature as the secondary bifurcation parameter. The stable solutions are plotted with solid lines (—) and the unstable solutions with dashed lines (---)

caused to have lower monomer conversion for the same residence time this appears because the reaction is exothermic and its progress is favored by lower inlet temperatures. Moreover, this behavior has some interesting implications; for example, it can be seen from the monomer conversion plot that it is possible to achieve any desired value for this variable with considerably low residence times. However, these results must be taken with care because it is possible to see that such low residence times are in the order of a few minutes so these results could be somewhat inexact. This situation holds for the molecular weights, PDI, and both temperatures as well. In this case, the self-intersecting curves behavior for the TEMPO conversion is in the range of 0.8 to 0.95 that which includes both of the stable and unstable segments.

It is important to keep in mind that there is no correlation for the gel effect has been used in the mathematical model, so that some inaccuracy in the high conversion region results should be expected as it can be seen in the reactor temperature plot, it is not practical to operate the reactor under 450°C because the acceptable operating temperature should lay inside the range between 120 and 180°C. In contrast, acceptable operating jacket temperature for the high conversion region can be achieved. It is interesting to note that the number and weight average molecular weights profiles have low values for the medium conversion segment. The maximum value one can get for both number and weight average molecular weights is less than (1.5×10^4 g/mol). Finally, not like the former cases, the PDI has got lower values, around 1.7, for high conversion region.

At this point it is worthwhile to compare our work when the residence time is the main bifurcation parameter and the feed stream temperature is the secondary parameter with previous work has been done by Roberto et al. (2006) on the unimolecular nitroxide mediated radical polymerization of styrene in CSTR. Clearly, their system have different behaviors, the reason for the discrepancy is in their work all the plots for monomer conversion, molecular weights, PDI as well as both temperatures show input output multiplicities in such a way that makes the curves to have a mushroom like shape.

Figure 4.9 shows the steady state bifurcation behavior when the residence time is the main bifurcation parameter and the coolant flow rate used as the secondary parameter. Clearly, increasing the coolant flow rate did not affect the results as all the lines are overlapping in a way

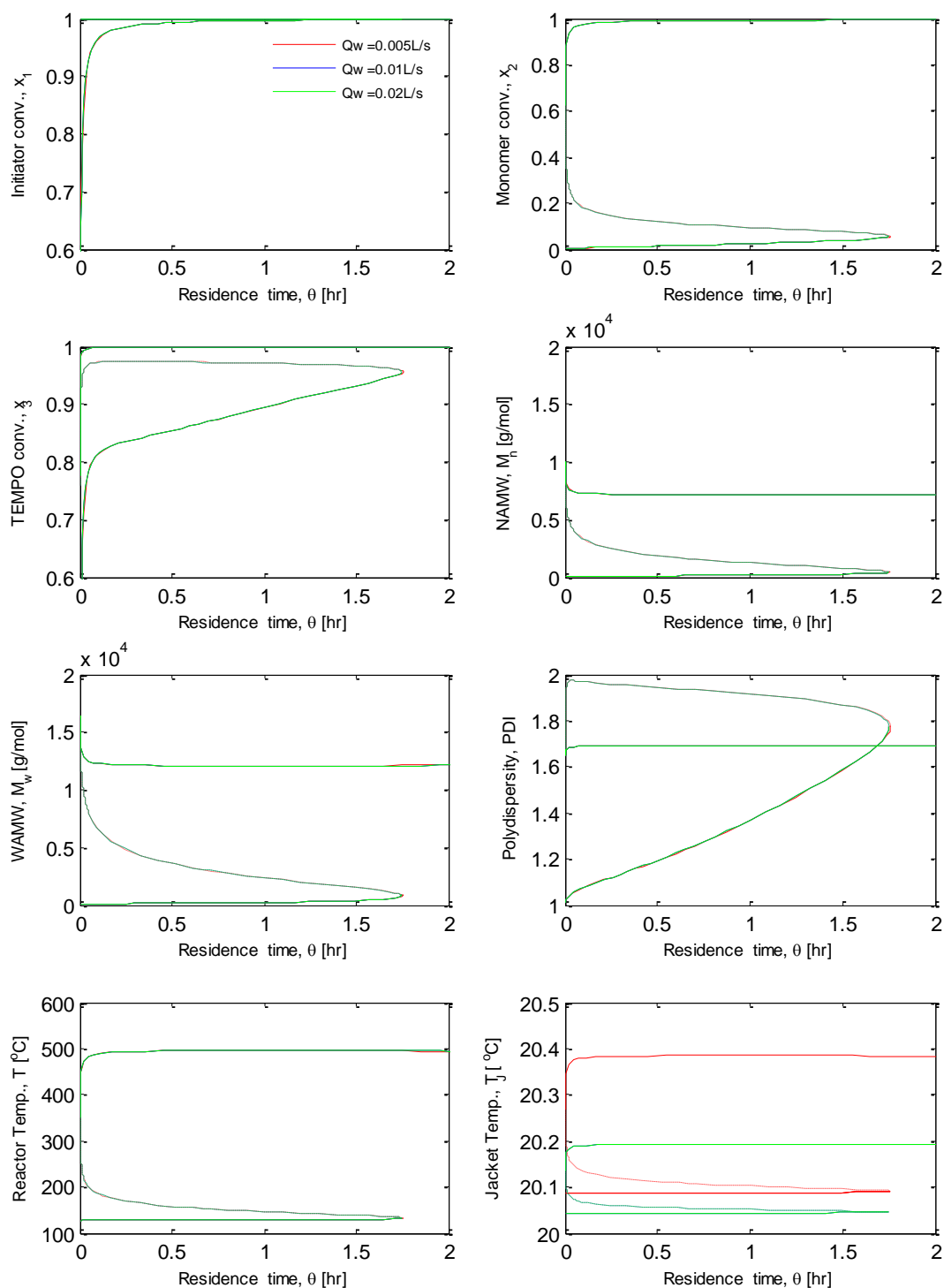


Figure 4.9: Bifurcation diagrams with residence time as the main bifurcation parameter and coolant flow rate as the secondary bifurcation parameter. The stable solutions are plotted with solid lines (—) and the unstable solutions with dashed lines (---)

that it looks like there is one line only. This situation holds for all the plots except the jacket temperature as it decreases by increasing the coolant flow rate.

Observably, the initiator conversion has got its high conversion from the first minutes whereas the hysteresis behavior is the behavior for the monomer conversion, TEMPO conversion, molecular weights, reactor and jacket temperature except the PDI which show self-intersecting curves as well as input and output multiplicities.

In this case, the TEMPO conversions self-intersecting curve ranges from 0.65 to 0.95 which includes the stable and unstable branches. In addition, the number and weight average molecular weights profiles show that as the monomer conversion increases, the molecular weight increases to a maximum value of 1.5×10^4 g/mol. Moreover, the self-intersecting curves behavior for the PDI in this case is between 1.7 and 2, as it can be seen the medium conversion branch has got the PDI value close to 2 while the situation changes in the high conversion branch as the PDI decreases to a value close to 1.7. Also, the jacket temperature plot show acceptable values even in the high conversion branch as the highest jacket temperature value reported here is around 20.4°C. However, the reactor temperature shows unrealistic values in the high conversion branch.

The last part of this section is to analyze Figure 4.10, in which the steady state bifurcation behavior described when the main bifurcation parameter is the residence time and the secondary parameter is the [TEMPO]/[BPO] ratio. In this case the monomer conversion, molecular weights as well as the reactor and the jacket temperatures demonstrate typical hysteresis behavior whereas the output multiplicity is the case for TEMPO conversion and just as the previous cases the PDI show self-intersecting curves as well as input and output multiplicities. Clearly, wider ranges for the residence time can be achieved when increasing the [TEMPO]/[BPO] molar ratio; however, the desired value for the monomer conversion can be achieved with considerably low residence times. The same situation holds for the TEMPO conversion profiles. Low number and weight average molecular weight values are reported in this case with a maximum value of 1.5×10^4 g/mol for the weight average molecular weight and 1×10^4 g/mol for the number average molecular weight. However, there is a quite high value for PDI appears in the medium conversion branch around 1.95. Finally, from analyzing the reactor temperature profile

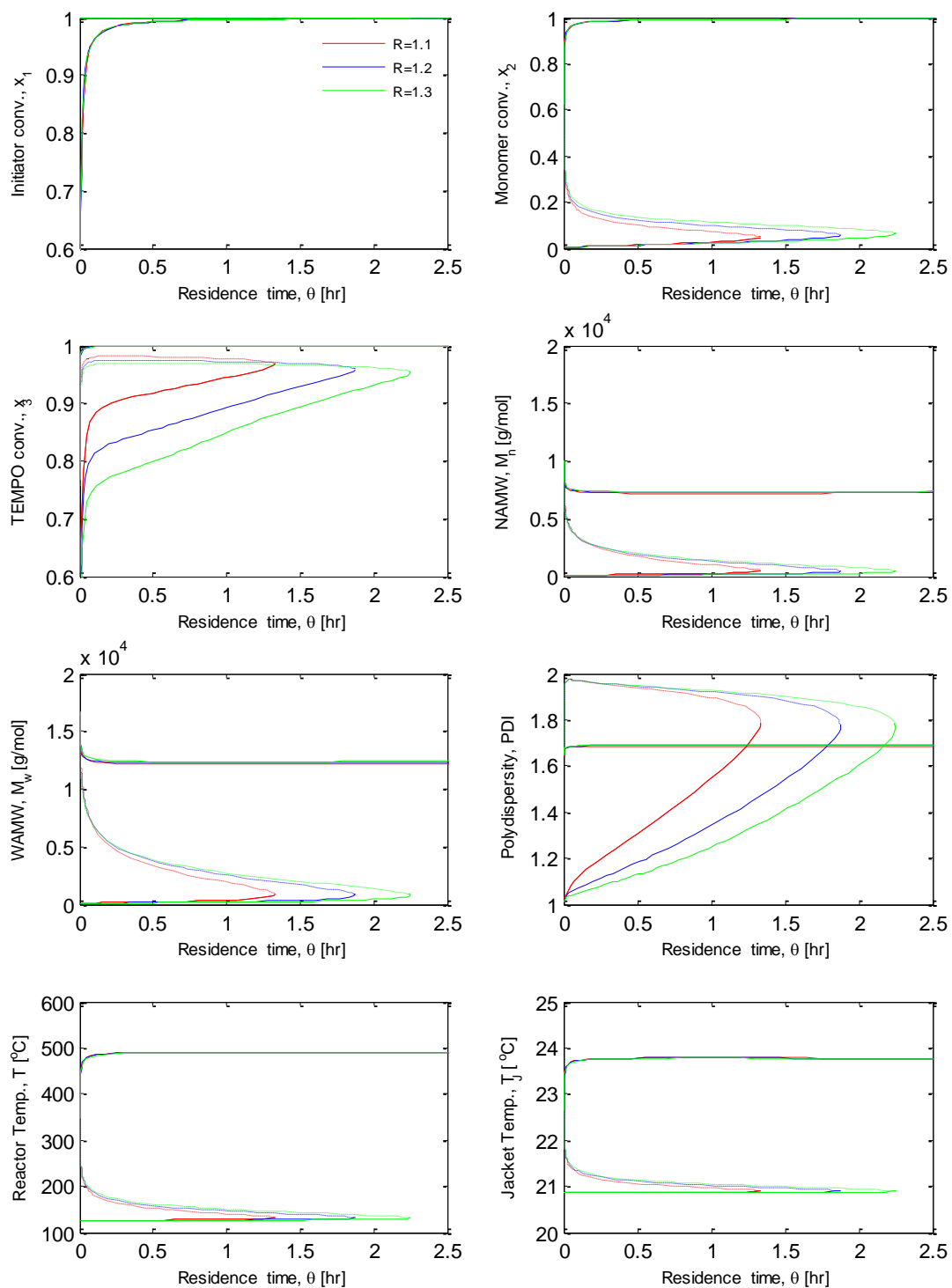


Figure 4.10: Bifurcation diagrams with residence time as the main bifurcation parameter and $[\text{TEMPO}]/[\text{BPO}]$ ratio as the secondary bifurcation parameter. The stable solutions are plotted with solid lines (—) and the unstable solutions with dashed lines (---)

for this case, unrealistic high temperature values has been found for the high conversion branch whereas acceptable jacket temperature has been reported with the maximum value of 23.5°C for the high conversion branch.

4.5.4 The Effect of Initiator Feed Stream Concentration as a Main Bifurcation Parameter

In this section the steady state bifurcation behavior of the mathematical model has been analyzed when the initiator feed stream concentration are the main bifurcation parameter and the feed stream temperature, coolant flow rate, and the residence time as secondary parameters, respectively. The system has a qualitative behavior different from the ones shown in previous cases and for the mentioned cases there is no reference available for result comparison.

Figure 4.11 show the steady state bifurcation behavior when the initiator feed stream concentration is the main bifurcation parameter and the feed stream temperature is the secondary parameter. For the first time the initiator concentration exhibit both input and output multiplicities; nevertheless, the same situation holds for the TEMPO conversion, molecular weights and PDI but with expressing self-intersecting curve behavior also. However, the monomer conversion, reactor and jacket temperatures demonstrate the typical hysteresis behavior. As the feed stream temperature rises, a lower initiator feed stream concentration is required to achieve the same monomer conversion; however there is a slight difference between the lines at the medium conversion branch.

Now, the monomer conversion profile shows the medium conversion segment in the range of 0.2 to 0.9. Also, interesting results can be found when analyzing the TEMPO conversion, as it can be seen that the medium conversion branch starts from 0.15 and ends at 1. Also, all the lines are overlapping in the same segment. The self-intersecting curves behavior for the molecular weights has both stable and unstable segments. The self-intersecting curves in the number average molecular weight plot are in the range of 1.25×10^4 to 2×10^4 g/mol. Here again, low number average molecular weight can be achieved in the high conversion branch. The same situation holds for the weight average molecular weight but within the range of 2.5×10^4 to 4×10^4 g/mol.

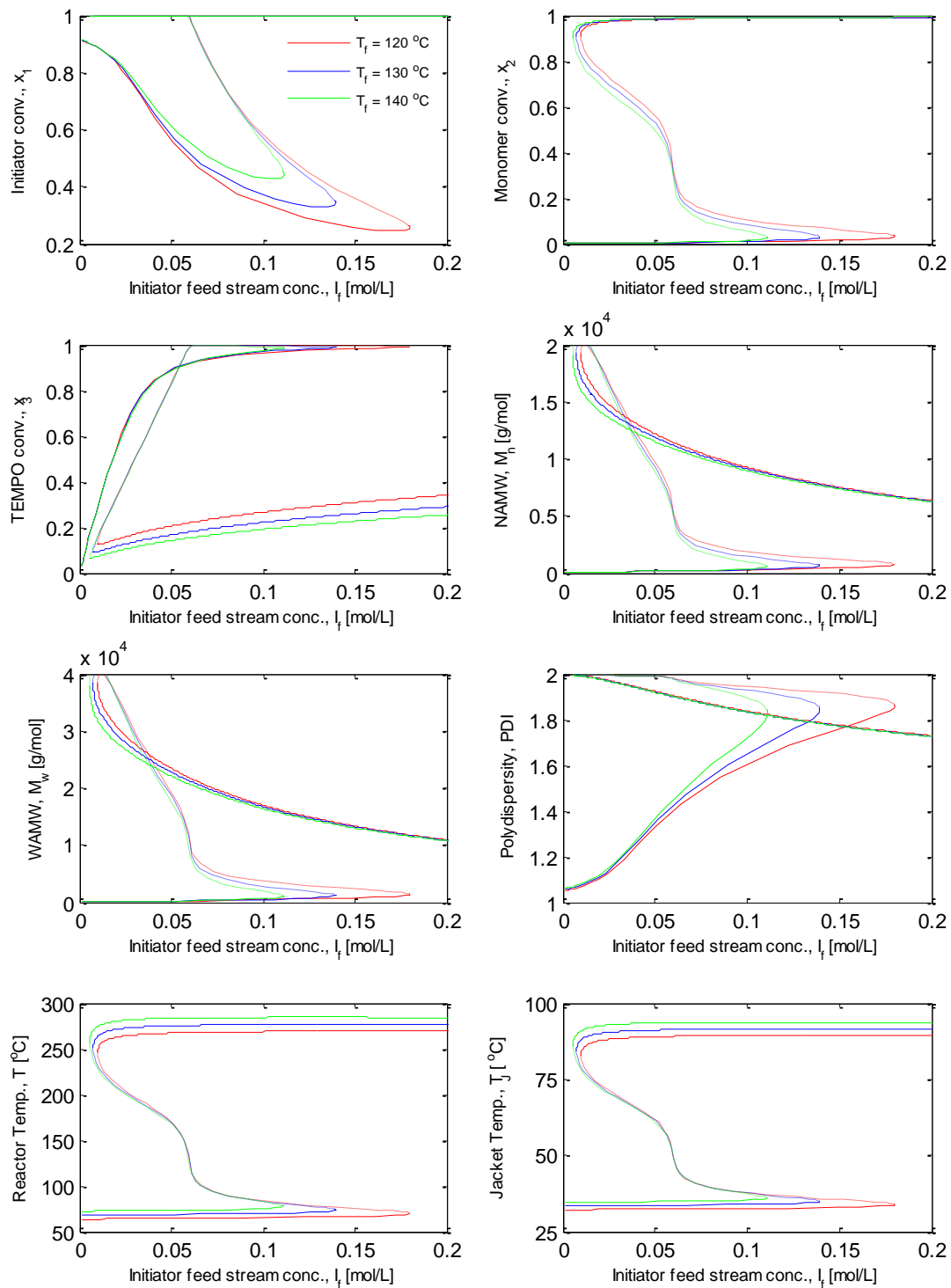


Figure 4.11: Bifurcation diagrams with initiator feed stream concentration as the main bifurcation parameter and feed stream temperature as the secondary bifurcation parameter. The stable solutions are plotted with solid lines (—) and the unstable solutions with dashed lines (---)

Low weight average molecular weight value, close to 1×10^4 g/mol, can be achieved at the high conversion segment. Nevertheless, the PDI has a value close to 1.9 for the medium conversion branch, and then it decreases to 1.7 at the high conversion segment.

In one hand, the reactor temperature has acceptable operating values for most of the unstable branch; however, unrealistic values arise in the high conversion branch. On the other hand, the jacket temperature has acceptable values for the full profile. Furthermore, it can be seen that the lines are overlapping in the reactor and jacket temperature plots for the same medium conversion branch. Moreover, an interesting fact can be observed, there is obviously acceptable operating condition if one analyze the medium conversion branch but we should keep in mind that the PDI show high values in this case also.

If attention paid to Figure 4.12 that show the steady state bifurcation behavior when the initiator feed stream concentration is the main bifurcation parameter and the coolant flow rate is the secondary parameter. It appears that a higher initiator feed stream concentration is required to achieve the same monomer conversion as the coolant flow rate increases.

Clearly, the initiator conversion has got the input and output multiplicities behavior whereas the monomer conversion, reactor and jacket temperatures exhibit typical hysteresis behavior. The medium conversion segment is in a wide range of 0.1 to 0.9. Also, the reactor and jacket temperatures profiles have realistic results for the medium conversion branch, but unrealistic values appear for the high conversion branch of the lowest coolant flow rate 0.005L/s.

Furthermore, as it can be seen in the molecular weight plots that a noticeable behavior changes happened when the coolant flow rate raises, as at the lower value 0.005L/s, the model expresses self-intersecting curve as well as input and output multiplicities but the situation is different when increasing the coolant flow rate as the model here expresses output multiplicity behavior and the self-intersecting curve disappeared. This observation will lead us to think that for lower values of the coolant flow rate the system might shift to the 0-like disjoint region and this behavior might be a start formation for isola.

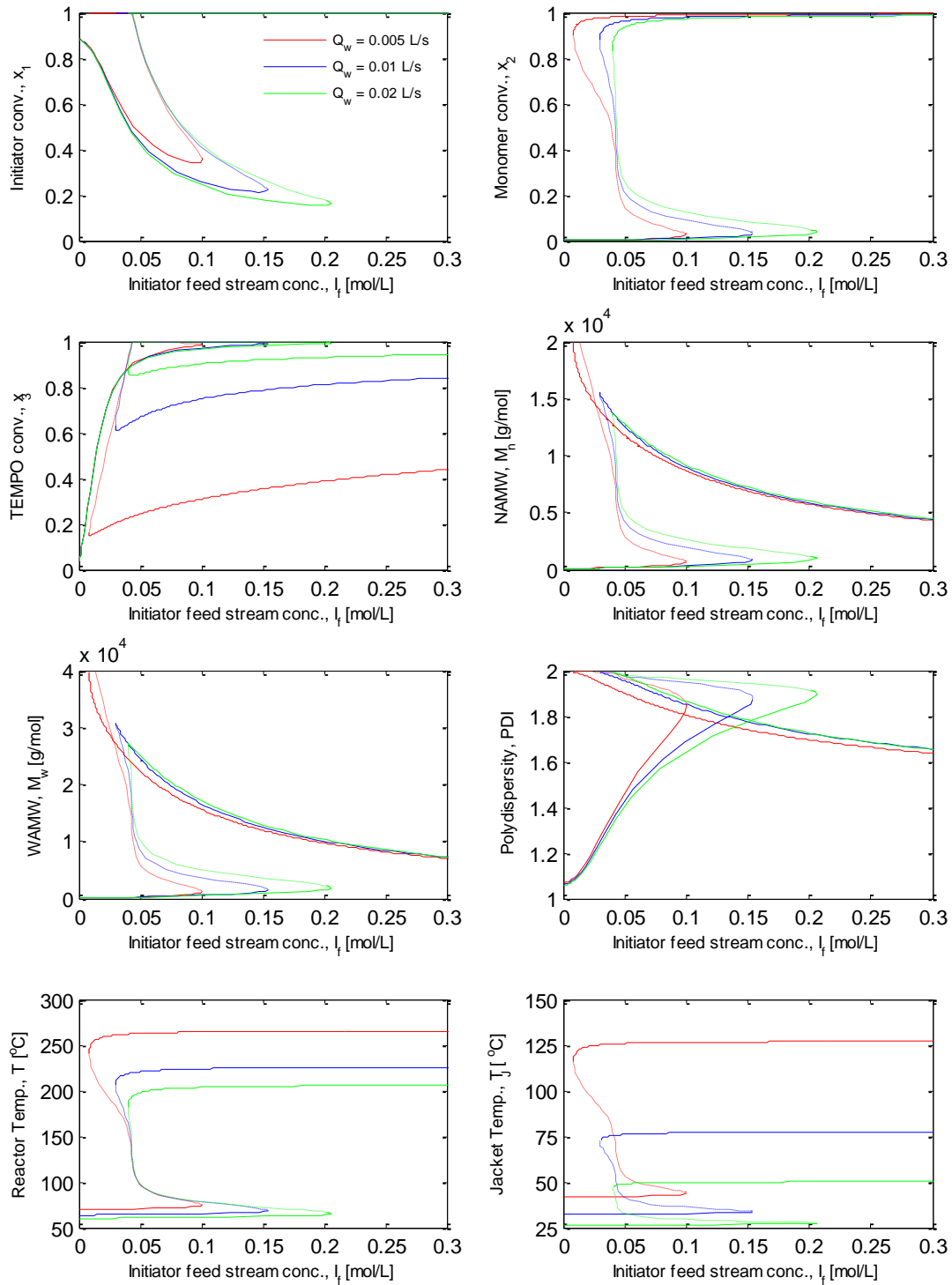


Figure 4.12: Bifurcation diagrams with initiator feed stream concentration as the main bifurcation parameter and coolant flow rate as the secondary bifurcation parameter. The stable solutions are plotted with solid lines (—) and the unstable solutions with dashed lines (---)

In addition, the TEMPO conversion and the PDI plots show self-intersecting curve with input and output multiplicity behavior. The PDI has high values for the medium conversion branch but for the high conversion branch the PDI is close to 1.6. However, remarkable operating values takes place for reactor and jacket temperatures as well as the molecular weights for the medium conversion branch.

In fact, when looking at Figure 4.13 where analyzing the steady state bifurcation behavior when the initiator feed stream concentration is the main bifurcation parameter and the residence time is the secondary parameter, it can be realized that the molecular weight plots hold the same behavior that mentioned in the prior case; also, the normal hysteresis behavior demonstrated by the monomer conversion, reactor and jacket temperatures whereas self-intersecting curve with input and output multiplicities is the PDI behavior for the current case. In addition, an input and output multiplicity is the behavior shown for both the initiator conversion and the TEMPO conversion.

It is interesting to notice that increasing the residence time have made noticeable shifting in the monomer conversion curves to high initiator feed stream concentration values which is unrealistic, so this observation could confirm our nominal residence time value 0.5hr to be the most realistic value. Moreover, all the other variables have got acceptable operating condition for the most interested medium conversion. For example, if the aim is to produce polymer with a monomer conversion close to 0.75, then the reactor temperature show values below 180°C plus the jacket temperature is less than the boiling point. However, the PDI has high values in the range of 1.8 to 2 for this case just like the former cases.

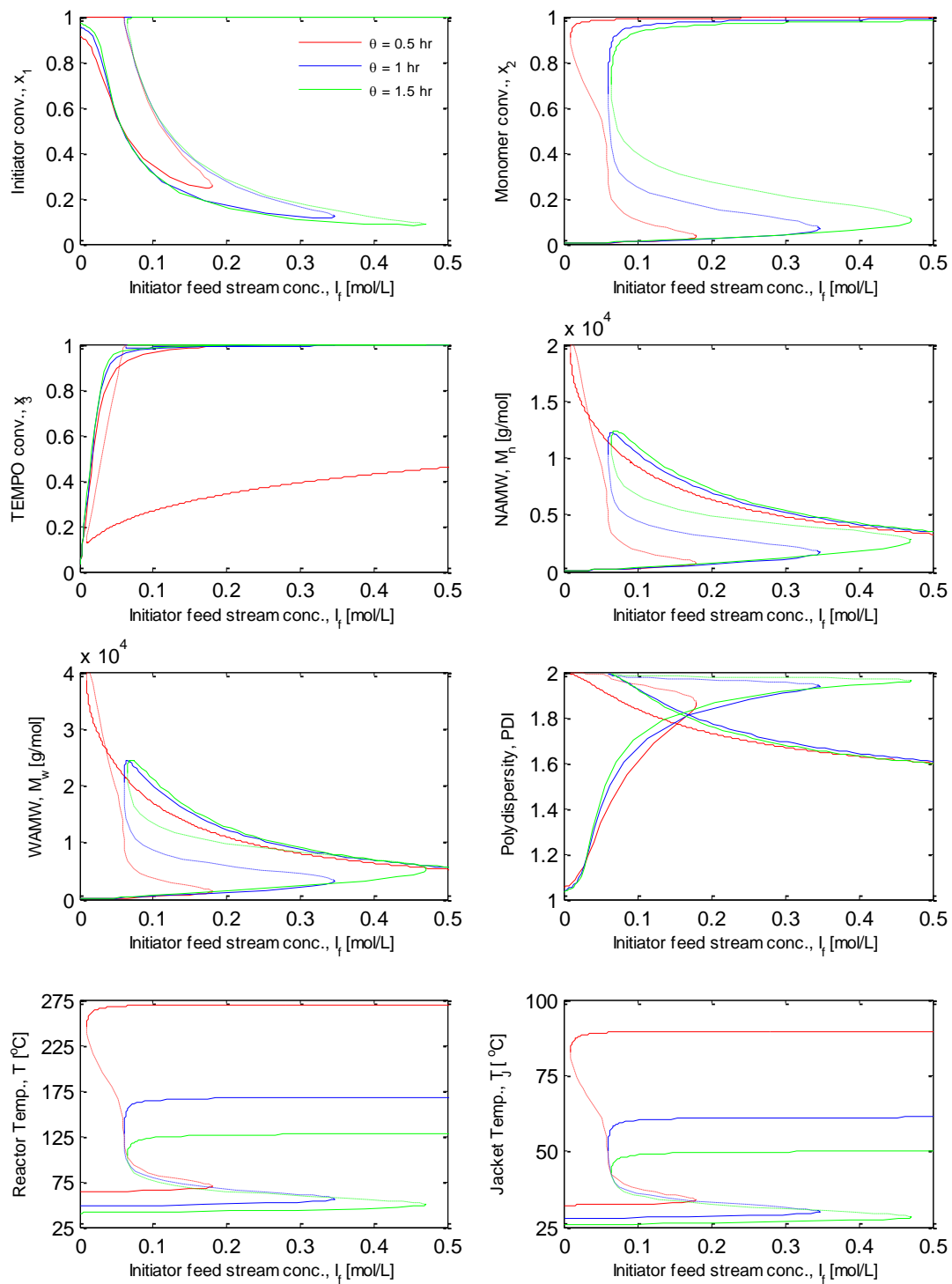


Figure 4.13: Bifurcation diagrams with initiator feed stream concentration as the main bifurcation parameter and residence time as the secondary bifurcation parameter. The stable solutions are plotted with solid lines (—) and the unstable solutions with dashed lines (---)

4.5.5 The Effect of Controller Feed Stream Concentration as a Main Bifurcation Parameter

In fact, the mentioned observations in the last section could lead us to think that it is very interesting to investigate the steady state bifurcation behavior of the model when the main bifurcation parameter is the controller feed stream concentration whereas the feed stream temperature, coolant flow rate and the residence time are the secondary parameters, respectively. For the mentioned cases there is no reference available for result comparison.

Now looking at Figure 4.14, where the steady state bifurcation behavior when the controller feed stream concentration is the main bifurcation parameter and the feed stream temperature is the secondary parameter has been examined. It is clear that increasing the temperature did not affect the system performance since all the curves show the same trend with slight difference.

Typical hysteresis behavior exhibits by the monomer conversion, molecular weights as well as the reactor and jacket temperatures. But the situation is different for the initiator conversion as it expresses input and output multiplicity behavior whereas the self-intersecting curve as well as input and output multiplicities is the behavior for TEMPO conversion and PDI.

As the feed stream temperature decreases, less amount of the controller feed stream concentration will be required to achieve the same monomer conversion. In addition, there is a wide range for the medium conversion branch which allows achieving almost 0.75 monomer conversion at TEMPO feed stream concentration similar to the nominal value of 0.432 mol/L. Moreover, these results can be supported by looking at the reactor temperature plot where the value related to the medium conversion is less than the high limit of 180°C as well as the jacket temperature has realistic value of less than 75°C for the mentioned branch. Again, the same high values of the PDI is the problem as it is close to 2 for the medium conversion branch.

Figure 4.15 show the steady state bifurcation behavior when the controller feed stream concentration is the main bifurcation parameter and the coolant flow rate is the secondary bifurcation parameter. As it can be seen, in the monomer conversion profile, for the case of lower coolant flow rate the system show two segments only. But when the coolant flow rate

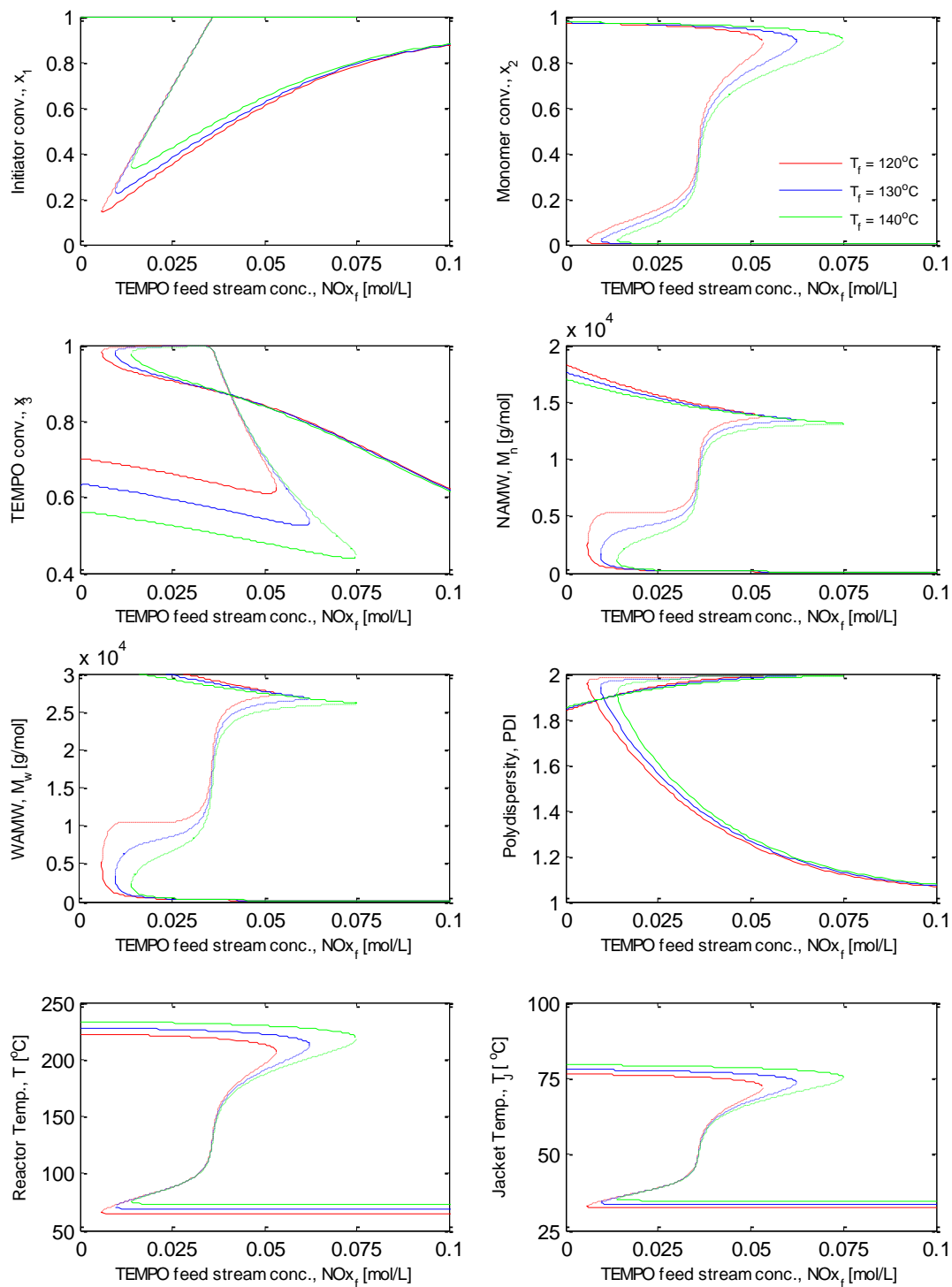


Figure 4.14: Bifurcation diagrams with TEMPO feed stream concentration as the main bifurcation parameter and feed stream temperature as the secondary bifurcation parameter. The stable solutions are plotted with solid lines (—) and the unstable solutions with dashed lines (---)

doubled, this behavior changed to show the typical hysteresis behavior with three segments which all lay in the realistic region.

Now, the initiator conversion profile show input and output multiplicities and all the lines are overlapping which indicates that increasing the coolant flow rate has no effect on the initiator conversion. Looking at the TEMPO conversion profile, the self-intersecting curves appeared in the high TEMPO conversion value close to 0.9. Here the lines are overlapping in the medium conversion branch only.

Noticeable interaction between the curves for the jacket temperature profile, these results indicates that the nominal coolant flow rate value of 0.01L/s is acceptable since it gives wider range for the controller feed stream concentration in the medium conversion segment. Moreover, the reactor temperature profile confirm the analysis as it has a value less than 180°C for the mentioned medium conversion branch. In addition, the molecular weight profiles have realistic values as well. Just as the previous cases the PDI expresses values close to 2 for the medium conversion branch.

Now, if attention paid to Figure 4.16 which illustrates the steady state bifurcation behavior when the controller feed stream concentration as the main bifurcation parameter and the residence time is our secondary bifurcation parameter. It is possible to find input and output multiplicities for the initiator conversion while the profile of monomer conversion show hysteresis behavior with noticeable affect when the residence time increases, as at 15min only two segments appear but for higher residence time one can see three segments. Furthermore, the same monomer conversion can be reached with less TEMPO feed stream concentration.

Just like the former cases, the initiator conversion profile show input and output multiplicities with line overlapping which indicates that there is no effect of increasing the residence time on the initiator conversion. The TEMPO conversion and the PDI show input and output multiplicities as well as self-intersecting curve. Here also the PDI values for the medium monomer conversion branch are high, but it is close to 1.7 for the high conversion branch.

The most interesting point in this part is the molecular weights profiles, as increasing the residence time affected the behavior noticeably. For both plots it can be seen that at lower

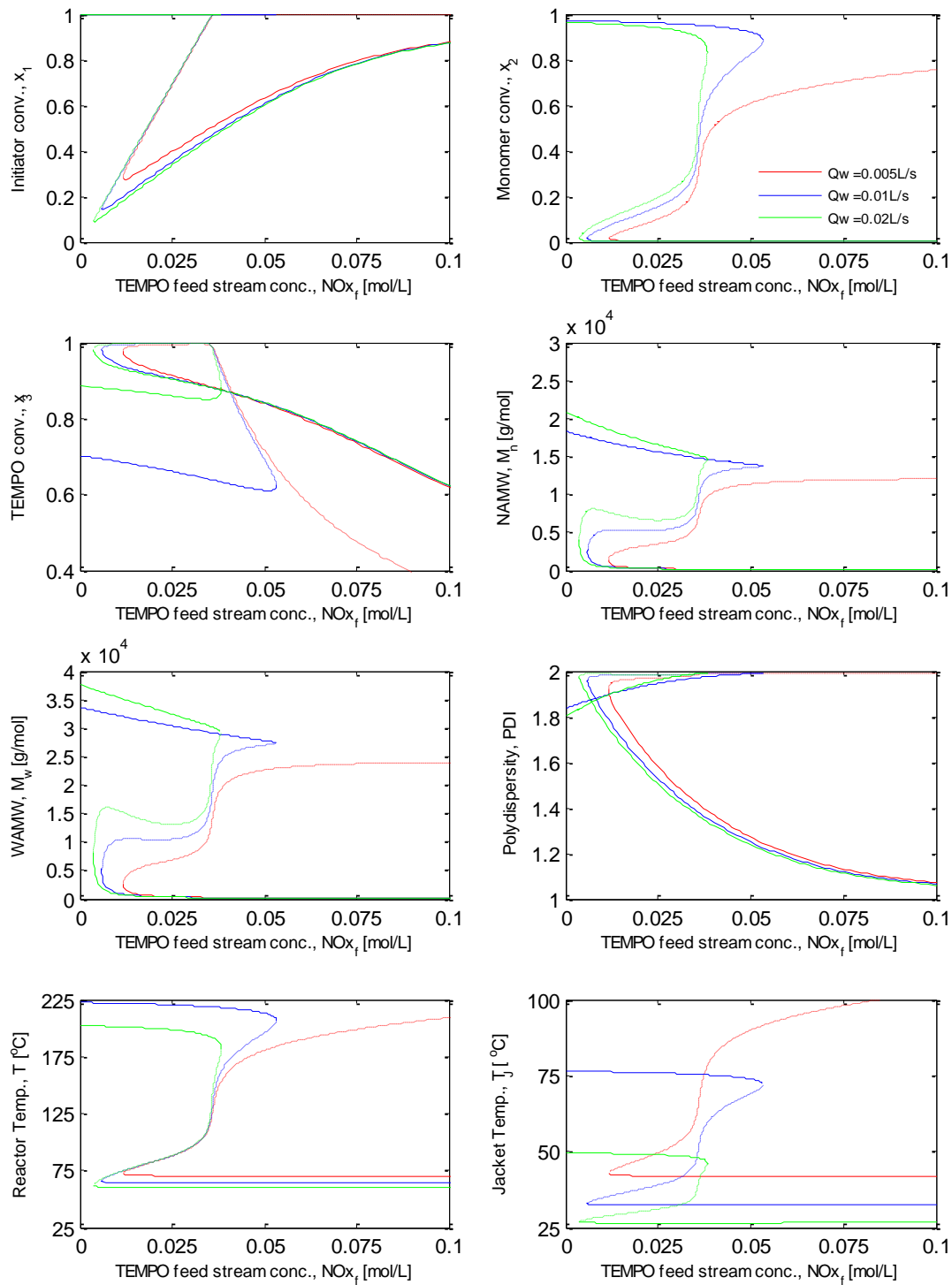


Figure 4.15: Bifurcation diagrams with TEMPO feed stream concentration as the main bifurcation parameter and coolant flow rate as the secondary bifurcation parameter. The stable solutions are plotted with solid lines (—) and the unstable solutions with dashed lines (---)

residence time the model expresses two segments only and most of the medium conversion branch lies in the area where the values of the TEMPO feed stream concentration should be high which is unrealistic. In other words, the medium conversion lies in the 0-like disjoint region; moreover, if the residence time increases, typical hysteresis behavior will appear. With further increasing of the residence time, the system will obviously show the input and output multiplicity behavior with a clear singe for isola formation.

Now looking at the reactor and jacket temperature profiles, it expresses hysteresis behavior; in addition, is an interaction with over lapping in the curves. Although the temperature plots has this behavior, acceptable values can be observed when looking at the medium monomer conversion branch.

The steady state bifurcation analysis of bimolecular nitroxide mediated radical polymerization of styrene done in this chapter gives us a general idea of the right operating region of the CSTR. These results are useful as starting points for the reactor optimization studies carried out in chapter 5.

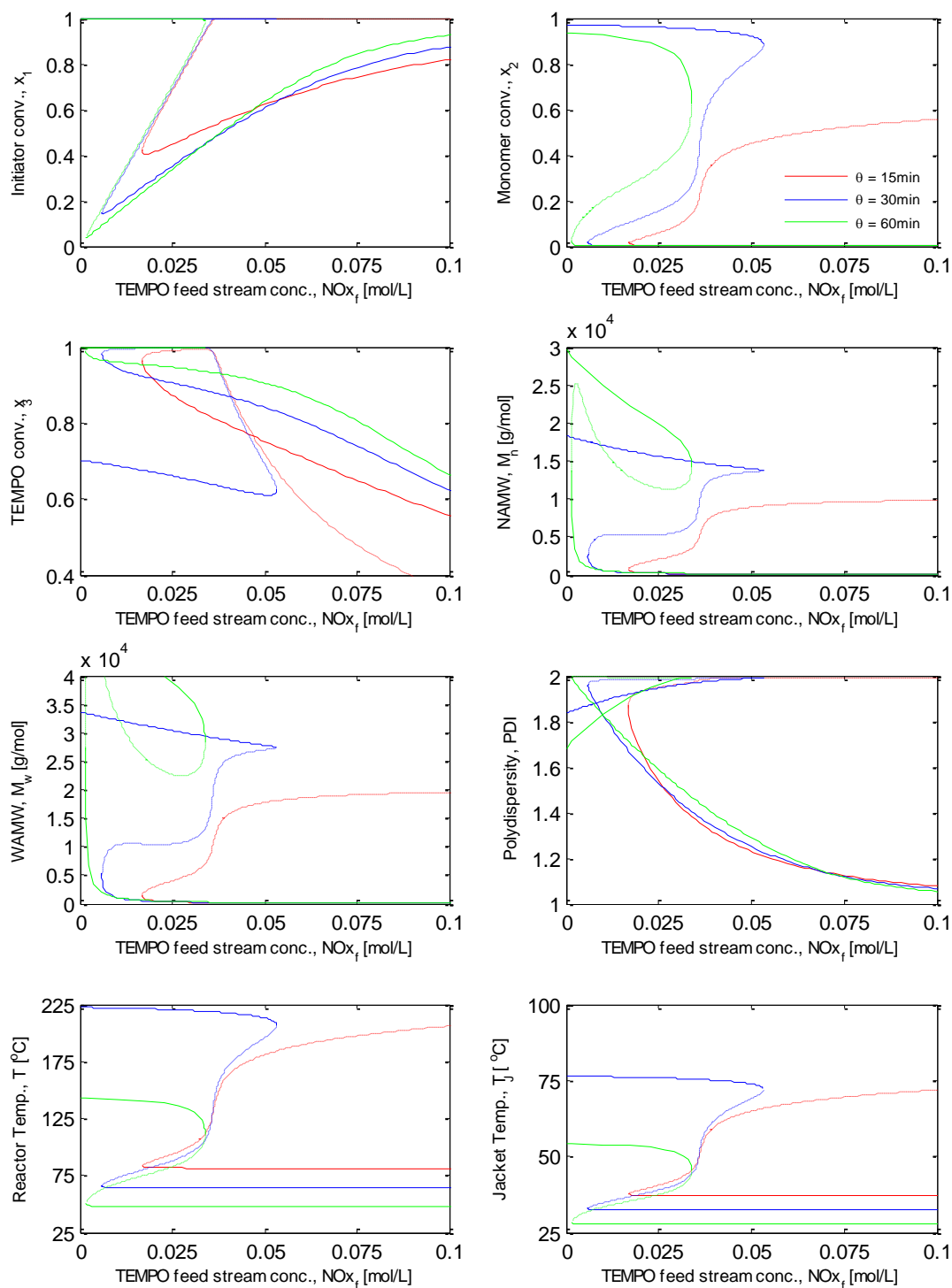


Figure 4.16: Bifurcation diagrams with TEMPO feed stream concentration as the main bifurcation parameter and residence time as the secondary bifurcation parameter. The stable solutions are plotted with solid lines (—) and the unstable solutions with dashed lines (---)

Chapter 5: Optimal Operating Conditions of CSTR

In this chapter, optimum operating conditions will be discussed for continuous stirred tank reactor (CSTR). The operation of nonisothermal jacketed continually stirred tank reactors involves a high degree of nonlinearity. Under certain operating conditions, this nonlinearity may cause steady state multiplicity; therefore, an optimization problem should be solved in order to find the best operating conditions.

Chemical engineers have become very interested in studying the features of steady state multiplicity of reacting systems of multiparameter space using bifurcation analysis as mentioned earlier in Section 4.1. The objective of the bifurcation theory is to describe quantitative changes in the behaviour of a system as a control parameter is smoothly varied. The CSTR reactor operating at steady state might give multiple steady states as the main bifurcation parameter is varied. The possibilities of changes are obtained in the form of bifurcation diagrams as discussed in Chapter 4.

The high nonlinearity and complexity entailed in the operation of CSTRs present a real challenge to process designers and engineers. Difficulties such as input-output steady state multiplicities, limit cycles, etc. are challenging phenomena, which are usually encountered. In this case, the CSTR operation will have the probability of attaining more than one equilibrium condition where some of these conditions are inaccessible and unstable even under close loop conditions. Because of the existence of such unstable steady states, design engineers try to avoid such regions by identifying them and design for reasonably safe operating conditions. Russo and Bequette (1998) studied the existence of such multiplicity for a jacketed CSTR with n^{th} order kinetics. In their analysis, they linked the bifurcation results to the multiplicity behaviour of CSTRs under certain operating conditions. Also, Gao et al. (2004) reviewed the commonly used optimization policies for the manufacture of polystyrene. In addition, Bhat et al. (2004) first studied the model of styrene polymerization in continuous tower process then optimized it to see whether the temperature profiles used are optimal in practice.

Optimal design of chemical processes are based on the optimization of objective functions that measure the economics of steady-state operating points. Therefore, extensive research has been performed on steady state optimization of polymerization processes. For instance, Astasuain et al. (2006) presented a comprehensive approach to the simultaneous design and control of a continuously stirred tank reactor for styrene solution polymerization in order to produce different polymer grades. In their work, a multiobjective optimization was implemented to minimize the annualized reactor cost, the operating costs, and the transition time between steady states.

In the following sections, a steady state optimization technique was applied to the bimolecular NMRP of styrene in CSTR in order to identify the optimum reactor operating conditions. An optimization problem was solved in order to find the “best” operating conditions required to produce a polymer with the desired properties. The control or input variables employed to optimize the reactor operation were the feed temperature, feed [TEMPO]/[BPO] ratio $[N_{O_{xf}}]/[I_f]$, the coolant flow rate, and the reactor residence time.

Therefore, the following general optimization problem was solved:

$$\min_{x,u} \Phi(x,u) \quad (5.1)$$

subject to:

$$f(x,u) = 0 \quad (5.2)$$

$$x_L \leq x \leq x_U \quad (5.3)$$

$$u_L \leq u \leq u_U \quad (5.4)$$

$$g_L \leq g(x,u) \leq g_U \quad (5.5)$$

Where the states $x \in R^n$ and the inputs $u \in R^m$ are the decision variables in this problem. Eq. (5.2) denotes the steady state conditions of the NMRP of styrene in CSTR model which is represented by the scaled model equations (4.24) to (4.43). Eqs. (5.3) and (5.4) denote the upper and lower bounds on the states as well as the inputs respectively, and Eq. (5.5) denotes a nonlinear process constraint on the PDI which is given by:

$$g(x,u) = PDI = \frac{\overline{Mw}}{\overline{Mn}} \quad (5.6)$$

The vector $x \in R^n$ represents the state variables from the NMRP of styrene model, and it is defined in Table 4.2; whereas the vector u represents the inputs and it is given below:

$$u = [I_f, NOx_f, T_f, Q_w, \theta]^T \quad (5.7)$$

In order to avoid numerical errors due to ill-conditioning in the optimization algorithm, the following input variables were rescaled as $u_1 = (I_f - I_{fs})/I_{fs}$, $u_2 = (NOx_f - NOx_{fs})/NOx_{fs}$, and $u_3 = (T_f - T_{fs})/T_{fs}$. Here, I_{fs} is the initiator feed stream concentration scaling factor, NOx_{fs} is the controller feed stream concentration scaling factor, and T_{fs} is the reactor feed stream temperature scaling factor. The sequential quadratic programming (SQP) algorithm was applied. This algorithm is one of the most popular and robust algorithms for nonlinear optimization. The method is based on solving a series of sub-problems designed to minimize a quadratic model of the objective subject to a linearization of the constraints. The optimization scenarios considered here are discussed next.

5.1 Conversion Maximization

First, a maximization of styrene conversion in the bimolecular NMRP was performed. The objective function maximizing the monomer conversion is expressed as:

$$\min_{x,u} \quad \Phi = -C \quad (5.8)$$

subject to:

Process model equations (4.24) to (4.43)

$$0 \leq I_f \leq 1 \text{ mol/L} \quad (5.9)$$

$$0 \leq NOx_f \leq 1 \text{ mol/L} \quad (5.10)$$

$$100 \leq T_f \leq 140^\circ\text{C} \quad (5.11)$$

$$10^{-6} \leq Q_w \leq 5 \text{ L/s} \quad (5.12)$$

$$10^{-6} \leq \theta \leq 5 \text{ hr} \quad (5.13)$$

$$0 \leq T_{reactor} \leq 180^\circ\text{C} \quad (5.14)$$

$$5 \leq T_{jacket} \leq 50^\circ\text{C} \quad (5.15)$$

$$0 \leq C \leq 1 \quad (5.16)$$

Process constraints on the polydispersity index (PDI) and weight average molecular weight (WAMW) were also considered:

$$1 \leq PDI \leq 1.7 \quad (5.17)$$

$$25 \times 10^3 \leq \overline{Mw} \leq 40 \times 10^3 \text{ g/mol} \quad (5.18)$$

In general, most optimization functions execute minimization of functions, not maximization. Therefore, maximization of monomer conversion is achieved according to the well-known optimization rule $\min(\Phi) = -\max(\Phi)$, the monomer conversion is represented by C . Table 5.1 provides the optimal values of the decision variables for this case. It can be seen that all the values of the decision variables are within the bounds while getting the maximum monomer conversion (close to 95%).

Furthermore, the previous objective function Eq. (5.8) was augmented with the coolant flow rate Q_w and reactor residence time θ . Here, the objective is to minimize the coolant flow rate and residence time, while at the same time maximizing the conversion. The augmented objective function is given by Eq. (5.19). This objective function will give a high production rate in a short time.

$$\min_{x,u} \quad \Phi = -w_1(C) + w_2(Q_w) + w_3(\theta) \quad (5.19)$$

subject to:

Process model Eqs. (4.24) to (4.43)

Constraints Eqs. (5.9) to (5.18)

Moreover, w_1 , w_2 as well as w_3 denote weighting factors used to obtain better conversion, coolant flow rate, and residence time fitting, respectively, and they set equal to one. As one can see that the range of the upper and lower bounds chosen for the coolant flow rate as well as the residence time is a wide range, as those variables are part of the objective function for this case.

Looking at the optimization results in Table 5.1, the monomer conversion in the second case is close to 96% and the [TEMPO]/[BPO] molar ratio is 1.215. Both values are similar to the first case. However, adding the coolant flow rate and the residence time affected the other variables, i.e giving lower values for feed stream temperature, coolant flow rate, and residence time. Whereas higher optimal values were found for the reactor and jacket temperature and the weight average molecular weight. It is clear that all the results are within the upper and lower bounds, but one can see that both values of the reactor temperature and the PDI were hit the upper limits.

Table 5.1: Optimal operating conditions of NMRP of styrene to maximize conversion

Variables in the objective function			
Decision variables	Units	Case I	Case II
Conversion		0.9582	0.9614
Q_w	L/s		0.0441
θ	hr		0.537
Non- optimal values			
Polydispersity index		1.640	1.696
$\overline{M_w}$	g/mol	26.5×10^3	30.7×10^3
Corresponding optimal operating conditions in the constraints			
[TEMPO]/[BPO]		1.235	1.215
T_f	°C	136.996	120.118
$T_{reactor}$	°C	158.369	179.951
T_{jacket}	°C	25.737	28.301
Q_w	L/s	0.0478	
θ	hr	0.688	

5.2 Conversion and PDI Optimization

In this section, the objective of the optimization algorithm was to maximize the monomer conversion while simultaneously attempting to achieve a certain desired polydispersity index $PDI_{desired}$. The optimization problem solved in this case is given by Eqs. (5.20) to (5.29) below:

$$\min_{x,u} \quad \Phi = -w_1(C) + w_2(PDI / PDI_{desired} - 1)^2 \quad (5.20)$$

subject to:

Process model equations (4.24) to (4.43)

$$0 \leq I_f \leq 1 \text{ mol/L} \quad (5.21)$$

$$0 \leq NOx_f \leq 1 \text{ mol/L} \quad (5.22)$$

$$100 \leq T_f \leq 140 \text{ }^\circ\text{C} \quad (5.23)$$

$$10^{-6} \leq Q_w \leq 5 \text{ L/s} \quad (5.24)$$

$$10^{-6} \leq \theta \leq 5 \text{ hr} \quad (5.25)$$

$$0 \leq T_{reactor} \leq 180 \text{ }^\circ\text{C} \quad (5.26)$$

$$5 \leq T_{jacket} \leq 50 \text{ }^\circ\text{C} \quad (5.27)$$

$$0 \leq C \leq 1 \quad (5.28)$$

Here, in addition to the above constraints, a single nonlinear process constraint on the weight average molecular weight (WAMW) is added.

$$25 \times 10^3 \leq \overline{Mw} \leq 40 \times 10^3 \text{ g/mol} \quad (5.29)$$

Here, C represents the monomer conversion, PDI represents the polydispersity index, $PDI_{desired}$ represents the desired polydispersity index. Finally, the weighting factors w_1 and w_2 are employed to weight the relative importance of the two terms. In this study, the weighting

factors selected were: $w_1 = w_2 = 1$. All the results are presented in Table 5.2 and it shows that the optimal results satisfied within the selected value of the constraint. However, the optimal values of the feed stream temperature, reactor and jacket temperatures are all hit their upper limits, whereas the weight average molecular weight hit the lower bound.

In this section, another optimization problem was solved but this time by adding the coolant flow rate Q_w and the residence time θ to the objective function addressed above, Eq.(5.20). Now, the second optimization problem in this section is listed in Eq. (5.30):

$$\min_{x,u} \quad \Phi = -w_1(C) + w_2(PDI / PDI_{desired} - 1)^2 + w_3(Q_w) + w_4(\theta) \quad (5.30)$$

This problem is subject to the same constraints appeared in the first case, Eqs. (5.21) to (5.29) as well as the process model Eqs. (4.24) to (4.43). Again, w_1, w_2, w_3 and w_4 denote weight factors used to obtain better conversion, PDI, coolant flow rate, and residence time fitting, respectively.

Table 5.2 illustrates the optimal results for the first and the second cases of this section, as it can be seen that all the results satisfied the upper and lower bounds. From comparing the optimal results for both cases, one can see that the monomer conversion achieved 96% in both cases, the molar ratio is almost the same, the PDI value reached the desired PDI value but interesting results appeared for the jacket temperature as it decreases in the same time of increasing the coolant flow rate. One might explain decreasing the residence time combined with higher coolant flow rate helped to remove the heat from the reactor and decreased the jacket temperature whereas this did not affect the reactor temperature as it is still hit the upper bound for this case as well. In addition, lower value for the feed stream temperature has been achieved in this case. Furthermore, the polymer produced in this case has higher molecular weight.

Table 5.2: Optimal operating conditions of NMRP of styrene conversion and PDI

Variables in the objective function			
Decision variables	Units	Case III	Case IV
Conversion		0.968	0.960
Polydispersity index		1.695	1.699
Q_w	L/s		0.0441
θ	hr		0.536
Non- optimal values			
$\overline{M_w}$	g/mol	25×10^3	31.7×10^3
Corresponding optimal operating conditions in the constraints			
[TEMPO]/[BPO]		1.238	1.263
T_f	°C	139.967	120.038
$T_{reactor}$	°C	179.995	179.984
T_{jacket}	°C	49.986	28.314
Q_w	L/s	0.0144	
θ	hr	0.675	

5.3 Conversion, PDI and Mw Optimization

In the first case, the objective was to maximize the monomer conversion while minimize the polydispersity index (PDI) and the weight average molecular weight (\overline{Mw}) as it can be seen in Eq. (5.31):

$$\min_{x,u} \Phi = -w_1(C) + w_2(PDI / PDI_{desired} - 1)^2 + w_3(\overline{Mw} / \overline{Mw}_{desired} - 1)^2 \quad (5.31)$$

subject to:

Process model equations (4.24) to (4.43)

$$0 \leq I_f \leq 1 \text{ mol/L} \quad (5.32)$$

$$0 \leq NOx_f \leq 1 \text{ mol/L} \quad (5.33)$$

$$100 \leq T_f \leq 140^\circ\text{C} \quad (5.34)$$

$$10^{-6} \leq Q_w \leq 5 \text{ L/s} \quad (5.35)$$

$$10^{-6} \leq \theta \leq 5 \text{ hr} \quad (5.36)$$

$$0 \leq T_{reactor} \leq 180^\circ\text{C} \quad (5.37)$$

$$5 \leq T_{jacket} \leq 50^\circ\text{C} \quad (5.38)$$

$$0 \leq C \leq 1 \quad (5.39)$$

Whereas the nonlinear process constraints are not included for this case as both of PDI and the weight average molecular weight are parts of the optimization problem, Eq. (5.31).

Here C is representing the model monomer conversion, PDI is representing the model polydispersity index, $PDI_{desired}$ represents the desired value for polydispersity index, finally, \overline{Mw} represents the weight average molecular weight and $\overline{Mw}_{desired}$ represents the desired value of the weight average molecular weight. Also, w_1 , w_2 as well as w_3 denote weight factors used to

obtain better fitting. All the results were presented in Table 5.3 and it shows that the optimal results satisfied within the selected value of the constraint. The optimal results of the PDI as well as the weight average molecular weight satisfied the desired values.

Furthermore, second optimization problem has been solved, in this case the coolant flow rate Q_w and the residence time θ have been included in to the objective function, so the optimization problem is represented in Eq. (5.40):

$$\begin{aligned} \min_{x,u} \quad \Phi = & -w_1(C) + w_2(PDI / PDI_{desired} - 1)^2 + w_3(\overline{Mw} / \overline{Mw}_{desired} - 1)^2 + w_4(Q_w) \\ & + w_5(\theta) \end{aligned} \quad (5.40)$$

This problem is subject to the same constraints appeared in the previous case, Eqs. (5.32) to (5.39) and the process model Eqs. (4.24) to (4.43). Table 5.3 shows the optimal results for the two cases discussed in this section. In both cases, the conversion achieved is close to 96%, the molar ratio is quite the same in both cases. Moreover, including the coolant flow rate and the residence time helped in decreasing the jacket temperature, this happened due to the increase of the coolant flow rate which helped in remove the heat from the system. Looking at the reactor temperature, the optimal value in the second case hit the upper bound. The polymer produced here has the same properties as the previous case as it has the same PDI and weight average molecular weight.

Table 5.3: Optimal operating conditions of NMRP of styrene conversion, PDI and \overline{M}_w

Variables in the objective function			
Decision variables	Units	Case V	Case VI
Conversion		0.964	0.962
Polydispersity index		1.697	1.692
\overline{M}_w	g/mol	29.9×10^3	29.8×10^3
Q_w	L/s		0.0435
θ	hr		0.538
Corresponding optimal operating conditions in the constraints			
[TEMPO]/[BPO]		1.272	1.269
T_f	°C	134.431	120.171
$T_{reactor}$	°C	178.249	179.936
T_{jacket}	°C	46.189	28.458
Q_w	L/s	0.0164	
θ	hr	0.653	

Chapter 6: Conclusions and Recommendations

6.1 Concluding Remarks

Nitroxide Mediated Radical Polymerization (NMRP) of styrene provides a variety of special polymerization systems that are particularly interesting from the viewpoint of the production of polymers with highly controlled structure, narrow molecular weight distribution and polydispersity index. Under thermal heating, the polymerization is initiated by benzoyl peroxide (BPO) and controlled by nitroxide stable free radical (TEMPO).

A kinetic mechanism describing the bimolecular NMRP was thoroughly discussed, reviewed and improved. For the NMRP system, two side reactions were added to compensate for the theoretical model discrepancy reflected in the literature. These reactions are the promoted dissociation reaction between BPO and TEMPO, and the dormant living exchange which produces dimeric alkoxyamine. The thermal polymerization of styrene was carefully investigated, and the kinetic parameters were validated. Two kinetic models, one based on thermal polymerization of styrene and one on the use of TEMPO/BPO mixture, were proposed and then validated with data obtained at temperature 120°C and [TEMPO]/[BPO] molar ratio 1.1.

The NMRP kinetic model obtained is highly nonlinear and reveals stiffness characteristics in the differential equations, which can make the integration difficult. Therefore, the differential model was transformed into a dimensionless form in order to avoid numerical difficulties in the integration. Optimization tool box in Matlab was employed to determine the optimal kinetic parameters of the rate constants. To test the validity of the kinetic parameters obtained, the model predictions were compared with data at 120 and 130°C for [TEMPO]/[BPO] molar ratios of 0.9, 1.1, 1.2, and 1.3. A good to very good agreement was obtained between the prediction and data.

Besides, the non-linear behavior of styrene bimolecular NMRP model was investigated. Use of the Matlab continuation program Matcont generated the bifurcation diagrams and the eigenvalues of each of their points. The bifurcation diagrams were plotted for the main

bifurcation variables: the initiator conversion, monomer conversion, controller conversion, molecular weights, polydispersity index, reactor temperature and jacket temperatures. In most cases, typical hysteresis behavior has been determined and contains more practical features, such as input/output multiplicities, self-intersecting curves, 0-like disjoint region, and isola formation. In addition, some values obtained in the CSTR bifurcation work are not practically feasible. However, they have been included in order to give a better idea of the theoretical nonlinear behavior of the system.

Also, some important operational difficulties were revealed such as an efficient value of the polydispersity index could not be achieved using single CSTR. In addition, the operation of the reactor was very constrained due to the tight range of temperatures in which the reaction should take place.

Steady state optimization of the NMRP of styrene model has been carried out in order to identify the best operating conditions of the process. Three different objective functions cases were selected. All the optimal results obtained satisfied the process constraints.

The optimal values obtained for monomer conversion, PDI, weight average molecular weight, coolant flow rate and residence time were about 0.96, 1.70, 30×10^3 g/mol, 157L/hr and 0.54hr, respectively. These optimal values correspond to the optimal operating reactor data such as [TEMPO]/[BPO] molar ratio about 1.27, feed stream temperature equals to 120°C, jacket temperature with value of 28.5°C, and reactor temperature with value of 179°C (upper limit).

6.2 Recommendations

As discussed in Chapter 2, due to the relatively high strength of the C-O bond in the TEMPO polymer adduct, TEMPO-mediated NMRP needs long reaction times and higher polymerization temperatures. To overcome this deficiency, changes in the structure of the nitroxide are recommended so it would be worth to examine the effect of other nitroxide on NMRP of styrene and compare it with TEMPO-mediated NMRP. Also, it might be useful to use different initiators to start the polymerization. It is also advisable to include the correlations of the gel-effect in the NMRP kinetic model.

The use of a series of CSTR reactors may help to resolve the problem of controlling the PDI. Finally, a closed-loop control scheme is highly recommended to operate the reactor system under unstable conditions.

Nomenclature

Symbols	Definition
A	Jacketed area of the reactor, m^2
A_{in}	Total inner area of the reactor, m^2
C	Monomer conversion
CP_m	Heat capacity of reaction mixture, $J/(kgK)$
CP_w	Heat capacity of coolant, $J/(kgK)$
D	Dimer concentration (Diels-Alder adduct), mol/L
D_a	Agitator diameter, m
D^\bullet	Dimeric radical concentration, mol/L
d_e	Hydraulic mean diameter, m
D_{in}	Inner reactor diameter, m
DNO_x	Dimeric alkoxyamine concentration, mol/L
D_{out}	Outer reactor diameter, m
f	Efficiency of initiator decomposition
H	Reactor height, m
h_j	Heat transfer coefficient from vessel wall to cooling fluid, W/m^2K
HNO_x	Hydroxylamine concentration, mol/L
ΔH_R	Heat of reaction, J/mol
h_v	Heat transfer coefficient to vessel wall, W/m^2K
I	Initiator concentration (Benzoyl peroxide), mol/L
I_f	Initiator feed concentration, mol/L

k	Constant
k_a	Rate constant for activation, min^{-1}
k_{a1}	Rate constant for activation, min^{-1}
k_{a2}	Rate constant for activation, min^{-1}
k_d	Rate constant for initiation, min^{-1}
k_{da}	Rate constant for deactivation, $L \cdot \text{mol}^{-1} \text{min}^{-1}$
k_{da1}	Rate c Rate constant for deactivation, $L \cdot \text{mol}^{-1} \text{min}^{-1}$
k_{da2}	Rate constant for deactivation, $L \cdot \text{mol}^{-1} \text{min}^{-1}$
k_{decomp}	Rate constant for decomposition of alkoxyamines, min^{-1}
k_{dim}	Rate constant for Mayo dimerization, $L \cdot \text{mol}^{-1} \text{min}^{-1}$
K_{exch}	The equilibrium rate constant
k_f	Thermal conductivity of reactor contents, W / mK
k_f	Thermal conductivity of cooling fluid, W / mK
k_{fD}	Rate constant for transfer to dimer, $L \cdot \text{mol}^{-1} \text{min}^{-1}$
k_{fM}	Rate constant for transfer to monomer, $L \cdot \text{mol}^{-1} \text{min}^{-1}$
k_{h3}	Rate constant for rate enhancement reaction
k_{ia}	Rate constant for thermal initiation, $L \cdot \text{mol}^{-1} \text{min}^{-1}$
k_p	Rate constant for propogation, $L \cdot \text{mol}^{-1} \text{min}^{-1}$
k_{p1}	Rate constant for thermal initiation, $L^2 \cdot \text{mol}^{-2} \text{min}^{-1}$
k_{PR}	Rate constant of promoted dissociation, $L \cdot \text{mol}^{-1} \text{min}^{-1}$
k_t	Overall termination rate constant, $L \cdot \text{mol}^{-1} \text{min}^{-1}$

M	Monomer concentration (Styrene), mol/L
M^\bullet	Monomeric radical concentration, mol/L
M_f	Monomer feed concentration, mol/L
\overline{M}_n	Number average molecular weight, g/mol
MNO_x	Monomeric alkoxyamine concentration, mol/L
\overline{M}_w	Weight average molecular weight, g/mol
MW_M	Monomer molecular weight, g/mol
N	Agitator speed, rps
NO_x^\bullet	Nitroxide radical concentration, mol/L
NO_{xf}^\bullet	Nitroxide radical feed concentration, mol/L
Nu	Nusselt number, dimensionless
PDI	Polydispersity index
$P_r^\bullet, P_{r+s}^\bullet$	non-growing (dead) polymer chain having r or $r+s$ monomeric units, mol/L
Pr	Prandtl number, dimensionless
Q_w	Cooling water flow rate, L/s
R_1^\bullet	Primary radicals concentration, mol/L
Re	Reynolds number, dimensionless
R_{in}^\bullet	Benzoyloxy primary radicals concentration, mol/L
R_p	Rate of polymerization
R_r^\bullet	Active radical of chain length r , mol/L
R_r^\bullet, R_s^\bullet	Polymeric radical species, mol/L
R_{r+1}^\bullet	Live polymeric radicals of chain length $r+1$, mol/L

$R_r NO_x$	Polymeric alkoxyamine concentration of chain length r, mol/L
T	Reactor temperature, K
t	Time, s
T_f	Feed stream temperature, K
$T_{f,j}$	Jacket feed stream temperature, K
T_j	Jacket temperature, K
U	Heat transfer coefficient, $J/(m^2sK)$
u	Velocity of cooling fluid, m/s
V	Reactor volume, L
V_{in}	Inner reactor volume, L
V_j	Jacket volume, L
w_i	Weight fraction
w_p	Polymer weight fraction

Greek letters

λ_i	i^{th} moment of the growing polymer radicals
μ_i	i^{th} moment of the dead polymer chains
δ_i	i^{th} moment of the dormant species
θ	Residence time, s
ρ_m	Density of reaction mixture, kg/L
ρ_w	Density of cooling water, kg/L
μ	Viscosity of cooling fluid, $N.s/m^2$

μ_m	Viscosity of reaction mixture, $N.s/m^2$
μ_w	Viscosity of water, $N.s/m^2$
α	Constant
β	Constant
γ_{avg}	Average shear rate in the reactor, s^{-1}

Subscripts

0	Initial value
0	Zeroth moment
1	First moment
2	Second moment
mi	Theoretical values
di	Experimental values

Acronyms

AIBN	Azobisisobutyronitrile
ATRP	Atomic transfer radical polymerization
BPO	Benzoyl peroxide
CRP	Controlled radical polymerization
CSTR	Continuous stirred tank reactor
LFRP	Living free radical polymerization
LRP	Living radical polymerization
MMA	Methyl methacrylate
NAMW	Number average molecular weights

NMRP	Nitroxide mediated radical polymerization
PRE	Persistent radical effect
RAFT	Reversible addition fragmentation transfer
SNR	Stable nitroxyl radical
WAMW	Weight average molecular weights

References

- Almeida, A. S., Wada, K. and Secchi, A. R., (2008). Simulation of styrene polymerization reactors: kinetic and thermodynamic modeling. *Brazilian Journal of Chemical Engineering*, 25, (2), 337-349.
- Asteasuain, M., Bandoni, A., Sarmoria, C. and Brandolin, A., (2006). Simultaneous process and control system design for grade transition in styrene polymerization. *Chemical Engineering Science*, 61, 3362 – 3378.
- Avery, H.E. (1974), *Basic Reaction Kinetics Mechanisms*. London, UK: Macmillan.
- Belincanta-Ximenes, J., Mesa, P. V. R., Lona, L. M. F., Vivaldo-Lima, E., McManus, N.T., Penlidis, A., (2007). Simulation of styrene polymerization by monomolecular and bimolecular Nitroxide mediated radical processes over a range of reaction conditions. *Macromolecular Theory and Simulations*, 16, 194-208.
- Bhat, S. A., Sharma, R. and Gupta, S. K., (2004). Simulation and optimization of the continuous tower process for styrene polymerization. *Journal of Applied Polymer Science*, 94, 775-788.
- Bird, R. B., Stewart, W. E., Lightfoot, E. N., (2007). *Transport phenomena* (Second edition). New York: Wiley.
- Bonilla, J., Saldivar, E., Flores-Tlacuabuac, A., Vivaldo-Lima, E., Pfaendner, R., Tiscareno-Lechuga, F., (2002). Detailed modeling, simulation, and parameter estimation of nitroxide mediated living free radical polymerization of styrene. *Polymer Reaction Engineering Journal*, 10, 227-263.
- Boutevin, B. and Bertin, D., (1999). Controlled free radical polymerization of styrene in the presence of nitroxide radicals. I. Thermal initiation. *European Polymer Journal*, 35, 815-825.
- Butte, A., Storti, G., Morbidelli, M., (1999). Kinetics of living free radical polymerization. *Chemical Engineering Science*, 54, 3225-3231.

- Chiefari, J., Chong, Y. K. B., Ercole, F., Krstina, J., Jeffery, J., Le, T. P. T., Mayadunne, R. T. A., Meijs, G. F., Moad, C. L., Moad, G., Rizzardo, E. and Thang, S. H., (1998). Living free radical polymerization by Reversible Addition Fragmentation chain Transfer: The RAFT Process. *Macromolecules*, 31, 5559-5562.
- Connolly, T. J. and Scaiano, J. C., (1997). Reaction of the stable nitroxide radical TEMPO. Relevant to living free radical polymerization and autopolymerization of styrene. *Tetrahedron Letters*, 38, (7), 1133-1136.
- Dhib, R., Gao, J., Penlidis, A., (2000). Simulation of free radical bulk/solution homopolymerization using mono-and bi-functional initiators. *Polymer Reaction Engineering Journal*, 8, 4, 299-464.
- Dhooge A., Govaerts W., Kuznetsov Y. A., and Sautois B., (2006), Matcont: A Matlab package for dynamical systems with applications to neural activity. *Program Documentation*.
- Dhooge, A., Govaerts, W., Kuznetsov, Y., (2003). MATCONT: a Matlab package for numerical bifurcation analysis of ODEs. *ACM Transactions on Mathematical Software*, 29, 141.
- Dou, H. S., Khoo, B. C. and Tsai, H. M. Critical condition for flow transition in a full- developed annulus flow Retrieved on October 20 2009 from <http://arxiv.org/ftp/physics/papers/0504/0504193.pdf>
- Filho, I. P. F., Biscaia Jr, E. C. and Pinto, J. C., (1994). Steady state multiplicity in continuous bulk polymerization reactors – A general approach. *Chemical Engineering Science*, 49, (22), 3745-3755.
- Fischer, H., (2001). The persistent radical effect: A principle for selective radical reactions and living radical polymerization. *Chemical Reviews*, 101, 3581-3610.
- Flory, P. J., (1937). The mechanism of vinyl polymerizations. *Journal of the American Chemical Society*, 59, (2) 241-253

- Fogler, H. S., (1999). *Elements of Chemical Reaction Engineering* (Third edition). NJ: Prentice Hall PTR.
- Fukuda, T., Goto, A. and Ohno, K., (2000). Mechanism and kinetics of living radical polymerization. *Macromolecular Rapid Communications*, 21, 151-165.
- Fukuda, T., Terauchi, T., Goto, A., Ohno, K., Tsujii, Y. and Miyamoto, T., (1996). Mechanism and kinetics of nitroxide controlled free radical polymerization. *Macromolecules*, 29, 6393-6398.
- Gao, J., Hungenberg, K. D., Penlidis, A., (2004). Process modelling and optimization of styrene polymerization. *Macromolecular Symposium*, 206, 509-522.
- Georges, M. K., Veregin, R. P. N., Kazmaier, P. M. and Hamer, G. K., (1993). Narrow molecular weight resins by a free- radical polymerization process. *Macromolecules*, 26, 2987-2988.
- Georges, M. K., Veregin, R. P. N., Kazmaier, P. M., Hamer, G. K. and Saban, M., (1994). Narrow polydispersity polystyrene by a free radical polymerization process-rate enhancement. *Macromolecules*, 27, 7228-7229.
- Greszta, D. and Matyjaszewski, K., (1996). Mechanism of controlled/"living" radical polymerization of styrene in the presence of nitroxyl radicals. Kinetics and simulations. *Macromolecules*, 29, 7661-7670.
- Hamer, J. W., Akramov, T. A. and Ray, W. H., (1981). The dynamic behavior of continuous polymerization reactors—II. Nonisothermal solution homopolymerization and copolymerization in a CSTR. *Chemical Engineering Science*, 36, (12), 1897–1914.
- Hawker, C. J., Bosman, A. W. and Harth, E., (2001). New Polymer Synthesis by Nitroxide Mediated Living Radical Polymerizations. *Chemical Reviews*, 101, 3661-3688.
- He, J., Li, L., Yang, Y., (2000). Effect of hydrogen transfer reaction on kinetics of nitroxide mediated free radical polymerization. *Macromolecules*, 33, 2286-2289.

- Hui, A.W. and Hamielec A.E., (1972). Thermal polymerization of styrene at high conversions and temperatures, an experimental study. *Journal of Applied Polymer Science*, 16, 749-769.
- Jaisinghani, R. and Ray, W. H., (1977). On the dynamic behavior of a class of homogeneous continuous stirred tank polymerization reactors. *Chemical Engineering Science*, 32, 811-825.
- Judovits, L. H., Bopp, R. C., Gaur, U. and Wunderlich, B., (1986). The heat capacity of solid and liquid polystyrene, p-substituted polystyrenes, and crosslinked polystyrenes. *Journal of Polymer Science*, 24, 2725-2741.
- Kim K.J. and Choi K.Y. (1988), Steady state behavior of a continuous stirred tank reactor for styrene polymerization with bifunctional free radical initiators. *Chemical Engineering Science*, 43, 965-977.
- Kiparissides, C., (1996). Polymerization reactor modeling: a review of recent developments and future directions. *Chemical Engineering Science*, 51, (10), 1637–1659.
- Lemoine-Nava, R., Antonio Flores-Tlacuahuac, A. and Saldívar-Guerra, E., (2006). Non-linear bifurcation analysis of the living nitroxide mediated radical polymerization of styrene in a CSTR. *Chemical Engineering Science*, 61, 370-387.
- Luyben, W. L. (2007). *Chemical Reactor Design and Control*. NJ: Wiley.
- Mayo, F. R. (1968), The Dimerization of Styrene, *J. Am. Chem. Soc.*, 90, 1289-1295.
- Melo, P. A., Sampaio, J. G., Biscaia Jr., E. C., Pinto, J. C., (2001). Periodic oscillations in continuous free radical solution polymerization reactors- a general approach, *Chemical Engineering Science*, 56, 3469–3482.
- Mesa, P. V. R., Belincanta, J. and Lona, L. M. F., (2005). Modeling and parameter estimation of Nitroxide Mediated Living Free Radical Polymerization (NMRP) of styrene. European Symposium on Computer Aided Process Engineering – 15.

- Moad, G., Rizzardo, E, Soloman, D. H., (1981) The reaction of acyl peroxides with 2,2,6,6-tetramethylpiperidinyl-1-oxy. *Tetrahedron Letters*, 22 (12), 1165-1168.
- Moad, G., Rizzardo, E. and Solomon D. H., (1982). A product study of the nitroxide inhibited thermal polymerization of styrene. *Polymer Bulletin*, 6, 589-593.
- Moad, G., Rizzardo, E. and Thang, S. H., (2005). Living radical polymerization by RAFT process. *Australian Journal of Chemistry*, 58, 379-410.
- Nabifar, A., McManus, N. T., Lima, E. V., Lona, L. M. F., Penlidis, A., (2009). Thermal polymerization of styrene in the presence of TEMPO. *Chemical Engineering Science*, 64, 304-312.
- Nabifar, A., McManus, N. T., Lima, E. V., Lona, L. M. F., Penlidis, A., (2008). A replicated investigation of nitroxide mediated radical polymerization of styrene over a range of reaction conditions. *The Canadian Journal of Chemical Engineering*, 86, 879-892.
- Otsu, T. and Yoshida, M., (1982). Role of initiator transfer agent terminator (Iniferter) in radical polymerizations: polymer design by organic disulfides as iniferters. *Macromolecular Rapid Communications*, 3, 127-132.
- Patel, H., (2007). Computational fluid dynamics (CFD) analysis of mixing in styrene polymerization. A Master's thesis, Ryerson University.
- Pfaendner, R., (2006). Nitroxyl radicals and nitroxylethers beyond stabilization: radical generators for efficient polymer modification. *Comptes Rendus Chimie*, 9, 1338–1344.
- Pinto J. C., (1995), The dynamic behavior of continuous solution polymerization reactors—A full bifurcation analysis of a full scale copolymerization reactor. *Chemical Engineering Science*, 50, (21), 3455-3475.
- Pyun, J. and Matyjaszewski, K., (2001). Synthesis of nanocomposite organic/inorganic hybrid materials using controlled/"living" radical polymerization. *Chemical Material*, 13, 3436-3448.

- Roa-Luna, M., Nabifar, A., Diaz-Barber, M. P., Mcmanus, N. T., Vivaldo-Lima, E., Lona, L. M. F. and Penlidis, A., (2007). Another perspective on the Nitroxide Mediated radical Polymerization (NMRP) of styrene using 2,2,6,6-Tetramethyl-1-piperidinyloxy (TEMPO) and dibenzoyl peroxide (BPO). *Journal of Macromolecular Science*, 44, 337-349.
- Roa-Luna, M., Nabifar, A., Mcmanus, N. T., Vivaldo-Lima, E., Lona, L. M. F. and Penlidis, A., (2008). Effect of the addition inert of TEMPO-capped prepolymer on polymerization rate and molecular weight development in the nitroxide mediated radical polymerization of styrene. *Journal of Applied Polymer Science*, 109, 3665-3678.
- Roberto L. N., Anotnio F. T. and Enrique S. G. (2006), Non-linear bifurcation analysis of living Nitroxide Mediated Radical Polymerization of styrene in a CSTR, *Chemical Engineering Science*, 61, 370-387.
- Russo, L. P. and Bequette, B. W., (1992). CSTR performance limitations due to cooling jacket dynamics-open and closed loop considerations. Rensselaer polytechnic institute, Troy, NY, 12180-3590.
- Russo, L. P. and Bequette, B. W., (1998). Operability of chemical reactors: multiplicity behavior of a jacketed styrene polymerization reactor. *Chemical Engineering Science*, 53, (1), 27–45.
- Saldivar-Guerra, E., Bonilla, J., Zcahua, G., Albores-Velasco, M., (2006). Incubation period in the 2,2,4,4-Tetramethyl-1-piperidinyloxy-mediated thermal autopolymerization of styrene: Kinetics and simulations. *Journal of Polymer Science, Part A, Polymer Chemistry*, 44, 6962–6979.
- Schmidt, A. D. and Ray, W. H. (1981). The dynamic behavior of continuous polymerization reactors—I. Isothermal solution polymerization in a CSTR. *Chemical Engineering Science*, 36, (8), 1401–1410.
- Schork, F. J. and Smulders, W., (2004). On the molecular weight distribution polydispersity of continuous living radical polymerization. *Journal of Applied Polymer Science*, 92, 539-542.

- Schulte, T., Knoop, C. A. and Studer, A., (2004). Nitroxide mediated living free radical polymerization of styrene: Asystematic study of the variation of the alkoxyamine concentration. . *Journal of Polymer Science, Part A, Polymer Chemistry*, 42, 3342-3351.
- Sinnott, R. K.; Coulson, J. M. and Richardson, J. F., (1999). *Chemical Engineering Design* (Third edition). Oxford, UK: Elsevier.
- Solomon, D. H., Rizzardo, E., and Cacioli, P., (1986) U.S. Patent. 4,581,429.
- Verazaluce-Garcia, J. C., Flores-Tlacuahuac, A. and Saldívar-Guerra, E., (2000). Steady-state nonlinear bifurcation analysis of a high impact polystyrene continuous stirred tank reactor. *Industrial and Engineering Chemistry Research*, 39, (6), 1972-1979.
- Veregin, R. P. N., Georges, M. K., Kazmaier, P. M., and Hamer, G. K., (1993). Free radical polymerization for narrow polydispersity resins: Electron spin resonance studies of the kinetics and mechanism. *Macromolecular*, 26, 5316-5320.
- Veregin, R. P. N., Odell, P. G., Michalak, L. M., and Georges, M. K., (1996). The pivotal role of excess nitroxide radical in living free radical polymerization with narrow polydispersity. *Macromolecules*, 29, (8), 2746-2754.
- Wang, J., S. and Matyjaszewski, K., (1995). Controlled/living radical polymerization. Atom transfer radical polymerization in the presence of transition metal complexes. *Journal of American Chemical Society*, 117, 5614-5615.
- Zhang, M. and Ray, W. H., (2001). Modeling of “Living” free-radical polymerization with RAFT chemistry. *Industrial and Engineering Chemistry Research*, 40, 4336-4352.
- Zhang, M. and Ray, W. H., (2002). Modeling of living free radical polymerization processes. I. Batch, semibatch and continuous tank reactors. *Journal of Applied Polymer Science*, 86, 1630-1662.

Appendix A : Molar Balances for Kinetic Model Development

This Appendix presents the use of the initiator primary radical equation in the kinetic model shown in Chapter 3.

The initiator primary radical R_{in}^\bullet has a very short life time. However, the kinetic model still depends on R_{in}^\bullet . Molar balance of R_{in}^\bullet gives:

$$\frac{d[R_{in}^\bullet]}{dt} = +2fk_d[I] - k_1[M][R_{in}^\bullet] + k_{PR}[I][NO_x^\bullet] = 0 \quad (A.1)$$

Which gives:

$$R_{in}^\bullet = \frac{2fk_d[I] + k_{PR}[I][NO_x^\bullet]}{k_1[M]} \quad (A.2)$$

Participation of the initiator primary radical R_{in}^\bullet in the kinetic model:

$$\begin{aligned} \frac{d[M]}{dt} = & -k_1[R_{in}^\bullet][M] - 2k_{dim}[M]^2 - k_{ia}[M][D] - k_{p1}[M]([D^\bullet] + [M^\bullet]) \\ & - k_p[M][\lambda_0] + k_{decomp}[MNO_x] - k_{fM}[M][\lambda_0] \end{aligned} \quad (A.3)$$

$$\begin{aligned} \frac{d(\lambda_0)}{dt} = & +k_1[R_{in}^\bullet][M] + k_{p1}[M]([M^\bullet] + [D^\bullet]) - k_{da}[NO_x^\bullet][\lambda_0] + k_a[\delta_0] \\ & - k_t[\lambda_0]^2 - k_{fM}[\lambda_0][M] - k_{fD}[D][\lambda_0] \end{aligned} \quad (A.4)$$

By substituting Eq. (A.2) into Eqs. (A.3) and (A.4), the following expressions were obtained. These are identical to Eqs. (3.28) and (3.39), respectively.

$$\begin{aligned} \frac{d[M]}{dt} = & -2fk_d[I] - k_{PR}[I][NO_x^\bullet] - 2k_{dim}[M]^2 - k_{ia}[M][D] - k_{p1}[M]([D^\bullet] + [M^\bullet]) \\ & - k_p[M][\lambda_0] + k_{decomp}[MNO_x] - k_{fM}[M][\lambda_0] \end{aligned} \quad (A.5)$$

$$\frac{d(\lambda_0)}{dt} = 2fk_d[I] + k_{PR}[I][NO_x^\bullet] + k_{p1}[M]([M^\bullet] + [D^\bullet]) - k_{da}[NO_x^\bullet][\lambda_0] + k_a[\delta_0] - k_t[\lambda_0]^2 - k_{fM}[\lambda_0][M] - k_{fD}[\lambda_0][D] \quad (\text{A.6})$$

Appendix B :Calculating the Heat Transfer Coefficient

The heat transfer coefficient for the inner wall of an agitated vessel such as the jacketed CSTR discussed in this study can be given by the following general expression. (Sinnott, 1999)

$$Nu = \frac{h_v D}{k_f} = C Re^a Pr^b \left(\frac{\mu}{\mu_w} \right)^c = C \left(\frac{ND_a^2 \rho}{\mu} \right)^a \left(\frac{CP\mu}{k_f} \right)^b \left(\frac{\mu}{\mu_w} \right)^c \quad (B.1)$$

The physical properties have been calculated according to the equations below (Patel, 2007):

$$\rho_m = (1174.7 - 0.918T)(1 - w_p) + (1250 - 0.605T)w_p \quad (B.2)$$

$$\mu_m = \frac{\mu_0}{\left(1 + \frac{\mu_0 \gamma^{1.2}}{35000} \right)^{0.6}} \quad (B.3)$$

$$\ln(\mu_0) = -11.091 + 1109/T + M_{w,p}^{0.1413} [12.032w_p - 19.501w_p^2 + 2.92w_p^3 + (-1327w_p + 1359w_p^2 + 3597w_p^3)/T] \quad (B.4)$$

$$\gamma_{avg} = k * N \quad (B.5)$$

The heat capacity CP_m of the reaction mixture is given by the following correlation (Judo vits et al., 1986):

$$CP_m = \alpha + \beta T \quad (B.6)$$

Where: Nu = Nusselt number, dimensionless

Re = Reynolds number, dimensionless

Pr = Prandtl number, dimensionless

h_v = heat transfer coefficient to vessel wall, W/m^2K

D_a = agitator diameter, m

k_f = thermal conductivity of reactor contents, W/mK

N = agitator speed, rps (revolutions per second)

ρ_m = density of reaction mixture, kg/m^3

μ_m = viscosity of reaction mixture, $N.s/m^2$

μ_w = viscosity of water, $N.s/m^2$

CP_m = heat capacity of reaction mixture, J/kgK

$\alpha = 95.12$,

$\beta = 0.2653$,

C, a, b, c = constants that depend on agitator type,

w_p = polymer weight fraction,

γ_{avg} = average shear rate in the reactor, s^{-1}

$k = 11$,

$M_{w,p}$ = molecular weight of the polymer,

T = temperature, K

For impeller type 45° pitched blade, Coulson and Richardson (Sinnott, 1999) provides constants (C, a, b, c) in Eq. (B.1). The final expression is as shown below.

$$Nu_v = \frac{h_v D}{k_f} = 0.64 \left(\frac{ND_a^2 \rho_m}{\mu_m} \right)^{0.67} \left(\frac{CP_m \mu_m}{k_f} \right)^{0.33} \left(\frac{\mu_m}{\mu_w} \right)^{0.14} \quad (B.7)$$

The heat transfer coefficient in a liquid-cooled jacket is also given by the general Nusselt number expression Eq. (B.8). For a spirally baffled jacket, Coulson and Richardson (Sinnott, 1999) provides the constants (C, a, b, c).

$$Nu_j = \frac{h_j d_e}{k_f} = C Re^a Pr^b \left(\frac{\mu}{\mu_w} \right)^c = 0.023 \left(\frac{\rho_w u d_e}{\mu} \right)^{0.80} \left(\frac{CP_w \mu_w}{k_f} \right)^{0.33} \left(\frac{\mu}{\mu_w} \right)^{0.14} \quad (B.8)$$

Where: h_j = heat transfer coefficient from vessel wall to cooling fluid, W/m^2K

d_e = hydraulic mean diameter, m

k_f = thermal conductivity of cooling fluid, W/mK

ρ_w = density of cooling fluid, kg/m^3

u = velocity of cooling fluid, m/s

μ = viscosity of cooling fluid, $N.s/m^2$

μ_w = viscosity of water, $N.s/m^2$

CP_w = heat capacity of cooling fluid, J/kgK

Since the cooling fluid is water, the viscosity correction ratio (μ/μ_w) is equal to unity and therefore can be ignored. Eq. (B.7) and (B.8) can be used to calculate h_v and h_j , respectively.

The overall heat transfer coefficient (U), neglecting heat transfer resistance due to the reactor wall and fouling, can then be calculated using the following expression.

$$U = \frac{h_v h_j}{h_v + h_j} \quad (B.9)$$

where U is the overall heat transfer coefficient, W/m^2K .

Appendix C : Steady State Bifurcation Plots

In this appendix, the plots of steady state bifurcation behavior when the feed stream temperature is the main bifurcation parameter whereas the coolant flow rate, and the residence time as the secondary bifurcation parameter, respectively, as it can be seen in Figure (C.1) and Figure (C.2). Those figures represent the model behavior in the 0-like disjoint region.

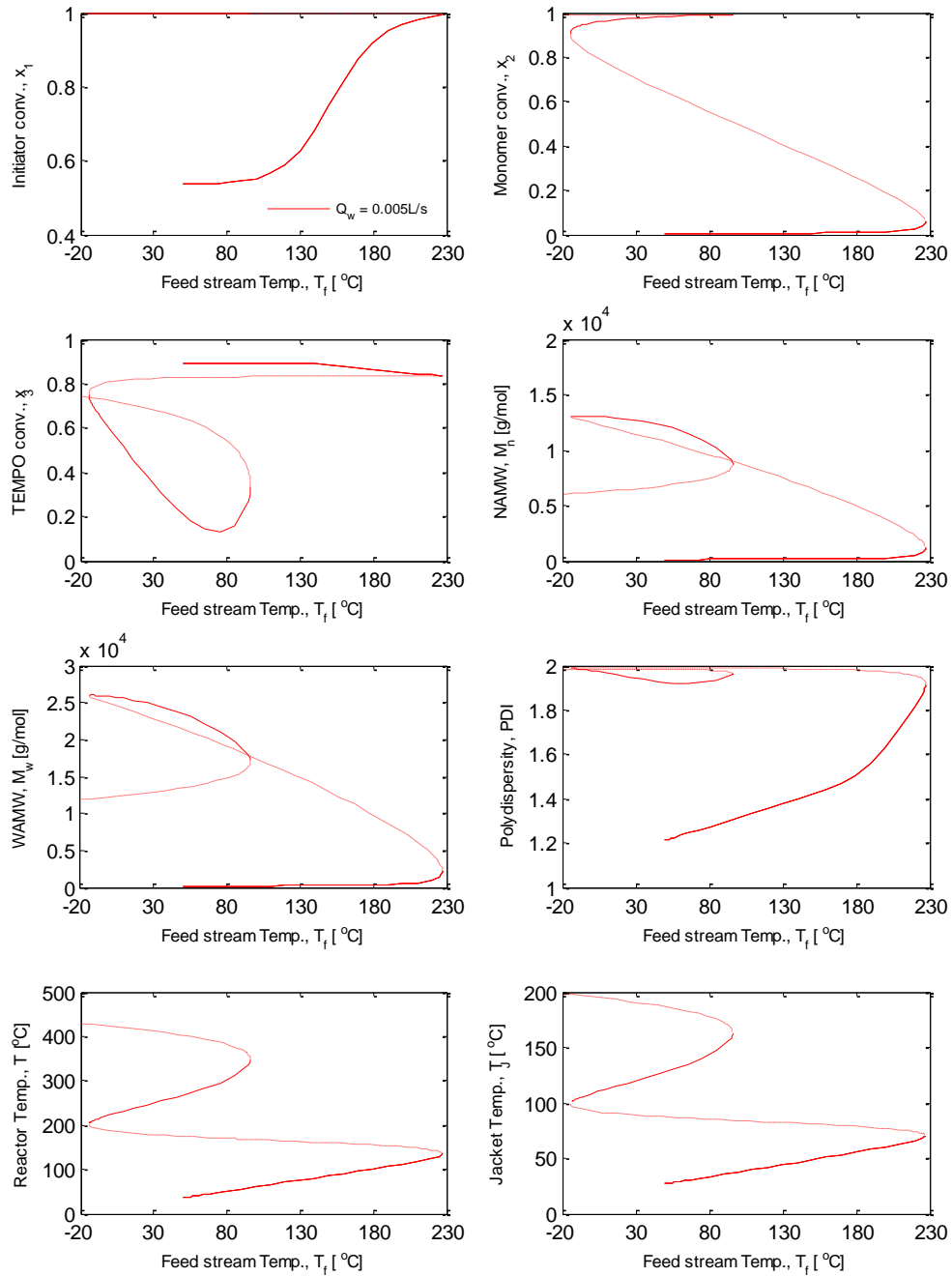


Figure C.1: Bifurcation diagrams with feed stream temperature as the main bifurcation parameter and coolant flow rate as the secondary bifurcation parameter. The stable solutions are plotted with solid lines (—) and unstable solutions with dashed lines (---)

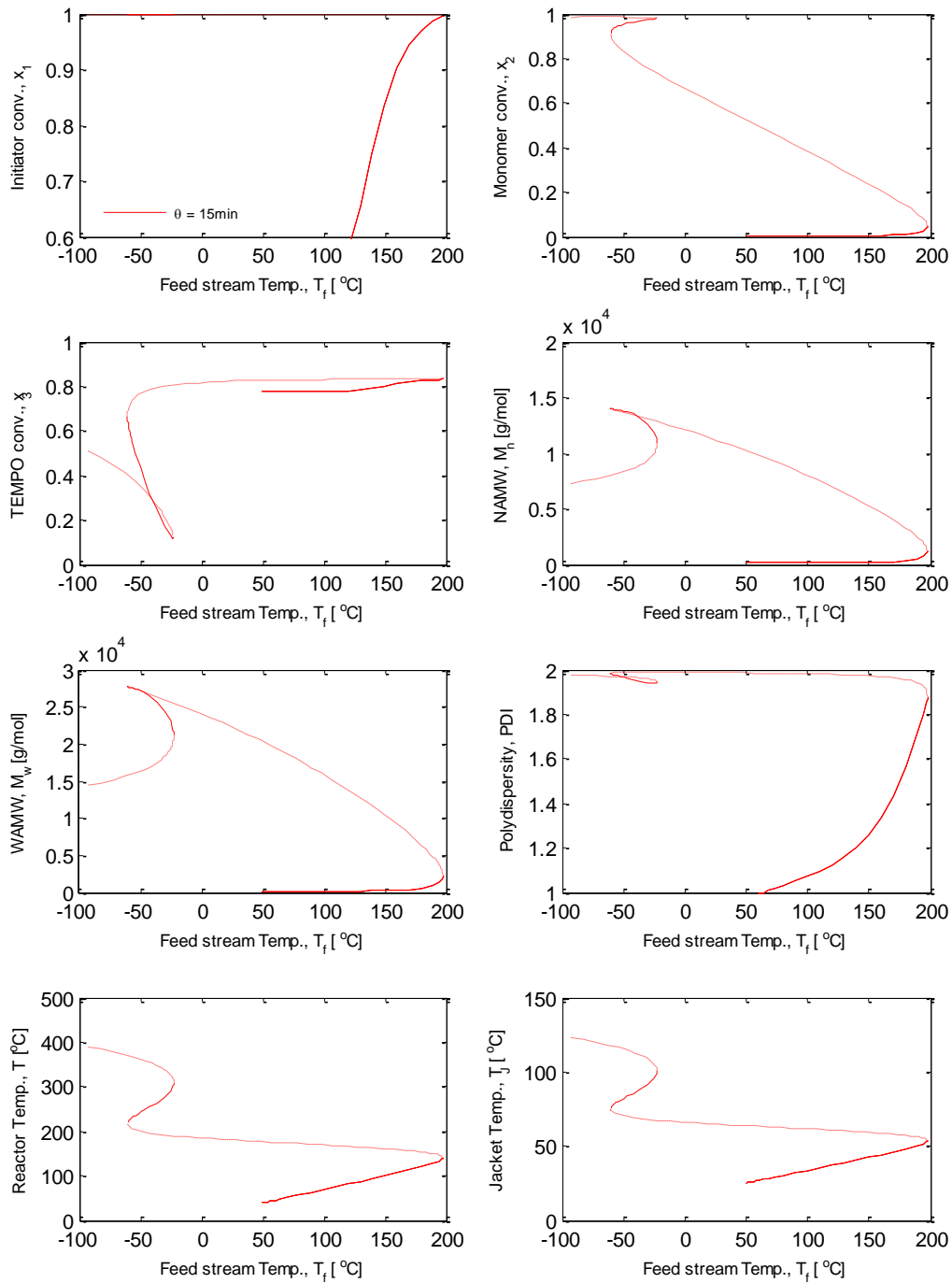


Figure C.2: Bifurcation diagrams with feed stream temperature as the main bifurcation parameter and residence time as the secondary bifurcation parameter. The stable solutions are plotted with solid lines (—) and the unstable solutions with dashed lines (---)